Enhanced Photocatalytic Oxidation of Polycyclic Aromatic Hydrocarbons in Offshore Produced Water

by

©Bo Liu, BSc, MASc

A Thesis submitted to the School of Graduate Studies

in partial fulfillment of the requirements for the

Degree of Doctor of Philosophy

Faculty of Engineering & Applied Science
Memorial University of Newfoundland

April 2018

St. John's Newfoundland and Labrador Canada

Abstract

The growing amount and environmental impact of offshore oily wastewater especially offshore produced water (OPW) have drawn significant attention in recent years. The petroleum hydrocarbons in wastewater can have severe negative effects in a long term on coastal and marine ecosystems if without sufficient treatment before discharge. Polycyclic aromatic hydrocarbons (PAHs) as a representative of dissolved chemical compounds or environmental pollutants in oily wastewater have been a major issue of marine environments due to their carcinogenic or mutagenic, toxic, persistent and bio-accumulative properties. To reduce the negative impact of produced water to the marine ecosystem, it is required to remove all toxicants especially PAHs before discharge. Various challenges have been identified in implementing conventional technologies (e.g., physical separation, chemical oxidation and biological remediation) for treating the dissolved organic pollutants (e.g., PAHs). Therefore, the research and development of more effective technologies to address these concerns are much desired. Photocatalysis generates powerful oxidative radicals which can rapidly mineralize organics especially aromatic compounds, offering a great potential use in removing PAHs from oily wastewater. However, the photocatalytic degradation of organics can be dramatically inhibited by the complex matrix of OPW. Limited in-depth studies were reported on the behaviors and interactions of different components in produced water during photocatalysis. The mechanisms of the interferences are of utmost importance to the development of highly efficiency treatment technologies. The generation of intermediates

caused by the complex matrix and inhibited treatment process could further lead to the increase in the toxicity of treated effluent to the marine ecosystem, and consequently reduce its potential in natural attenuation. In addressing these challenges and fulfill the knowledge gaps, this research is focused on the evaluation of the key factors and the mechanisms of OPW matrix in photocatalysis, and the development of enhanced photocatalytic oxidation processes to aid the OPW treatment, thus can achieve both high efficiency in removal of PAHs, and low toxicity and high biodegradability of the effluent.

The matrix effect was first investigated in a suspensive photocatalytic oxidation system, in which the synthesized TiO_2 nanoparticles were used. It is indicated that the degradation of PAHs was inhibited by the impurities in OPW matrix in many ways: the alkaline-earth cations caused the flocculation of the particle; the insoluble particulate matters competed with PAHs in the adsorption on TiO_2; the competition and the fouling effect of other dissolved organic matters were deteriorating the process.

To enhance the treatment process, immobilized TiO_2 was used instead and it was compared with the TiO_2 nano-particles. Improvements were found in both naphthalene adsorption and degradation in the immobilized photocatalytic oxidation system, indicating immobilized TiO_2 was more efficient and durable than TiO_2 nanoparticles in oily wastewater treatment. The competition of hydrocarbons especially phenols played a key role in the degradation of PAHs. The fouling on the catalyst surface was verified by the scaling of alkaline-earth metals and the deposition of organic matters.

Further improvement was aimed at developing a novel UV-light-emitted diode (UV-LED)/TiO_2 nanotube array (TNA)/ozonation process for treating OPW. The involvement of ozone was to reduce the competition of other organics and enhance the degradation efficiency. The TNA with hollow 1-D tubular nano-structures was applied because of the combined advantage of nano-particle and immobilization, as well as high quantum yield. UV-LED has the advantage of high energy efficiency and long-life time. In the integrated system, the removal of PAHs can be achieved within 30-min treatment with the half-lives reduced to less than 10 mins. Factorial analysis demonstrates that the best dose of TNA is 0.2 g/L. Light intensity affects the generation of iodine radicals, which is a strong scavenger of ozone thus reduces the efficiency of PAHs removal. Ozone dose is a dominated factor that promotes the degradation. Further results indicate that the degradation of phenols and PAHs with higher solubility favors to undergo to ozone-inducted oxidation, while PAHs with lower solubility are more likely oxidized on the catalyst surface.

The toxicity and biodegradability of OPW treated by photocatalytic oxidation were investigated during and after the treatment. Studies on the intermediates formed during the photocatalytic ozonation treatment in the presence of halogen ions reveal the mechanism and various reaction pathways of aromatic compounds. Iodization and bromination were the dominant interfering reactions in sequential stages. Two multivariable regression models were developed to quantify the contributions of key toxicants (e.g., total PAHs, total phenols, dibromo-pentane and bromoform) to the acute toxicity of OPW during the treatment processes. It was observed that by removing the

total PAHs and total phenols, the acute toxicity was increased from 3% to 57%, and the biodegradability (BOD_{28}/COD ratio) was doubled more than 80% by the integrated UV-LED/TNA/ozonation process. Further, the biodegradation rate of bromoform was much faster than those of phenols, indicating that the proposed technology features high efficiency and has low impact on marine environment.

In this research, I have investigated the matrix effect of OPW on photocatalysis and the impacts to the suspended and immobilized TiO_2. A novel integrated UV-LED/TNA/ozonation process was developed to treat OPW. The efficiency of the process, the effects of operational parameters, the intermediates and degradation pathways, and their contribution to the acute toxicity and biodegradability of treated effluent were investigated.

The scientific contributions of the research are: 1) revealing and summarizing the key mechanisms of OPW matrix and their key effects on photocatalysis, 2) understanding the interactions of OPW composition with catalyst surface, 3) fulfilling the knowledge gaps on the removal of PAHs from OPW by the UV-A (365 nm) photocatalytic ozonation process, including the interactive mechanisms of the adsorption and photocatalytic oxidation, the behaviors of halogenic ions, and the effects of the operational factors, 4) proposing the altered photodegradation pathways of aromatic organic matter in the presence of halogen ions, and 5) proposing toxicity contribution models targeted on the most toxic compounds in OPW with/without photocatalytic ozonation.

The findings of this thesis work also help 1) develop a better strategy to countermeasure the difficulties in the application of photocatalytic oxidation for treating OPW, 2) develop an advanced alternative option for the OPW management, and 3) monitor the composition and toxicity changes during the process and hence the production of by-products in the OPW treatment practice.

Acknowledgement

I would first like to thank my supervisors Dr. Bing Chen and Dr. Baiyu Zhang from the Faculty of Engineering and Applied Science at the Memorial University, Canada. They were always there whenever I ran into a problem or had a question about my research or life. They consistently provided kind advices and encouragement on both my Ph.D. research and my career development. They always steered me in the right direction. I would also like to thank Dr. Kenneth Lee, on my supervising committee from the Fisheries and Oceans Canada (DFO). His valuable advices particularly from the regulatory and practical aspects guided me to conduct more meaningful research.

I would like to acknowledge that my research work was funded by Natural Sciences and Engineering Research Council of Canada (NSERC), Canadian Foundation of Innovation (CFI), Research & Development Corporation of Newfoundland and Labrador (RDC NL), Petroleum Research Newfoundland and Labrador (PRNL) and Mitacs. Special Thanks also go to Memorial University which proved me such a good research environment and financial support and, DFO and local industrial partners for their technical support and advice.

I must express my very profound gratitude to my parents and to my wife for providing me with unfailing support and continuous encouragement throughout my years of study and through the process of thesis writing. This accomplishment would not be possible without them.

Additional gratitude is given to my colleagues Dr. Pu Li, Dr. Liang Jing, Dr. Jisi Zheng, Dr. Jing Ping, Dr. Hongjing Wu, Dr. Yinchen Ma, Xing Song, Qinhong Cai, Tong Cao, Yunwen Tao, Fuqiang Fan, Kedong Zhang, Zelin Li, Weiyun Lin, Zhiwen Zhu, Xudong Ye, and Xiao Zheng, for their friendship and assistance in the course of my research program.

Table of Contents

List of Tables

List of Figures

List of Abbreviations

A	Electron Acceptor	IPY	Indeno(1,2,3-cd)Pyrene
ANA	Acenaphthene	IS	Internal Standard
ANT	Anthracene	LED	Light-Emitting Diode
ANY	Acenaphthylene	LLME	Liquid-Liquid Micro-Extraction
AOPs	Advanced Oxidation Processes	NAP	Naphthalene
BaA	Benzo(a)Anthracene	NBOD	Nitrogenous Biochemical Oxygen Demand
BaP	Benzo(a)Pyrene	NL	Newfoundland and Labrador
BbF	Benzo(b)Fluoranthene	NTU	Nephelometric Turbidity Unit
BET	Brunauer–Emmett–Teller	OPW	Offshore Produced Water
BkF	Benzo(k)Fluoranthene	OUR	Oxygen Uptake Rate
BOD	Biological Oxygen Demand	PAHs	Polycyclic Aromatic Hydrocarbons
BPY	Benzo(g,h,i)Perylene	PHE	Phenanthrene
BTEX	Benzene, Toluene, Ethyl Benzene and Xylene	ppm	Part Per Million
CB	Conduction Band	ppmv	Part Per Million in Volume
CBOD	Carbonaceous Biochemical Oxygen Demand	PWRI	Produced Water Reinjection
CHR	Chrysene	PYR	Pyrene
COD	Chemical Oxygen Demand	SEM	Scanning Electron Microscope
D	Electron Donor	SIM	Selected Ion Monitoring
DBA	Dibenzo(a,h)Anthracene	TDS	Total Dissolved Solid
DCM	Dichloromethane	TEM	Transmission Electron Microscopy
DOC	Dissolved Organic Carbon	TIC	Total Ion Current

EDS	Energy-Dispersive X-Ray Spectroscopy	TNA	TiO_2 Nanotube Array
EGC	Expended Graphite	TPH	Total Petroleum Hydrocarbon
FLT	Fluoranthene	TSS	Total Suspended Solid
FLU	Fluorene	TTIP	Titanium (IV) Tetra-Isopropoxide
FTIR	Fourier-Transform Infrared Spectroscopy	UV	Ultraviolet
GC-MS	Gas Chromatograph – Mass Spectrometer	VB	Valence Band
ICP-MS	Inductively Coupled Plasma Mass Spectrometry	XRD	X-Ray Diffractometer

List of Symbols

hv	Photon energy
t	Reaction time (e.g., second, minute, day)
k	First-order reaction rate constant (min^{-1})
Kads	Adsorption rate constant (g/mg min)
C_0	Initial concentration of the reactant (µg/L)
C_t	Concentration of a reactant at time *t* (µg/L)
e	Mathematical constant
q_e	Amount of naphthalene adsorbed per unit mass of adsorbent at equilibrium (mg/g)
q_t	Amount of naphthalene adsorbed per unit mass of adsorbent at different time (mg/g)
I	Light flux per volume (Einstein/L s)
Δn	Photo-generated ferrous ion (mole)
∅	Quantum yield
V	Volume (e.g., mL, L)
Y	Dependent variable
X	Independent variable
α	Slop
β	Intercept
R^2	Regression coefficient

Chapter 1 Introduction

1.1 Background

The offshore industry generates a range of wastewater streams and causes marine oil pollutions by routinely discharging of oily wastewater particularly during oil and gas operations and shipping, such as produced water, bilge water, and ballast water (Jing et al., 2012; Jing et al., 2014b). Bilge water is the wastewater commonly found in the lowest part of a vessel and it is a mixture of oil and grease leaked from engine, piping and other mechanical parts inside the vessel (Asselin et al., 2008; Cazoir et al., 2012; McLaughlin et al., 2014). Ballast water may be contaminated by seeped oil from below decks, resulting in a small content of oil (Jing et al., 2012; Jing et al., 2015). Offshore produced water (OPW) is generated from the offshore oil and gas exploitation and production, which includes the formation water, injection water and process water (Jaji, 2012; Zheng et al., 2016). It presents the largest in oily wastewaters, which is approximately 14 billion barrels annually worldwide (Jaji, 2012; Zheng et al., 2016). Due to its enormous quantity, OPW is targeted as a representative of offshore oily wastewater.

The generation of OPW was highly dependent on the age of oil and gas wells. For example, the Hibernia project in Newfoundland and Labrador, Canada has been in service since 1997. As the operation time goes, the amount of OPW generated from this project has been dramatically increased; in the year of 2016, it reached to 6 million m^3/year (NLOPB, 2017). A similar trend can be seen in the annual OPW production from offshore Newfoundland (Figure 1.1).

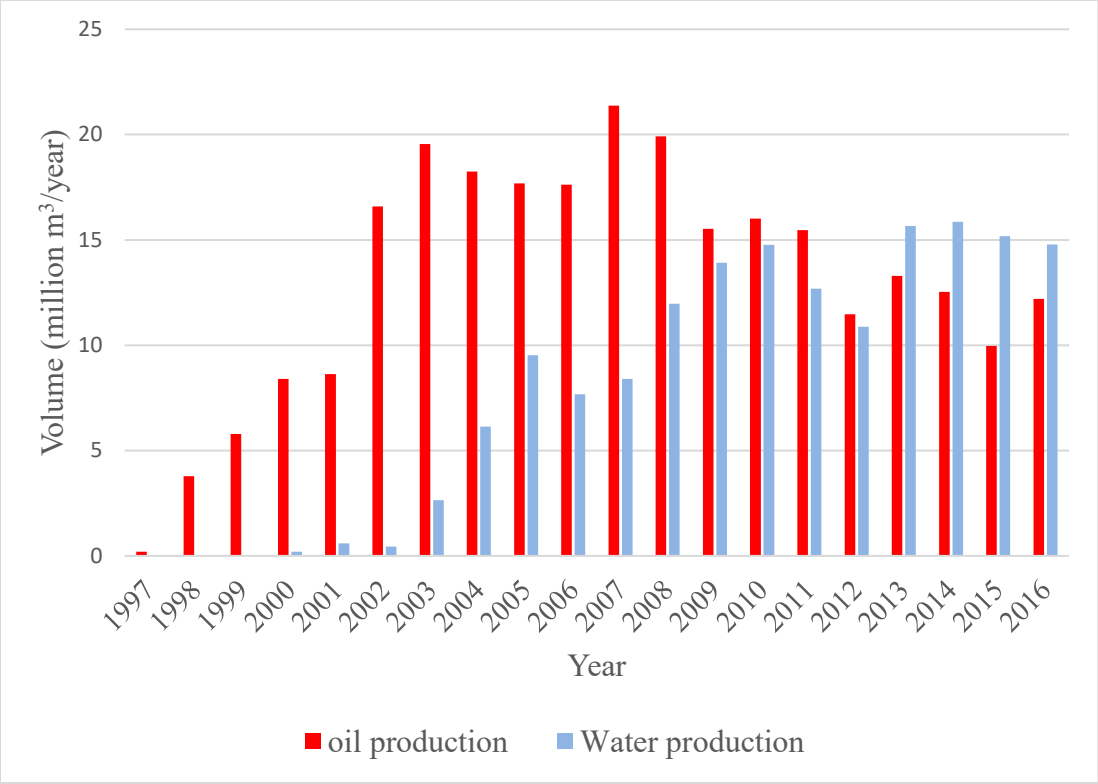

Figure 1.1 Oil and water production in the offshore Newfoundland (1997-2016)

Common practices of OPW management are discharge and reinjection (NEB et al., 2010; Oil & Gas UK, 2017). In some countries, OPW discharge is still a predominant option. For example, the production of OPW in the UK was 202 million m^3 in 2016, in which 165 million m^3 was discharged to sea (NEB et al., 2010; Oil & Gas UK, 2017). The continuous discharge of OPW on a daily basis is referred to as "chronic oil pollution". Recent studies have showed the negative impacts of discharged OPW on marine organisms, including bioaccumulation, endocrine disruption and suppression of bioactivities (Henderson et al., 1999; Nakata et al., 2003; Thomas et al., 2004; Hasselberg et al., 2004; Meier et al., 2007). Chronic exposure could lead to acute and chronic toxicity. To prevent the negative impact of OPW discharge, a practical management approach can be used which is to control the oil-in-water concentration. For example, the Canadian regulation for the the oil-in-water concentration in discharged OPW allows a monthly average of 30 mg/L and a daily average of 44 mg/L (NEB et al., 2010). However, the composition of OPW, including suspended solids, salt, petroleum hydrocarbons, organic acids, heavy metals, radionuclide and treating chemicals, is more complex than oil-in-water: (Li et al., 2005; Neff et al., 2011). The large discharge volume, the complex composition of contaminants and the lack of knowledge on the long term ecological impact have thus raised many concerns.

Among many organics in OPW, polycyclic aromatic hydrocarbons (PAHs) have drawn growing attention due to their long-term mutagenic and carcinogenic effects on marine biota and their resistance to biodegradation (OGP, 2002; Holth et al., 2009; Pérez-Casanova et al., 2012; Jing et al., 2014a; 2014b; 2015). Concentrations of PAHs in OPW

are relatively low, and the associated acute toxicity to aquatic organisms can be as low as 0.2-10 μg/g (Neff, 1985). However, even low-level exposure can result in bioaccumulation and development of cancer (Camacho et al., 2012). Therefore, it is recommended to eliminate PAHs before discharge of OPW.

1.2 Statement of Problems

The management of OPW has been recently emphasized by the industry and government as the increasing awareness. To reduce the environmental impact of OPW discharge, certain policies and actions have been fortified (Veil and Clark, 2011). For example, in northern Norway, considers as a severe environment, produced water should be treated before discharge or re-injection into a reservoir. (Igunnu and Chen, 2012; Oil & Gas UK, 2017). Further, the 'Zero Discharge' policy has been enforced by OSPAR (OSPAR Commission, 2012). Transport Canada also has regulations that no contaminants shall be discharged into Arctic waters according to the Arctic Waters Pollution Prevention Act.

In order to meet the regulation, OPW is usually treated onsite prior to reinjection or disposal. The conventional on-site treatment technologies are mainly based on physical separation such as hydrocyclone, skimming, and dissolved air flotation (Figure 1.2); however, they have been criticized for their limited capacity in removing oil residual and dissolved organic compounds, particularly PAHs (OGP, 2002; Dórea et al., 2007; Fakhru'l-Razi et al., 2009). A polishing treatment is needed to further remove PAHs from OPW prior to discharge (Jing et al., 2014b).

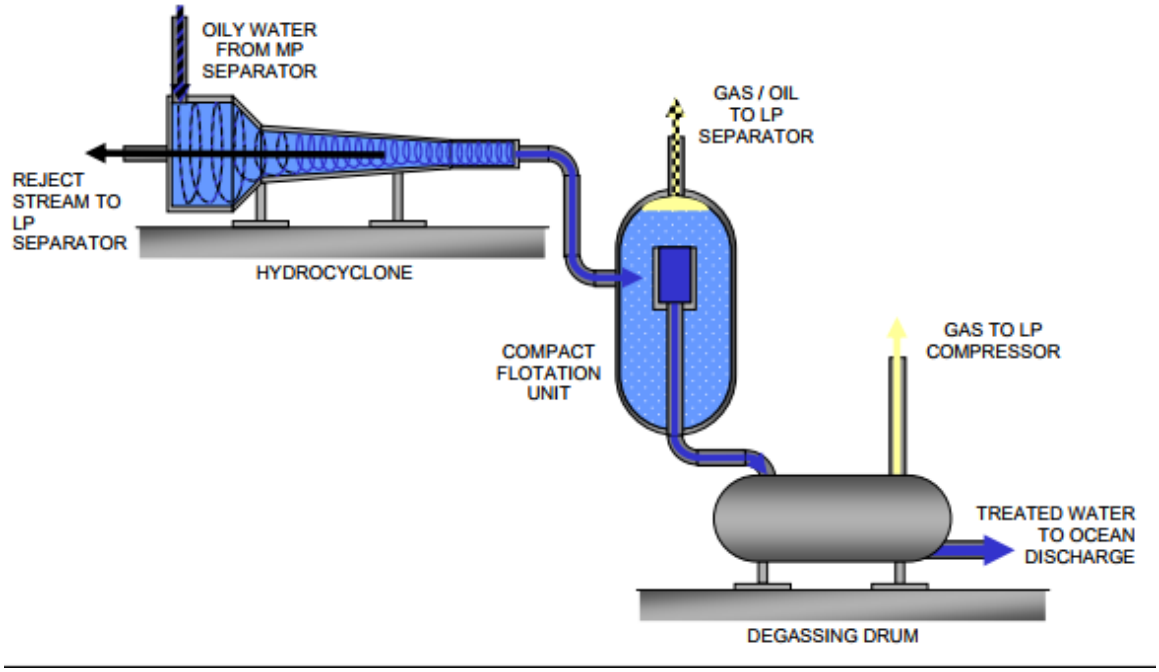

Figure 1.2 Scheme of on-site treatment process

Traditional PAH removal techniques such as biofiltration, biodegradation, adsorption, and phytoremediation are not directly suitable for offshore oil and gas production facilities or ships due to space, efficiency, cost, and safety concerns (Fakhru'l-Razi et al., 2009; Igunnu and Chen, 2012; Zheng et al., 2016). Photocatalytic oxidation has been regarded as one of the most promising means due to its high efficiency, small footprint, low selectivity for organic compounds, high level of mineralization and affordable cost. Less restrictions of weather and low maintenance requirement of photocatalytic oxidation make it more feasible in cold and harsh environments such as North Atlantic Canada. Nano-TiO_2 based photocatalysis has recently been proved to be a highly effective technology for treating various industrial and municipal wastewater (Pekakis et al., 2006; Shon et al., 2007; Armanious et al., 2011; Ghaly et al., 2011; Liu et al., 2016a; Liu et al., 2016b). It has also been recognized as an effective solution to the removal of PAHs from wastewater (Saien and Nejati, 2007; Ghaly et al., 2011).

It has been noticed that photocatalytic oxidation can be easily influenced by the complex matrix of wastewater. Ling et al. (2004) studied the photocatalytic degradation of phenol and pointed out that the turbidity of water body could reduce the penetration of UV light. Li et al. (2006) demonstrated chloride ions have competitive on the photoelectrocatalytic decontamination of oilfield produced wastewater. On the contrary, the presence of Fe^{3+} could promote photocatalysis by inhibiting the recombination of surface charges as well as photo-Fenton reactions (Rubio-Clemente et al., 2014). The presence of Cl^- can also enhance the degradation of naphthalene since the increase concentration of NaCl could enhance PAH aggregation and hence increase the adsorption of PAHs on the catalyst

surface (Lair et al., 2008). The composition of OPW is much more complex than that of the lab-synthesized water samples (Zheng et al., 2016; Liu et al., 2016b). The content of many inorganics and organics may cause dramatic changes in the efficacy and pathways of the photocatalysis.

The activity of catalyst surface plays an important role in affecting photocatalytic oxidation (Hidaka et al., 2003; 2006). The active surface of catalysts can be affected by the complex inorganic and organic composition of wastewater, resulting in lowered reactivity (Pablos et al., 2012). The presence of inhibitory ions (Mg^{2+}, Ca^{2+}, SO_4^{2-}, CO_3^{2-} etc.) can significantly reduce the effectiveness of catalyst, especially for suspended ones, by blocking the active sites and/or forcing the agglomeration of catalyst particles (Armanious et al., 2011; Alizadeh Fard et al., 2013). The high concentration of organic substrates can saturate the TiO_2 surface, reducing the photonic reactivity of the catalyst (Chong et al., 2010). These factors tend to cause the inhibition of photocatalysis, including catalyst agglomeration, surface fouling, competition of active sites on catalysts, and active radical scavenger. Therefore, the study of surface changes of catalyst is important to the investigation and application of photocatalytic oxidation for treating OPW.

To the author's best knowledge, no study has clearly identified the mechanisms of the matrix effect on OPW treatment by using nano-TiO_2. Furthermore, the influence of matrix on produced water (e.g., pH, turbidity, salinity, metals, and organic matters) and the selective adsorption/photocatalysis of petroleum hydrocarbons are rarely investigated.

The selectiveness of photocatalysis may result in different retention times for target compounds, thus affecting detoxication and overall performance of the treatment. It is necessary to jointly investigate the effects of matrix and the influence of different types of photocatalysts on OPW to fill the knowledge gaps and provide scientific guidance to the practice.

photocatalytic oxidation with low treatment efficiency makes the operation both costly and time-consuming. It also increases the levels of intermediates in the effluent due to insufficient treatment. It has been found that the oxy-intermediates could have higher persistence and wider spread occurrence in the environment, which magnify the toxicity (Lundstedt et al., 2007). Sufficient level of OPW detoxification is desired to afford non-toxic effluent by photocatalytic oxidation. Therefore, enhancement (e.g., development of highly efficient catalyst, addition of oxidant and use of high intensity light-emitting diode [LED] light) of photocatalytic oxidation for treating OPW would be more meaningful in supporting the sustainable offshore development and protecting the marine.

The mechanisms of the interferences are important to the development of high-efficiency treatment technologies. However, there is still a knowledge gap on the altered pathways of organics during photocatalytic oxidation caused by the complex matrix of OPW. The alternation would not only inhibit treatment process but also generate intermediates which may increase the toxicity of treated effluent to the marine ecosystem, and consequently reduce its potential in nature attenuation.

1.3 Objectives and Tasks

The research aims at the development of enhanced photocatalytic oxidation methods for treating OPW, a representative of oily wastewater. Focus has been placed on examining the key matrix effect, unveiling the mechanisms of photocatalytic oxidation, evaluating the suspended and immobilized catalysts, and testing the enhancement of the integration of advanced oxidation methods and their effects on the toxicity and biodegradability of treated OPW. OPW samples from the offshore oil fields were used and PAHs are the main target contaminants in the study. The main research tasks include:

(1) To examine and understand the behavior of key components in OPW matrix and their impact on the kinetics and mechanisms of nano-TiO_2 based photocatalytic oxidation of PAHs;

(2) To develop a nano-TiO_2 based photocatalytic oxidation technology for OPW treatment and to examine the efficiency and capacity of an immobilized nano-TiO_2 as enhanced system in removing PAHs;

(3) To design a highly efficient photocatalytic oxidation technology by integrating UV-LED, TiO_2 nanotube array (TNA) and ozonation for the degradation of hydrocarbons especially PAHs in OPW;

(4) To evaluate the compositional changes of OPW during the photocatalytic ozonation process and their influence on the toxicity and biodegradability of treated wastewater.

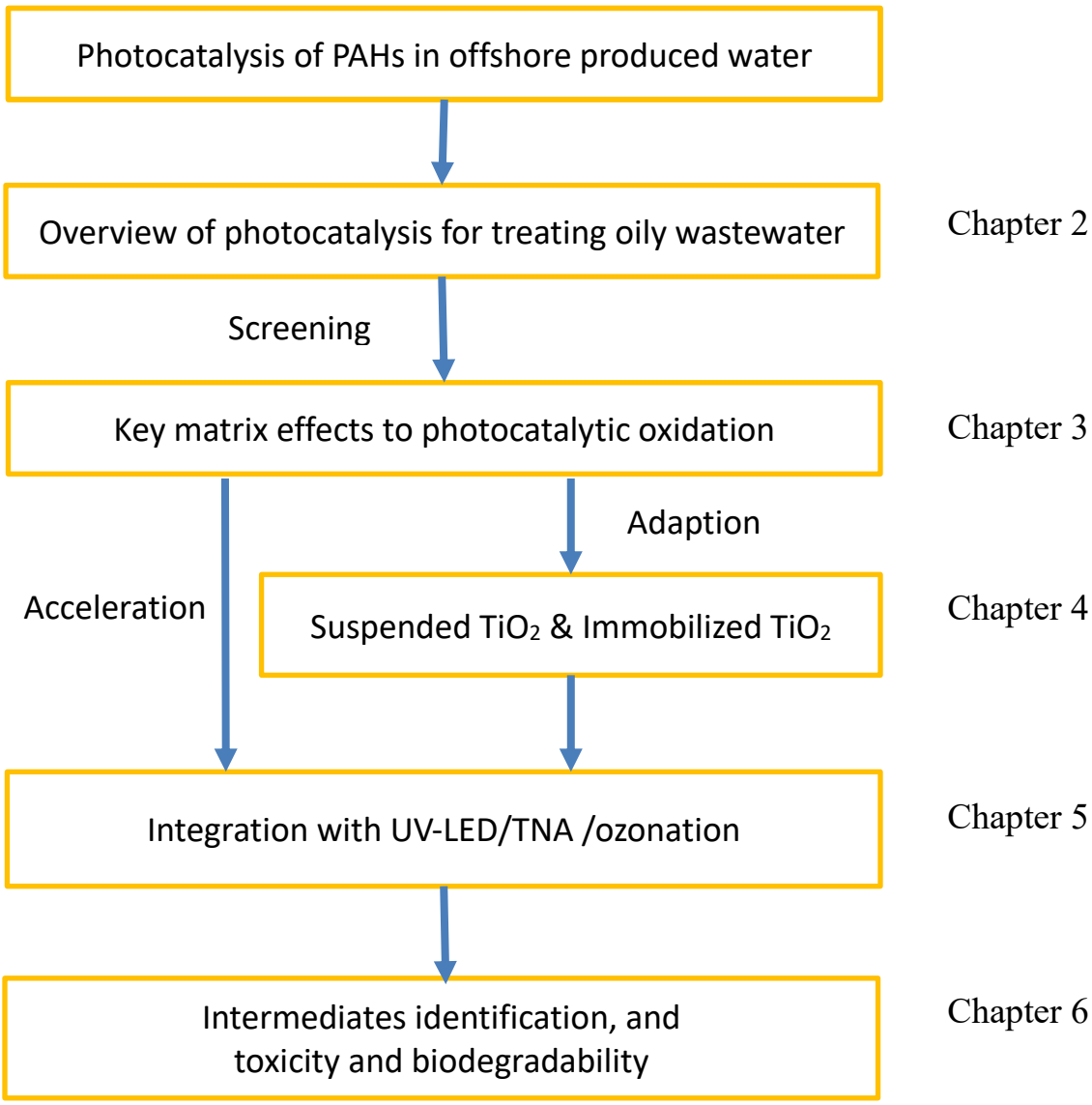

Figure 1.3 Flow chart of the research

1.4 Structure of the Thesis

Chapter 2 gives a comprehensive review of oily wastewater properties and the TiO_2 based photocatalytic technologies for oily wastewater treatments. The composition of wastewater, the matrix effects on photocatalysis, system configuration, and catalyst development were discussed.

Chapter 3 investigates the matrix effects arising from the individual components in OPW during the photocatalytic oxidation of PAHs. The kinetics of degradation and the effects of insoluble particles, inorganic ions and organic matters were examined.

Chapter 4 studies the applicability of different catalysts for treating PAHs in OPW. The adsorptive properties and photo-degradation of TiO_2 nanoparticles and immobilized TiO_2, and the surface changes of catalyst in relation to the composition of OPW are discussed.

Chapter 5 examines an integrated UV-LED/TiO_2 TNA photocatalysis/ozonation process for treating OPW. The efficiency of PAH removal in the single and integrated system, the effects of ozone dose, catalyst dose and light intensity are determined and analyzed.

Chapter 6 Investigates the influence of photocatalytic ozonation on the toxicity and the biodegradability of the treated effluent. The intermediates, the degradation pathways, and the interference of halogens were also discussed.

Chapter 7 summarizes the major findings and, the scientific and practical contributions of this research. Recommendations are made for future work.

Chapter 2 Literature Review[1]

[1] *The contents of this chapter are based and expanded on the following paper:*

Liu. B., Chen, B. and Zhang, B.Y. (2017) Oily Wastewater Treatment by Nano-TiO_2-Induced Photocatalysis, IEEE Nanotechnology Magazine, 11(3): 4-15, DOI: 10.1109/MNANO.2017.2708818
Role: Bo Liu solely worked on this study and acted as the first author of this manuscript under Dr. Bing Chen and Dr. Baiyu Zhang's guidance. Most contents of this paper were written by him and further edited by the other co-authors.

2.1 Offshore Oily Wastewater

The global booming of offshore industry has resulted in a dramatic increase in generation of oily wastewater (by far the largest waste by-product in oil and gas production) associated with produced water, bilge water and ballast water discharges. As the largest stream among the oily wastewater, offshore produced water (OPW) amounts to approximately14 billion barrels annually worldwide (Zheng et al., 2016). OPW contains a variety of contaminants such as petroleum hydrocarbons, nutrients, radionuclides, heavy metals and chemical additives (Ekins et al., 2005; Zheng et al., 2016). The impact of these toxic components in OPW, especially petroleum hydrocarbons and phenol derivations, to the marine ecosystem and environment, has aroused special concerns in the past years (Neff, 2002; Elias-Samlalsingh and Agard, 2004; Chen et al., 2010). Many offshore petroleum production fields are located in cold oceans such as the North Atlantic Ocean, which have more vulnerable ecosystems than other parts of the world because of short food chain and harsh environments featuring with low temperature, sea ice weather and rough seas etc. Hydrocarbons may have relatively slow biodegradation rates and the adverse chronic effects could be severe due to the extended period of low-level toxicant exposure (Zheng et al., 2016). Offshore produced water discharge guidelines are generally similar among countries with a trend towards the development of more stringent regulatory targets. Pressing needs have been recognized to develop more efficient treatment technologies that can not only remove the bulk of oil but extend the scope to the dispersed and dissolved hydrocarbons. The latter is still presenting a key challenge for research and practice.

To the author's knowledge, rare studies have been targeted on the OPW treatment by photocatalytic oxidation. Therefore, the scope of this review is focused on the development of photocatalytic technologies in treating oily wastewater.

2.2 Wastewater Characterization

Oily wastewater refers to any water containing oil from many industrial processes, such as oil and gas exploration, production and transportation, petroleum refining, and onshore/offshore oil spills (Fakhru'l-Razi et al., 2009; Srinivasan and Viraraghavan, 2010; An et al., 2017). The concentration of oil, the major contaminant in oily wastewater, varies widely among sources, ranging from 1 to 40000 mg/L (An et al., 2017). The effluents from oil and gas production and transportation are the largest waste streams of oily wastewater (e.g. produced water, bilge water, refinery wastewater) (Zheng et al., 2016). The total oil and grease concentration of OPW should be not higher than 42 mg/L based on the existing regulations (Fakhru'l-Razi et al., 2009). Not included are the soluble oil fractions such as carboxylic acids (0.001-10,000 mg/L), aliphatic hydrocarbons, BTEX (0.068-578 mg/L), PAHs (40-3000 μg/L), and phenols (0.4-23 mg/L), which results in the concentration of total organic carbon (TOC) being as high as 11000 mg/L (Neff et al., 2011; Zheng et al., 2016). Bilge water has a higher concentration of TOC (31-19,040 mg/L) and phenol (15-902 mg/L) than OPW does (U.S. EPA, 1999). Petroleum refinery effluent contains 20-4000 mg/L oil and grease, 200-600 mg/L chemical oxygen demand (COD), 20-200 mg/L phenol, and 1-100 mg/L benzene (Shahrezaei et al., 2012).

The toxicity of these chemical components in oily wastewater, especially petroleum hydrocarbons and phenol derivatives, has raised concerns over their effects on the marine ecosystems and the environment in general (Brendehaug et al., 1992; Flynn et al., 1996; Elias-Samlalsingh and Agard, 2004). The acute and chronic toxicity of PAHs and alkylated phenols have been well indicated (Johnsen et al., 1994). It was also disclosed that alkylphenols have higher potential of bioaccumulation because they have high hydrophobicity and can cause irreversible endocrine disruptive impacts to sexual development of young fish (Hasselberg et al., 2004; Ekins et al., 2005; Meier et al., 2007). Therefore, strict regulations have been established to control the emission of oil and grease in OPW (42 ppm daily maximum) (Zheng et al., 2016), bilge water (15 ppmv) (Cazoir et al., 2012) and refinery effluent (7.5 pounds per 1000 barrels of crude oil in daily maximum).

Table 2.1 Summary of oily wastewater composition

Chemical	Produced Water[a] Range	Bilge Water[b] Range
TSS (mg/L)	N/A	19 -1205
Salinity (TDS) (mg/L)	<5000 - >300,000,000	5,570 -16,620
Chloride (mg/L)	46,100 -14,100	3,616 - 9,742
Sulfate (mg/L)	210 - 1,170	411 - 1,290
Bromide (mg/L)	46 - 1,200	N/A
Ammonium (mg/L)	23 - 300	N/A
Bicarbonate (mg/L)	77 - 560	N/A
Iodide (mg/L)	3 - 210	N/A
Carbonate (mg/L)	30 - 450	N/A
Metals		
Sodium (mg/L)	23,000 - 57,300	2,680 - 5,200
Calcium (mg/L)	2,530 - 25,800	105 - 184
Magnesium (mg/L)	530 - 4,300	262 - 486
Potassium (mg/L)	130 - 3,100	N/A
Strontium (mg/L)	7 - 1,000	N/A
Barium (mg/L)	0.2 - 228	<0.67
Cadmium (µg/L)	0.5 - 5	<610
Copper (µg/L)	22 - 82	430 - 6,110
Mercury (µg/L)	<0.1 - 26	<10
Lead (µg/L)	0.4 - 8.3	<46
Zinc (mg/L)	0.5 - 13	0.5 - 13
Iron (mg/L)	0.1 - 15 (II) 4.5 - 6 (III)	0.2 - 1.2
Manganese (mg/L)	0.1 - 0.5	<0.2
Nickel (mg/L)	0.02 - 0.3	<0.4
Cobalt (mg/L)	0.3 - 1	N/A
Total Organic Carbon (mg/L)	<0.1 - >11,000	31 - 19,040
BTEX (mg/L)	0.068 - 578	>0.5
PAH (µg/L)	40 - 3,000	>64
Organic Acids (<C6) (mg/L)	<0.001 - 10,000	N/A
Phenols (mg/L)	0.4 - 23	15 - 902

a. Neff et al. (2011); b. U.S. EPA (1999)

2.3 Management Practice

To comply with the regulation, the oil and grease in produced water must be removed first. The main treatment technologies reported include gravity separation, hydrocyclone, sorption, chemical precipitation, flotation, membrane filtration, chemical oxidation and biodegradation (Zheng et al., 2016; An et al., 2017). The most widely applied on-site produced water treatment technology is water/oil separation which relies on gravity and density differences. To realize an effective water/oil separation, the most commonly used facility has been identified through the combination of a skim tank, a parallel plate separator, a hydrocyclone and a floatation device (Zheng et al., 2016). However, the water/oil separation encounters difficulty in removing very small droplets and dissolved hydrocarbons (OGP, 2002). To remove dissolved organic contaminants from wastewater, many available technologies have been used after the water/oil separation process, including coagulation, adsorption, membrane filtration, and chemical oxidation and activated sludge (Fakhru'l-Razi et al., 2009; Shahrezaei et al., 2012; Jamaly et al., 2015).

Coagulants added to oily wastewater can destabilize the oil emulsion, resulting in oil aggregation. Larger oil droplets can be subsequently removed by sedimentation or flotation (Hempoonsert et al., 2010). Adsorption is effective in removing most oil and other organic materials but requires continuous regeneration and replacement. In addition, the adsorbed wastes need to be shipped to shore for landfill which increases the treatment cost. Membrane and filtration technologies can remove small oil droplets and hydrocarbons larger than 0.005 microns (Janknecht et al., 2004), but fouling of the membranes is a major problem, and the technology is limited in oil field-type

applications. Bioremediation has the capability to remediate the organic matter in heavily loaded oily wastewater. However, this technology is time-consuming, inefficient in the degradation of aromatic organics, has a narrow range of appropriate reaction conditions (e.g., temperature and pH), and requires disposal of the spent, contaminated activated sludge (Zheng et al., 2016).

2.4 Photocatalytic Oxidation

2.4.1 Basics of Photocatalysis

Photocatalysis is an advanced oxidation processes (AOPs) that has been extensively studied in remediating environment samples contaminated by various organic pollutants (Chong et al., 2010; Zhang et al., 2014; Uyguner-Demirel et al., 2017). The photocatalytic process, which has shown promise in terms of complete mineralization of organic pollutants, has strongly attracted scholars' attentions. The photocatalytic degradation of aliphatic, aromatics, polymers, dyes, surfactants, pesticides and so forth into CO_2, water and mineral acids can be achieved under mild conditions without the need for waste disposal. Photocatalysis is the acceleration of photolysis by adding photo-sensitive semiconductors, such as TiO_2, ZnO, CdS, GaAs, GaP, GdSc, CdS, WO_3 etc. (Carp et al., 2004). Among these, TiO_2 has been discovered to be an ideal semiconductor for photocatalysis due to its high stability, low cost and safety to both humans and environment (Chong et al., 2010; Ibhadon and Fitzpatrick, 2013) .

The photocatalytic mechanism is initiated by the absorption of a photon with energy (*hv*) equal to or greater than the band gap of TiO_2, producing an electron-hole pair on the

surface of TiO_2. An electron is promoted to the conduction band (CB), while a positive hole is formed in the valence band (VB). Excited electrons and holes recombine and dissipate the input energy as heat, get trapped in metastable surface states, or react with electron donors (D) and electron acceptors (A) adsorbed on the semiconductor surface (Figure 2.1). After reaction with water, these holes produce hydroxyl radicals with high oxidation potentials. Depending upon the exact conditions, the holes, OH radicals, O_2^-, H_2O_2 and O_2 molecules play important roles in the photocatalytic mechanism (Hoffmann et al., 1995) as follows:

$$TiO_2 + hv \rightarrow e^- + h^+ \qquad (2.1)$$

$$h^+ + OH^-_{ads} \rightarrow OH\cdot_{ads} \qquad (2.2)$$

$$OH\cdot_{ads} + Orgnaics \rightarrow oxidized\ product \qquad (2.3)$$

$$e^- + O_{2,ads} \rightarrow O_2^{\cdot -} \qquad (2.4)$$

$$O_2^{\cdot -} + H^+ \rightarrow HO_2\cdot \qquad (2.5)$$

$$HO_2\cdot + HO_2\cdot \rightarrow H_2O_2 + O_2 \qquad (2.6)$$

$$H_2O_2 + e^- \rightarrow OH\cdot_{ads} + OH^- \qquad (2.7)$$

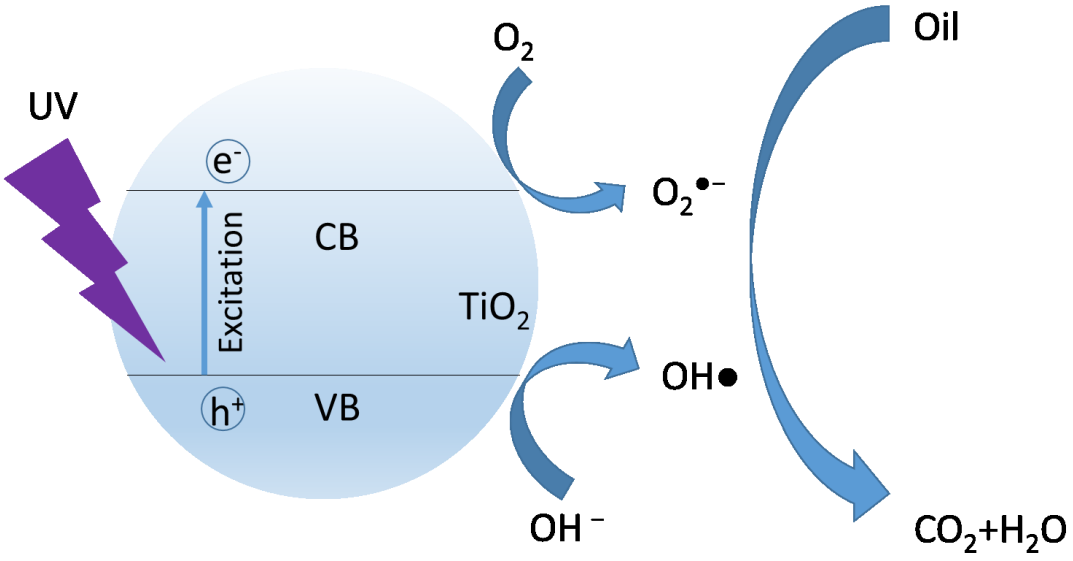

Figure 2.1 Mechanism of light absorption by TiO_2

TiO_2 polymorphs in nature include: anatase (tetragonal), brookite (orthorhombic), rutile (tetragonal), each of which has different optical properties (Gupta and Tripathi, 2011). The band gaps of anatase, rutile and brookite are 3.20, 3.02 and 2.96 eV respectively (Wunderlich et al., 2004). As a result, their absorption wavelengths are shorter than 400nm. In other words, only ultraviolet (UV) light and near ultraviolet light can excite TiO_2. The anatase structure has the largest band gap, and it is preferred over other polymorphs for photocatalysis applications because of its higher electron mobility, low dielectric constant and lower density (Carp et al., 2004) compared with rutile, which tends to recombine electrons and holes and hence prevents the transport of electrons.

Various studies have been reported, which confirm that TiO_2 is more effective in the form of nanoparticles than bulk powder (Gupta and Tripathi, 2011). When the crystallite diameter falls below a critical radius of about 10 nm, the band gap increases, and the band edges yield larger redox potential (Hoffmann et al., 1995). The higher redox potential provides stronger driving force, increases the rate constant of charge transfer (the rate-limiting step of photocatalysis) and then increases the photoactivity of nanoparticles. Additionally, the smaller the size of TiO_2 is, the higher efficiency the mass transfer can achieve, since size reduction leads to increased surface area and therefore improved photoactivity.

2.4.2 Applications in Oily Wastewater Treatment

Many attempts have been made to apply photocatalysis in treating oily wastewater and they are summarized in Table 2.2. Most of the studies utilized TiO_2 and UV and/or solar light to degrade the oil contents in different wastewater and gave good results

(Grzechulska et al., 2000; D'Auria et al., 2009; da Rocha et al., 2010; Yeber et al., 2012). The water types can be classified as artificial wastewater and authentic wastewater. The artificial water samples were prepared by spiking distilled water and/or seawater with the target pollutant (Vargas and Núñez, 2010; Zulfakar et al., 2011; McQueen et al., 2016). The authentic water samples were prepared by either contaminating the water samples with crude oil (Ziolli and Jardim, 2002) or diesel (Hu et al., 2012) or were obtained from already contaminated sources (Coelho et al., 2006; Liu et al., 2016a; Leshuk et al., 2016a). The target pollutants such as oil (Brame et al., 2013), COD (Gao et al., 2013), dissolved organic carbons (DOCs) (Santos et al., 2006), total petroleum hydrocarbons (TPHs) (Cho et al., 2006), BTEX (Cho et al., 2006), phenols (Shahrezaei et al., 2012), PAHs (King et al., 2014), aliphatic carbons (Hsu et al., 2008), organic acids (Leshuk et al., 2016b) and polymers (polyacrylamide, PAM) (Wang et al., 2006), constitute the major hazardous organic compounds in oily wastewater.

Table 2.2 Summary of photocatalysis for different oily wastewater

Wastewater type	Catalyst	Treatment process	Target pollutant	Major findings	reaction rate constant	Reference
Artificial water	Nano-TiO_2-SiO_2	fixed bed system+ sunlight	naphthenic acid	92% removal after 4 h		(McQueen et al., 2016)
	Nano-TiO_2	1000W xenon lamp	naphthalene		0.032~0.052 min^{-1};	(Vargas and Núñez, 2010)
			dibenzothiophene		0.009~0.019 min^{-1};	
			p-nitrophenol		0.009~0.068 min^{-1}	
	Nano-TiO_2 coated on quartz sand	20W UV lamp 254nm	phenol	50%-100% in 6 hours depend on the initial concentration		(Zulfakar et al., 2011)
Artificial water and seawater	Nitrogen-doped TiO_2 nanotube	6W black light lamp and 20W tungsten lamp	MB, toluene and 1-haxadecene	toluene 26% with N-TNT and 14% with TNT; less than 10% with visible light; 1-hexadecene: 10% degradation under UV light source	0.38 mg toluene/g N-TNT/h 0.25 mg 1-hexadecene /g N-TNT h	(Hsu et al., 2008)

Table 2.2 Summary of photocatalysis for different oily wastewater

	Degussa P25, Aerosil T805	1500W xenon lamp with 340nm ~79 mW	toluene dodecane		$2.7\times^{10-2}$~15 7.7×10^{-4}~0.82	(Minero et al., 1997)
Offshore produced water	Degussa P25 and Immobilized TiO_2 on glass plate	4.3 W UV lamp	Naphthalene		Dispersion 0.00219 min^{-1} fixed plate 0.00305 min^{-1}	(Liu et al., 2016a)
	TiO_2	8W UV lamp	PAHs	>50% PAHs removal in 24 h	>0.0005 min^{-1}	(Liu et al., 2016b)
	Immobilized TiO_2 on glass plate	4.3 W UV lamp + Ozone	PAHs	>90% removal in 1 h	0.05-0.29min^{-1}	(Liu et al., 2017)
Bilge water	K-TiO_2	UV lamp with light intensity of 49W·m^{-2}	COD	100% oil decompostion in 2 h		(Grzechulska et al., 2000)
	K-TiO_2	ultrafiltration and UV lamp with light intensity of 49W·m^{-2}	oil and COD	filtration: 96~98% removal; photocatalysis: 100% removal in 2 h		(Karakulski et al., 1998)
	TiO_2 PC500	air stripping+125 W UV lamp 365nm	oil	60% removal in 8.5 h	0.009×[HC]	(Cazoir et al., 2012)

Table 2.2 Summary of photocatalysis for different oily wastewater

	Nano-TiO_2 loaded on ceramic microbeads	near-UV solar irradiation 25~50 $W \cdot m^{-2}$	PAHs	100% removal		(Cho et al., 2006)
	Degussa P25	150W Hg lamp+H_2O_2	TOC	>50% TOC removal after 10 h		(Pernyeszi and Dékány, 2003)
	Exfoliated graphite/ZnO composites	UV irradiation 20W/m^2	oil	sorption: 50~57g/g, 85% removal after 160 h irradiations		(Yue et al., 2009)
Crude oil and contaminated water	Degussa P25, P25 supported on NaY zeolite	125 W high-pressure mercury arc for 100 hour	linear alkane, branched alkane, cyclic alkane and aromatic compounds	linear alkanes 98.66%, branched alkanes 97.31%, cyclic alkanes 96.04%, aromatic compounds 99.54%; with zeolite: linear alkanes 79.85%, branched alkanes 45.38%, cyclic alkanes 58.10%, aromatic compounds 91.85%		(D'Auria et al., 2009)
	TiO_2 nanotube and modified TiO_2 with stearic acid	irradiated with lamp of 765W/m^2 and 300-800nm	alkane, PAHs	alkane ineffective	PAHs removal: 0.08~0.14/h	(King et al., 2014)

Table 2.2 Summary of photocatalysis for different oily wastewater

	Nano-TiO_2	photocatalysis followed by biofilm	oil	90.0% of oil removal	0.027 min^{-1}	(Yeber et al., 2012)
Crude oil contaminated seawater	Degussa P25	125W Hg lamp 366nm	water-soluble fraction	100% removal after 1-2 d		(Ziolli and Jardim, 2003)
	Degussa P25	25W Hg lamp 366nm	DOC	adsorption: 25% in the first 12 h photocatalysis: 90% after 7 d		(Ziolli and Jardim, 2002)
Diesel in seawater	Nano-ZnO	UV irradiation	diesel	84% removal in 3 h		(Hu et al., 2012)
Diesel in water	Polyurethane foams modified with silver/titanium dioxide/graphene ternary nanoparticles (PU-Ag/P25/G)	UV irradiation	diesel	adsorption 96g/g; degradation 76% in 16 h		(Ni et al., 2016)
	Bi/N-doped TiO_2 on expanded graphite C/C (EGC) composite	500W xenon lamp with UV cut-off filters	diesel		0.0029-0.0062 min^{-1} depended on the Bi load	(Zhang et al., 2015)

Table 2.2 Summary of photocatalysis for different oily wastewater

Ground water contaminated by gasoline and diesel	TiO_2+SiO_2 sol dip-coated on ceramic beads.	irradiated by sunlight (1.6 mW/cm^2 measured at 365 nm) with H_2O_2	TPHs, BTEX，TOC	>70% degradation of BETX and TPH	(Cho et al., 2006)
Oil sands process-affected water	Degussa P25	nature sunlight 25J/m^2	acid extractable organics TOC	>90% removal over 14 days; 45% TOC removal	(Leshuk et al., 2016a)
Oil slick on water	Degussa P25 on floating substrate	420W cm^{-2} at 330~430nm+O_2	toluene 1-decene	100% degradation in 45 min; 30% removal in 2 h	(Berry and Mueller, 1994)
Oil sludge	Degussa P25	373 μW cm^{-2} at the wavelength range from 290 to 390 nm and 10.4 μW cm^{-2} at 254 nm with H_2O_2	PAHs TOCs	PAHs removal 100% after 96 h TOC removal 80%	(da Rocha et al., 2010)
Petroleum refinery sourwater	Degussa P25	250 W UV light	DOC	DOC removal 21% within 1 h	(Coelho et al., 2006)
Produced water	Fe doped TiO_2	n/a	oil and COD	oil removal 89.1% COD removal 98.5%	(Gao et al., 2013)

Table 2.2 Summary of photocatalysis for different oily wastewater

Refinery wastewater	Nano-TiO_2 loaded on Fe-ZSM-5	8W UV lamp	COD	photocatalytic removal 61.35%, adsorption removal 4% in 3 h		(Ghasemi et al., 2016)
	Nano-TiO_2	irradiated with UV lamp with 520 mw/cm^2	COD	70% removal in 2 h		(Saien and Nejati, 2007)
	ZnO, P25 and TiO_2	irradiated with 108 w/m^2 at 254 nm+H_2O_2	phenol	phenol removal 93%		(Santos et al., 2006)
			DOC	DOC removal 56% in 1 h		
	Nano-TiO_2	irradiated with UV lamp with 520 mw/cm^2	COD	COD removal 83% in 2 h	0.007–0.013 min^{-1}	(Shahrezaei et al., 2012)
Wastewater from polymer flooding	Nano-TiO_2	125 W Hg lamp	PAM	80% removal in 1.5 h		(Wang et al., 2006)
Weathered oil and contaminated water	food grade TiO_2 and Degussa P25	irradiated by UV lamp (350–400 nm at 18 W m^{-2})	soluble organic carbon bioavailability	soluble organic carbon content increased by 60% after 24 hours bioavailability enhanced by 37%		(Brame et al., 2013)

2.5 Factors Influencing Wastewater Composition

High organic load, high salinity, and various impurities compose a complex matrix of oily wastewater, which significantly deteriorates the performance of adsorption and photocatalysis (Liu et al., 2013). The surface charge of catalyst could be modified by the complex inorganic and organic composition of oily wastewater, which can result in lowered reactivity (Pablos et al., 2012; Liu et al., 2016b). The high concentration of organic substrates can saturate the TiO_2 surface, reducing the photonic activity of the catalyst (Chong et al., 2010).

2.5.1 Salinity

The presence of inhibitory ions (Mg^{2+}, Ca^{2+}, SO_4^{2-}, CO_3^{2-} etc.) could significantly reduce the effectiveness of catalyst, especially for suspended nanoparticles, by blocking the active sites and/or inducing the agglomeration of catalyst (Armanious et al., 2011; Alizadeh Fard et al., 2013). Hsu et al. (2008) indicated that the tendency toward agglomeration (particle–particle interaction) increases at high solid concentration, resulting in a reduction of surface area available for light absorption. The adsorption competition between cationic ions and diesel on the surface of catalyst becomes obvious in relative high salinity (Zhang et al., 2015). The competing ions might occupy the active sites, thus decreasing the photocatalytic efficiency of diesel. High concentration of anions further changes the catalyst surface, alters its point of zero charge, and thus changes the electrostatic interaction with the organics (Gulyas et al., 2005). The presence of halide anions could significantly affect photocatalysis by scavenging strong radicals (e.g. hydroxyl radicals) to weak halide radicals (Liu et al., 2016b). The radicals involved in the

photocatalytic degradation process could further alter the degradation pathways of organic compounds and potentially form toxic chlorinated by-products which have been observed in photocatalysis of saline waters (Li et al., 2006; Leshuk et al., 2016a).

2.5.2 Organic Composition

The composition of oily wastewater can significantly affect the effectiveness of photocatalysis. Each organic species in oily wastewater responses differently to photocatalysis. Liu et al. (2016b) investigated the change of organic composition during photocatalysis of OPW. Their findings suggest that organic compounds with aromatic rings (PAHs and phenols) are more degradable, while alkanes are inert to photocatalysis within 24 h of reaction time. It is probably because that aromatic organics can undergo photoexcitation more readily than alkanes (King et al., 2014; Jing et al., 2014b). The overall removal rates of oily wastewater could achieve as high as more than 90% after prolonged irradiation (100 h) (D'Auria et al., 2009). Aromatic compounds still have the highest rate of degradation compared with others, and the degradation rate of alkanes follows the order of n-alkanes > branched alkanes > cyclic alkanes.

The effectiveness of photocatalysis is also affected by organic load. When the organic load is small, photon flux and activated catalytic sites are sufficient for photodegradation. In this case, an increase in organic load should increase the degradation rate (Lair et al., 2008). At high concentration, the photon flux and activated sites become insufficient for treating organics. The reaction rate remains constant or decreases. Therefore, the removal rate of organics will decrease with increasing organic loads. The increase in the organic load can further hinder the reaction rates by 1) reducing the concentration of hydroxyl

radicals through a high consumption rate; 2) screening light through the increase of photo-sensitive organics; 3) accumulating organics on the catalyst because the adsorption rate are higher than degradation rate; and 4) generating more adsorptive intermediates thus occupy the activated sites on catalyst (Lair et al., 2008; Ahmed et al., 2011; Jing et al., 2014b).

The additives of oily wastewater can enhance or hinder photocatalysis. Zhang et al. (2015) evaluated the photocatalysis of diesel solutions with different concentrations of surfactants. It was indicated that low surfactant concentration could promote the diesel degradation by increasing its solubility. However, with a surfactant concentration higher than the critical micelle concentration, negative effects such as photo-attenuation and active site blockage were observed, which decreased the photodegradation of diesel.

2.5.3 Intermediates

The goal of photocatalysis is mineralization. Nevertheless, intermediates generated from incomplete mineralization are inevitable in treating oily wastewater with high organic load. Leshuk et al. (2016a) observed that over 90% of acid extractable organics were photo-transformed after one-day irradiation, but only 45% of the TOC was removed. The results suggested that acid extractable organics were transformed to oxidized intermediates instead of being completely mineralized. Ziolli and Jardim (2003) analyzed the compositional changes of soluble oil fraction in oil-contaminated marine waters during heterogeneous photocatalysis, and 63 new peaks were found in the gas chromatograph they measured. These peaks represent the oxidized intermediates formed during irradiation. They contain oxygen atoms and lose the aromatic character. The

researchers further suggested that these compounds might be more toxic to marine organisms than the originals.

Hashimoto et al. (1984) characterized the formation of by-products during photocatalysis of different organic species. For aliphatic hydrocarbons, the common intermediates are oxidized to alcohols, aldehydes, and carboxylic acids, while phenol, catechol, hydroquinone, and muconic acid are detected in the degradation of benzene. It is worth noting that, hydroquinone and benzoquinone are considered as a scavenger for oxidative radicals (Leshuk et al., 2016a). So further photocatalytic oxidation is dramatically inhibited in the presence of these species. Zulfakar et al. (2011) observed the formation of intermediates also significantly affects the rate of reaction by competing the active sites. Fouling of the catalyst surface can also occur through the polymerization of PAHs during photocatalytic process (King et al., 2014).

2.6 Configurable Factors of Photocatalytic Process

To remediate oily wastewater by photocatalysis, the optimization of configurable factors, such as light source, catalyst concentration, surface area, temperature, pH and oxidant concentration (O_2, H_2O_2 etc.) is important.

2.6.1 Light Sources

The light intensity among the studies varies from milliwatts per square centimeter (King et al., 2014) to microwatts per square centimeter (da Rocha et al., 2010) with the energy consumption of 4-1,500W (Minero et al., 1997; Liu et al., 2016a). Light intensity and wavelength directly affect the reaction rate. da Rocha et al. (2010) applied two lights of

the same wattage but different light intensity and wavelengths in treating oil sludge. The black light mercury lamp emitted 98 lux and 373 μW cm^{-2} at the wavelength range from 290 to 390 nm and 10.4 μW cm^{-2} at 254 nm, while the white light was 1900 lux and 74 μW cm^{-2} at wavelength range from 290 to 390 nm and 11.2 μW cm^{-2} at 254 nm. The results showed that white light with higher light intensity led to a higher TOC removal rate. Furthermore, compared with another study (King et al., 2014), the complete degradation of PAHs under 76.5 mW cm^{-2} was significantly accelerated, from four days to several hours, indicating that the higher light intensity resulted in a higher degradation rate increases with increasing light intensity applied.

Han et al. (2004) used two UV lamps (185 nm and 254 nm) in combination with TiO_2 to induce decomposition of *p*-chlorobenzoic acid. Their studies showed that the rate constants of TiO_2 at 185 nm were 3.0–6.5 times faster than those in TiO_2 at 254 nm. Photocatalysis with natural sunlight has attracted many researchers because sunlight as a form of free energy is sustainable and abundant. Berry (1994) evaluated the photocatalytic degradation of toluene and 1-decene under the irradiation of two different light sources, a UV lamp and sunlight. The results showed that the degradation rate of toluene under with UV/TiO_2/O_2 is slightly higher than that with sunlight/TiO_2/O_2, suggesting that the UV light of sunlight is sufficiently intense for the photolysis. Leshuk et al. (2016a) indicated a complete degradation of acid extractable organics in oil sands process-affected water could be achieved by solar photocatalysis within 1-7 days. Cho et al. (2006) found that more than 70% of BTEX and TPH in gasoline/diesel contaminated groundwater can be degraded by the solar light/TiO_2 slurry system. It should be noticed

that most of the lamps used in these studies were solar light simulators that are not energetically efficient, since only the light in the UV and near UV region (wavelength lower than 400 nm) was absorbed by the catalysts.

2.6.2 Catalysts

Karakulski et al. (1998) indicated the optimal catalytic content in the range of 0.8–1.2 g/L in treating the oil in ultrafiltration permeate. King et al. (2014) applied high dose (3% and 9%) of TiO_2 nanotubes on oil slick and found that the best dose of TiO_2 nanotube was 9%, by which a 93% enhancement in the observed degradation rate constant of very small PAHs (1-2 rings) was attained. The degradation of relative large PAHs was not sufficiently accelerated, while for some of the species even inhibited degradation was observed. They further concluded that addition of TiO_2 as catalyst could cause light attenuation, and hence inhibited the photolysis of PAHs, especially for large PAHs that are the highly photoactive. Saien and Neiati (2007) observed that photocatalytic degradation rate increased with the increase of suspended catalyst concentrations, up to about 100 mg L^{-1}. When the concentration was higher than this threshold, the turbidity of the solution increased, and the light transmission decreased. As a consequence of this effect, the photocatalytic degradation was decelerated.

Shahrezaei et al. (2012) found that a maximum reduction in COD was achieved when the catalyst concentration was 100 mg/L. It was further pointed out that the agglomeration of the catalyst in high doses could reduce the surface area for light adsorption and hence decrease the degradation rate. Santos et al. (2006) tested TiO_2 particles with different sizes as photocatalysts: TiO_2 (Brunauer-Emmett-Teller [BET] surface areas of 1.7 and

8.3 $m^2 g^{-1}$) and Degussa P25 (30 nm particle size and 50 ± 15 $m^2 g^{-1}$ BET surface area) for the photodegradation of phenols in petroleum wastewater samples. It was found that P25 in a low dose could lead to a great enhancement (5 times) in phenol removal. The results indicated that the larger surface area of the TiO_2 is, the more effective the photocatalysis becomes.

2.6.3 pH

pH value affects the surface charge of catalyst, the reduction potential of hydroxyl species, and the affinity of pollutant for the catalyst surface (Saien et al., 2010; Shahrezaei et al., 2012). pH could further enhance or hinder the efficiency of photo-degradation by affecting the electrostatic interactions between catalyst surface, organic molecules and generated radicals (Ghasemi et al., 2016). Saien and Neiati (2007) analyzed the removal of organic pollutants in PRW at different pH conditions. When the pH was lower than the pH of zero point of charge (pH_{zpc}), the positive charge of the catalyst would attract more anions and, thus increase the removal rate. Similar results were reported by Shahrezaei et al. (2012). Most of the organic matter in PRW consists of phenol and phenolic derivatives. They become negatively charged after ionization and are favoured to interact with positively charged TiO_2 surface through electrostatic attraction at relatively low pH.

Santos et al.(2006) pointed out that the optimum pH for degrading the non-polar components of the organic pollutants (e.g. alkanes) in the wastewater is pH_{zpc}, where the TiO_2 surface is neutral. Gimeno et al.(2007) investigated the adsorption of fluorene on TiO_2 at pH =2 and pH =5. High pH resulted in high adsorption and consequently high

degradation rate. Vargas and Nunez (2010) conducted photocatalytic degradation of several representative compounds at different pH value. The degradation rates of these compounds were found to decrease following the order of dibenzothiophene > naphthalene > *p*-nitrophenol at pH =3. Both naphthalene and *p*-nitrophenol showed high degradation rates under basic condition (e.g., pH =10). Generally speaking, the concentration of hydroxyl radicals a basic aqueous medium could be high; however, Zhang et al. (2015) reported that the agglomeration of catalytic particles could be accelerated in an acidic or alkaline solution, which eventually reduced the surface area of the catalyst. To achieve better efficiency, pH should be kept in the neutral range, which facilitates efficient particle dispersion and formation of hydroxyl radicals.

2.6.4 Temperature

The influence of temperature has been studied by many researchers. Saien and Neiati (2007) observed a positive influence of temperature on the photocatalysis of PRW. They further concluded that the photocatalytic degradation can be by increasing temperature because of enhanced electron transfer on TiO_2. Gahsemi et al. (2016) evaluated the correlation between catalyst dose and temperature. The outcome indicated that the efficiency of catalysis increased as temperature increased when the optimal dose of catalyst was used. Leshuk et al. (2016b) report that the effect of temperature on degrading the naphthenic acids in oil sands process-affected water. They rationalized that increasing temperature might enhance the aggregation of catalysts thus mitigate the overall reaction rate.

2.6.5 Oxidant

Oxidants play a vital role in the photocatalytic degradation, as they can combine with the free electrons on the catalyst surface to generate the hydroxyl radicals, which in turn dramatically accelerate the reaction rate. O_2 and H_2O_2 are often chosen as oxidants to enhance the photocatalysis (Li et al., 2006; Corrêa et al., 2009). Berry and Mueller (1994) reported that aeration of the photocatalytic system with O_2, resulted in significantly accelerated degradation of toluene, whereas the degradation of 1-decene in such system was only slightly increased. Cazoir (2012) proposed two important roles that oxygen plays in photocatalysis: 1) it prevents the electron–hole recombination by scavenging the photogenerated electron, and 2) it reacts with other species (O_2, OH^-) to produce reactive oxygen species such as $O_2^{\cdot-}$, $HO_2\cdot$ which improve the oxidation efficiency.

The addition of H_2O_2 increases the degradation in two ways (Li et al., 2006): 1) it reacts directly with organics and readily decomposes into OH radicals, and 2) it acts as a more active electron acceptor than O_2. Pernyeszi and Dekany (2003) applied H_2O_2 in photocatalytic oxidation of a crude oil emulsion. The results showed that the TOC removal rate was increased from 20% to 50%. Cho et al. (2006) reported that the presence of 10 mM H_2O_2 significantly increased the degradation efficiency in both the slurry and immobilized systems. With optimal dose (4~10 mM), the COD removal from oilfield produced wastewater was enhanced by 3.5 times (Li et al., 2006). Santo et al. (2006), by contrast, observed no significant changes after adding H_2O_2 to a continuous-aeration system, which suggests that air bubbling has already provide sufficient oxidant.

Therefore, it is necessary to have the dose of oxidant optimized according to specific different types of oily wastewater.

2.7 Enhancement of Photocatalytic Oxidation by Nanocatalyst

Photocatalysis shows great potential in treating oily wastewater. However, the application of this technology is hindered by the low reaction rates for some organic species, insufficient mass and photon contact rates for catalysts under high organic loads and sophisticated recovery of catalysts. Currently, research efforts have been focused on the modifications of catalyst to widen the range of light absorbance, increase photon-electron conversion rate, and improve the applicability of catalysts.

2.7.1 Doping of Nano-scaled TiO_2

Since the band gaps of TiO_2 are more than 3.0 eV, only UV light can be effectively absorbed by it, which means most of solar energy is of no use when the photocatalysis is operated with sunlight and TiO_2. To extend the applications of TiO_2 more widely, doping the TiO_2 surface with other materials has been studied (Zaleska, 2008; Gupta and Tripathi, 2011; Ni et al., 2016). Doped TiO_2 introduces intraband-gap states, which lead to decreased band gap and allow TiO_2 to be readily excited by lower-energy photons (Figure 2.2).

Transition metal ions provide additional energy levels within the band gap of a semiconductor; in other words, electrons can transfer from one of these levels to CB upon excitation by low energy photons (Zhang et al., 2015). Noble metals can capture the electrons from TiO_2, creating holes on TiO_2. This reduces the tendency towards

electron/hole recombination and hence increases the efficiency of photo-induction (Gupta and Tripathi, 2011). Nonmetallic elements, such as carbon, sulfur, halides, phosphorus and boron seem to have more significant advantages: as they are unlikely to form recombination centers but improve photocatalytic activity by reducing the band gap (Ni et al., 2007; Hsu et al., 2008). Zhang et al. (2015) prepared Bi and N doped nano-TiO_2 and examined its photocatalytic efficiency under a visible light source. $Bi_{1.0}$–N–TiO_2/expended graphite carbon composite (EGC) showed excellent performance in mineralizing diesels, which extended the applicability of doped TiO_2 under solar light. It further pointed out that the presence of low concentration of Bi on TiO_2 intensifies the absorption of visible light and reduces the electron-hole recombination rate, while high concentration of Bi resulted in the reduction of photon excitation.

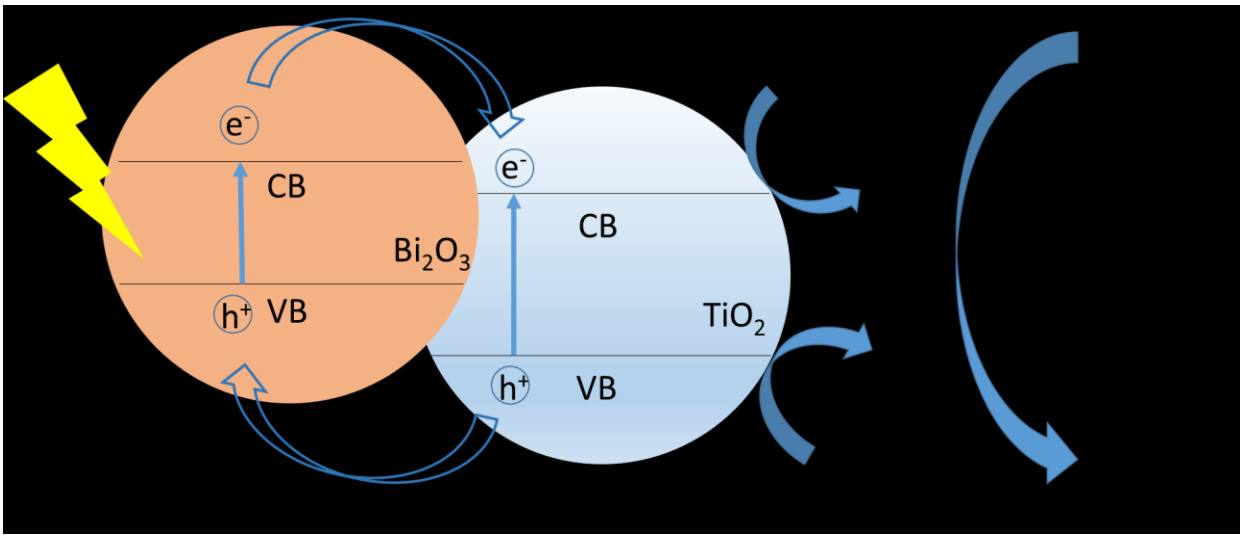

Figure 2.2 Mechanism of extended light absorption by TiO_2

2.7.2 Immobilization of Nano-scaled TiO_2

The industrial application of TiO_2 in treating of wastewater is still limited owing to the inconvenient catalyst-recovering step of suspended TiO_2 from the treated water at the end of operation. Membrane filtration, microfiltration and ultrafiltration may be able to collect fine particles, but they show drawbacks such as high transmembrane pressure, high fouling potential and great flux declination (Liu et al., 2016a). Therefore, to increase the efficiency and longevity of nano-scaled TiO_2 and circumvent the inconvenient catalyst-recovering step after treatment, methods based on immobilization of nano-scaled TiO_2 have been studied. It has been shown that immobilized TiO_2 is advantageous in terms of catalyst recovery and ease of handling, but the surface area of immobilized TiO_2 is much lower than that of suspended TiO_2, and the mass transfer rate of it is limited (Mascolo et al., 2007). Nano-scaled TiO_2 prepared in different structures (nanofiber, nanowire, nanorod etc.) can gain increased size without compromising the reduction in surface area. Another solution to increasing the surface area of catalyst is to coat TiO_2 on different substrates with relatively large surface areas such as quartz sand (Zulfakar et al., 2011), microbead (Cho et al., 2006), glass fiber (Erjavec et al., 2016), membrane (Athanasekou et al., 2015), carbon nanotube (Li et al., 2011) and absorbent (Wu et al., 2009; D'Auria et al., 2009).

Liu et al. (2016a) compared the photodegradation of PAHs in OPW by TiO_2 powder and immobilized TiO_2. The effectiveness of immobilized TiO_2 in photocatalysis was found to be slightly higher than that of TiO_2 powder, indicating that the immobilization approach is more resistant to the water matrix. Cho et al.(2006) demonstrated that the addition of

H_2O_2 could enhance the efficiency of immobilized TiO_2 and narrow its difference to that of TiO_2 slurry. Wang et al. (2006) applied the mixture of TiO_2 and surfactant in treating oily wastewater to trap the TiO_2 particles at the interface. Heller et al. (1993) attached TiO_2 to ceramic microbeads to maintained at the air-oil interface. These microbeads with catalysts can be deployed into environment, particularly in the arctic area, for long-term catalytic photolysis of spilled oil.

2.7.3 Modification of Adsorbent Surface with Nano-scaled TiO_2

The combination of photocatalyst and adsorbent has been studied in treating oily wastewater to enhance the effectiveness (Yue et al., 2009). Composite TiO_2 on the surface of an adsorbent has the combined advantages as follows: 1) large surface area adsorbent works as the support for nano-sized TiO_2 and concentrates the pollutants and intermediates around the TiO_2; 2) nano-sized TiO_2 facilitates the decomposition of pollutants and then refresh the surface of adsorbent in-situ; and 3) a TiO_2/adsorbent composite can capture photo-decomposed intermediates, preventing possible secondary pollution (Torimoto et al., 1996).

Ghasemi et al.(2016) coated TiO_2 onto Fe-ZSM-5 and applied the system to the treatment of refinery wastewater. The coating of TiO_2 resulted in the reduction of specific surface area, but the photocatalytic activity of the system was much higher than the catalytic systems based on simple mix of zeolite and Degussa P25. The addition of adsorbent could have a negative effect. D'Auria (2009) observed that the composite of TiO_2/zeolite could reduce the overall degradation rate of the organic species in crude oil due to light scattering. Zhang et al. (2015) used expanded graphite as an adsorbent to take advantage

of its extraordinary oil adsorption rate. It was found that after combination with catalyst, the specific surface area was enlarged. The adsorbent not only shortened the distance between organic species and photocatalytic sites but also plays a role as floating substrate to keep the catalyst between the air-liquid interface. The absorbent with a similar function, has also been used to treat diesel (Ni et al., 2016). The catalyst along with graphene significantly enhanced the adsorption effect to 96 g of diesel per gram catalyst. It should be noted, however, that the overwhelming effect of adsorption could inhibit the photocatalytic process because of the mass transfer reduction inside the adsorbent. Therefore, the balance between photocatalysis and adsorption should be carefully evaluated.

2.7.4 System Design

The effectiveness of photocatalysis depends critically on both the mass and photon contact rates of the catalyst. To optimize the photocatalytic effectiveness, various processes have been proposed aiming at increasing the contact efficacy and contact time. An annular photoreactor can shorten photon travel path (Lin and Valsaraj, 2003). Equipped with a tangential inlet and an outlet tube, the annular reactor increases the mixing rate within the system (Peres et al., 2015). Laoufi et al. (2008) used a helical photoreactor to maximize the irradiation time. Yu et al. (2016) coated TiO_2 on a helical support and applied it in an annular reactor to increase the contact time of pollutants and photon with the TiO_2 layer. A fixed-bed system with immobilized catalysts has shown advantages in terms of having no need of downstream separation processing and allowing the continuous flow treatment (McCullagh et al., 2011).

Combination with other technologies can also increase the applicability of photocatalysis. Karakulski et al. (1998) first filtered the bilge water using ultrafiltration. The filtration process removed 96~98% of oil which is more that 350 mg/L. The complete decomposition of oil in UF permeate was achieved after 2 h of UV illumination using a K-TiO_2 photocatalyst. Photocatalysis has the ability to treat organics with high toxicity and low biodegradability. Residual organic carbons were found to be significantly more biodegradable than the initial acid-extractable organics (Leshuk et al., 2016a). Therefore, photocatalysis followed by bioremediation could significantly reduce the overall intention time (Yeber et al., 2012). The combination of photocatalysis with ozone is could induce effective and prompt degradation of organics such as phenols in a short period (5 minutes) (Corrêa et al., 2009). It further increased the biodegradability of treated water from 13% to 40%.

2.7.5 Regeneration

The lifetime of a photocatalyst is an important parameter for evaluating its feasibility in real applications. Deactivation of a catalyst during photocatalytic degradation can significantly increase the operational cost as a result of the frequent replacement of catalyst that are needed. Leshuk (2016a) observed that reused catalyst loses some activity after five treatment cycles (apparent rate constant was lowered by about ~20%). The process of centrifugation and resuspension increases the aggregation of the catalyst particles thus reduces their specific surface area. They suggested that the deactivation of photocatalyst could be mitigated by better dispersion or particle-washing techniques. Ghasemi et al. (2016) reused the TiO_2/Fe-ZSM-5 nanocomposite three times.

A slightly decreasing trend of COD removal rate was observed, because of the blockage of the active sites of the catalyst by the accumulated organic substrate and intermediates.

To re-activate the catalyst, several approaches can be adopted. The organic fouling on the catalyst can be removed by calcination, which burns out the organics and keeps the catalyst stable and reusable (Ghasemi et al., 2016). The drawback of this technology is that it consumes additional energy. Zhu and Zou (2009) applied different technologies (e.g. UV, UV+H_2O_2 and UV/ultrasound) to re-activate the used photocatalysts and they found out that the combination of ultrasonic and UV requires has the shortest process time. They further showed that ultrasound could 1) generate hydroxyl radicals that oxidize the fouling organic on the catalyst surface; 2) produce ultrasonic waves to break the aggregation of catalyst particles into smaller size and mechanically clean their surface.

2.8 Summary

The review in this chapter summarizes various kinds of photocatalytic applications in oily wastewater treatment. Nano-TiO_2 induced photocatalysis has been demonstrated to be a promising technology in treating petroleum hydrocarbons because of its high mineral rate, low selectivity and low toxicity. However, the low efficiency and mineralization rate caused by the complex matrix of oily wastewater, high energy consumption, and sophisticated post-treatment could hinder the applicability of the technology.

Greater effectiveness with lower cost is the major goal of technology adaption. The main approaches to achieve this goal include system configuration and catalyst modification.

The use of solar light with doped TiO_2 can replace the more energy-consuming UV light source. LED (light-emitting diode) light can also be an option due to its high electro-photon conversion rate. Immobilization of TiO_2 on larger and porous structure with larger surface areas or on fixed surfaces allows for continuous treatment of OPW without subsequent separation. In combination with adsorptive substrates, the concentrate-and-treat approach allows for continuous treatment of the oil fraction thus can be used to remediate oil spill. These approaches therefore are of high performance and do not compromise the degradation efficiency in a significant degree.

Chapter 3 Photocatalytic Oxidation of Polycyclic Aromatic Hydrocarbons (PAHs) in Offshore Produced Water (OPW): the Effects of Water Matrix[2]

[2] *The contents of this chapter are based and expanded on the following paper:*

Liu. B., Zhang, B.Y., Chen, B., Jing, L., Zhang, H. and Lee, K. (2016) Photocatalytic Degradation of Polycyclic Aromatic Hydrocarbons (PAHs) in Offshore Produced Water (OPW): the Effects of Water Matrix. Journal of Environmental Engineering, 142(11): 04016054, DOI: 10.1061/(ASCE)EE.1943-7870.0001135
Role: Bo Liu solely worked on this study and acted as the first author of this manuscript under Dr. Bing Chen and Dr. Baiyu Zhang's guidance. Most contents of this paper were written by him and further edited by the other co-authors.

3.1 Introduction

Although the effectiveness of photocatalysis on oily wastewater treatment has been demonstrated in the literature (Santos et al., 2006; Saien and Nejati, 2007; Saien and Shahrezaei, 2012; Pavelescu et al., 2014), most studies mainly focused on the overall performance of different photocatalytic systems. The mechanisms of photocatalytic degradation of PAHs in OPW, especially those influenced by the OPW matrix, have not been reported. Therefore, in order to fulfill the aforementioned knowledge gaps, this study was carried out to evaluate the removal effectiveness of PAHs from both OPW and distilled water by using TiO_2 induced photocatalysis. The photocatalytic degradation kinetics of PAHs in OPW was determined. The matrix effects of OPW, including inorganic divalent cations, insoluble particulate matter, and dissolved organic matter, were discussed.

3.2 Materials and Method

3.2.1 Reagents and Standards

Titanium (IV) tetra-isopropoxide (TTIP) was obtained from Sigma-Aldrich (Canada). The 16 PAHs standard solution, containing 500 μg/mL of naphthalene (NAP), acenaphthylene (ANY), acenaphthene (ANA), fluorene (FLU), phenanthrene (PHE), anthracene (ANT), fluoranthene (FLT), pyrene (PYR), benzo(a)anthracene (BaA), chrysene (CHR), benzo(b)fluoranthene (BbF), benzo(k)fluoranthene (BkF), benzo(a)pyrene (BaP), dibenzo(a,h)anthracene (DBA), benzo(g,h,i)perylene (BPY), and indeno(1,2,3-cd)pyrene (IPY) was purchased from Agilent (USA). Naphthanlene-d_8, acenaphthene-d_{10}, phenanthrene-d_{10} and benzo(a)anthracene-d_{12} were purchased from

Cambridge Isotopes Labs (USA) and C/D/N Isotopes Inc. (Canada) as surrogates. Acetone (Honeywell Burdick and Jackson®, USA) and dichloromethane (Honeywell Burdick and Jackson®, USA) was used for preparing stock solutions and aqueous sample extraction, respectively. The commercial products were used as received without any further purification. Distilled water was produced on-site from a double fused-silica distillation unit. OPW samples were obtained from an offshore platform in the North Atlantic. Detailed location information is not provided here due to client confidentiality and non-disclosure. Laboratory tests on the OPW samples were performed using Inductively Coupled Plasma Mass Spectrometry (ICP-MS, PerkinElmer ELAN® DRCII) and the key parameters were measured by using pH meter (EL20, Mettler Toledo®), spectrophotometer (Genesys® 10S UV-Vis Spectrophotometer, USA) and turbidity meter (VWR Scientific®, USA) (Table 3.1).

The concentration of total PAHs, including their alkyl homologues, was measured as 60 μg/L. The concentrations of each individual PAH were also measured. Among them, naphthalene had the highest concentration around 9 μg/L. The concentrations of the other 15 PAHs presenting in the OPW samples were far less than that of naphthalene. The high concentrations of sodium, potassium, calcium and magnesium cations indicated a high salinity level. The pH was measured as 6.81, which was close to neutral. The turbidity was 17.59 NTU, indicating the presence of a large amount of insoluble particulate matters. The color of the OPW samples was light yellow. The absorbance of OPW in 254 nm (UV-C) was 0.220 A/cm in average.

Table 3.1 Background information of the OPW sample

Parameters	Concentration (mg/L)
Total alkane	2.16
Total PAHs	0.06
Sodium	16400
Potassium	240
Magnesium	417
Calcium	1100
Sulfur	730
pH	6.81
Turbidity	17.59 NTU
Absorbance in 254 nm wavelength	0.220 A/cm
Chemical Oxygen Demand (COD)	1247

3.2.2 TiO_2 Nanocatalyst Preparation

The synthesis of nano-scale TiO_2 catalyst was carried out by modifying the sol-gel method proposed by Li et al. (2006). Titanium tetraiso-propoxide was added dropwise into a vigorously stirred acetic acid solution. White slurry gradually formed during the reaction and was subsequently dissolved after further stirring for 3 hours. After aging for 3 days at room temperature (i.e., 20-25 ºC), the sol was transformed into gel. The gel was dried at 100 °C and then calcinated at 450 °C for 4 hours to obtain nano-scale TiO_2. A Rigaku Ultima IV X-ray diffractometer (XRD) with a copper x-ray source was used to determine the crystal phase of the synthesized nanocatalyst. The scan range was from 20° to 80° and the scan rate was 1°/min. The scanning electron microscope (SEM) images of nano-TiO_2 were acquired from FEI MLA 650F, which was set at 30 kV.

3.2.3 Photoreactor and Light Source

A 1.2 L cylindrical glass jar with a diameter of 10 cm was used as the photoreactor (Figure 3.1). A sampling valve was attached to the bottom of the jar. A total height of 500 mL water samples in the jar was measured as 6.3 cm. The jar was covered by a quartz cap and sealed with a PTFE o-ring to prevent the evaporation of PAHs. A high-pressure mercury lamp (UVLMS-38 EL series 3UV lamp, UVP®, USA) was used as irradiation source. The lamp was placed on top of the quartz cap and the UV-C lamp with a peak at 254 nm (3.7~3.8 mw/cm^2) was used. The emission peak has a full width half maximum (FWHM) of 15 nm.

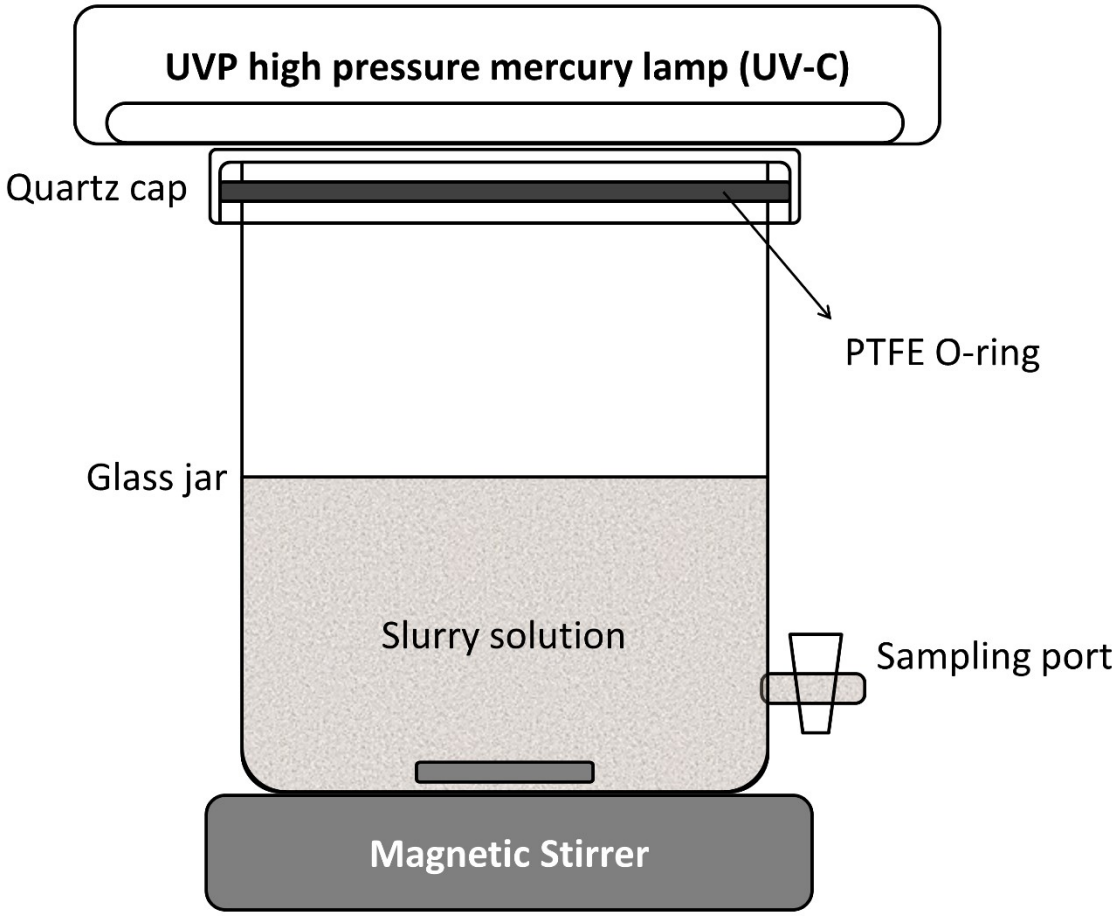

Figure 3.1 Scheme of the photocatalytic reactor

3.2.4 Irradiation Experiments

The detailed experimental design is shown in Table 3.2. The total number of runs was 6 including 4 runs under irradiation and 2 control runs. The control experiments were conducted in the presence of TiO_2 without irradiation to evaluate the adsorption of PAHs on the catalysts.

For each run, the stock solution was prepared by spiking 20 μL 16 PAHs standard solution (500 μg/mL) into 10 mL acetone. The concentration of each PAH in the stock solution was 10 μg/mL. Five hundred milliliter distilled water or OPW samples were spiked with 100 μL 16 PAHs stock solution and then transferred to the photoreactor. It should be noted that for distilled water samples, 5 mL acetone was added to increase the solubility of PAHs. After adding 0.05 g synthesized nanocatalyst, the mixture was vigorously stirred for 30 min prior to UV irradiation in order to reach the thermal and volatilization equilibria. The UV lamp was allowed to warm-up for 20 min before tests. The irradiation periods were set as 3 and 24 hours for distilled water and OPW samples, respectively. The aqueous suspension was kept homogeneous using a magnetic stirrer. A 20 mL water sample was collected periodically using a peristaltic pump and transferred into a 20 mL amber vial.

Table 3.2 Experimental design of photocatalytic degradation

Order of Run	Distilled water	OPW	UV irradiation	Synthesized TiO_2
1	+	-	+	-
2	-	+	+	-
3	+	-	+	+
4	-	+	+	+
5	+	-	-	+
6	-	+	-	+
7	synthesized brine sample		+	+
8	filtered OPW sample		+	+

Note: "+" refers to presence and "-" refers to absence.

3.2.5 Analytical Methods

Ten milliliter water sample was spiked with 20 µL surrogate solution (contains 5 µg/mL naphthanlene-d_8 and 0.5 µg/mL acenaphthene-d_{10}, phenanthrene-d_{10} and benzo(a)anthracene-d_{12}) and transferred from an amber vial into a 15 mL glass-centrifuge tube. Dichloromethane (1 mL) was then added into the water sample for extraction. The mixture was shaken at 1,000 rpm for 15 min at room temperature and then centrifuged at 1,500 rpm for 10 min to achieve phase separation. The organic phase was filtered through a 0.2 µm syringe filter (Whatman® Spartan® RC, Canada) to remove residual catalyst particles and transferred into a 150 µL micro-vial. Instrumental analysis was performed using an Agilent 7890A/5975C gas chromatograph – mass spectrometer (GC-MS) equipped with an Agilent 7693 autosampler. The analytes were separated by a 30 m × 0.25 mm id × 0.25 µm DB-5MS UI fused silica capillary columns. The injected mode was splitless at 300 °C. The temperature program used for GC-MS analysis was set as: initial temperature holds at 65 °C for 1 minute; temperature ramp from 65 to 300 °C at 4 °C/min; temperature hold at 300 °C for 1 minute. The PAH analyses were performed in the selected ion monitoring (SIM) mode using an electron energy of 70 eV. The ion-source was set at 350 °C. Recovery of filtration was conducted. The average recovery of standard working solution was 99%. The average recovery of standard working solution with dispersive TiO_2 was 112%. The method was verified by analyzing quadruplicate produced water samples. The average coefficient of variation of samples was 5.12%.

3.3 Results and Discussion

3.3.1 Characterization of the Synthesized TiO_2 Nanocatalyst

The XRD spectra of the synthesized TiO_2 nanocatalyst are depicted in Figure 3.2, where the typical spectrum of anatase shows a strong peak at 25.3°. No peak for rutile or brookite in the spectra indicated that a highly pure anatase was synthesized. The average crystallite size was calculated as around 13.5 nm by the Scherrer formula. The BET specific surface area of the synthesized catalyst was 110 m^2/g. Based on the relationship between the BET specific surface area and the average size of TiO_2 powder (Li et al., 2004), the particle size of the catalyst was estimated to be within the range of 12-17 nm. This range was also in a reasonable agreement with the result of transmission electron microscopic (TEM) analysis of the TiO_2 nanocatalyst reported by Li et al. (2006), where nano-TiO_2 was synthesized by the similar method. The surface morphology of the synthesized TiO_2 nanocatalyst was characterized by SEM. The agglomeration of the synthesized TiO_2 nanocatalyst was confirmed by examining the compact stack of particles that resulted in dense and non-uniform particle aggregates. The agglomeration could be attributed to the hydrolytic step of the precursor in the sol (Gupta et al., 2008). As the hydrolysis continued, the TiO_2 particles agglomerated and the dispersion stability of nano-sol was therefore reduced.

3.3.2 Photocatalytic Performance

Typically, the photocatalytic process can be characterized by the Langmuir-Hinshelwood model, which has been widely used to describe solid-liquid reactions (Lazar et al., 2012).

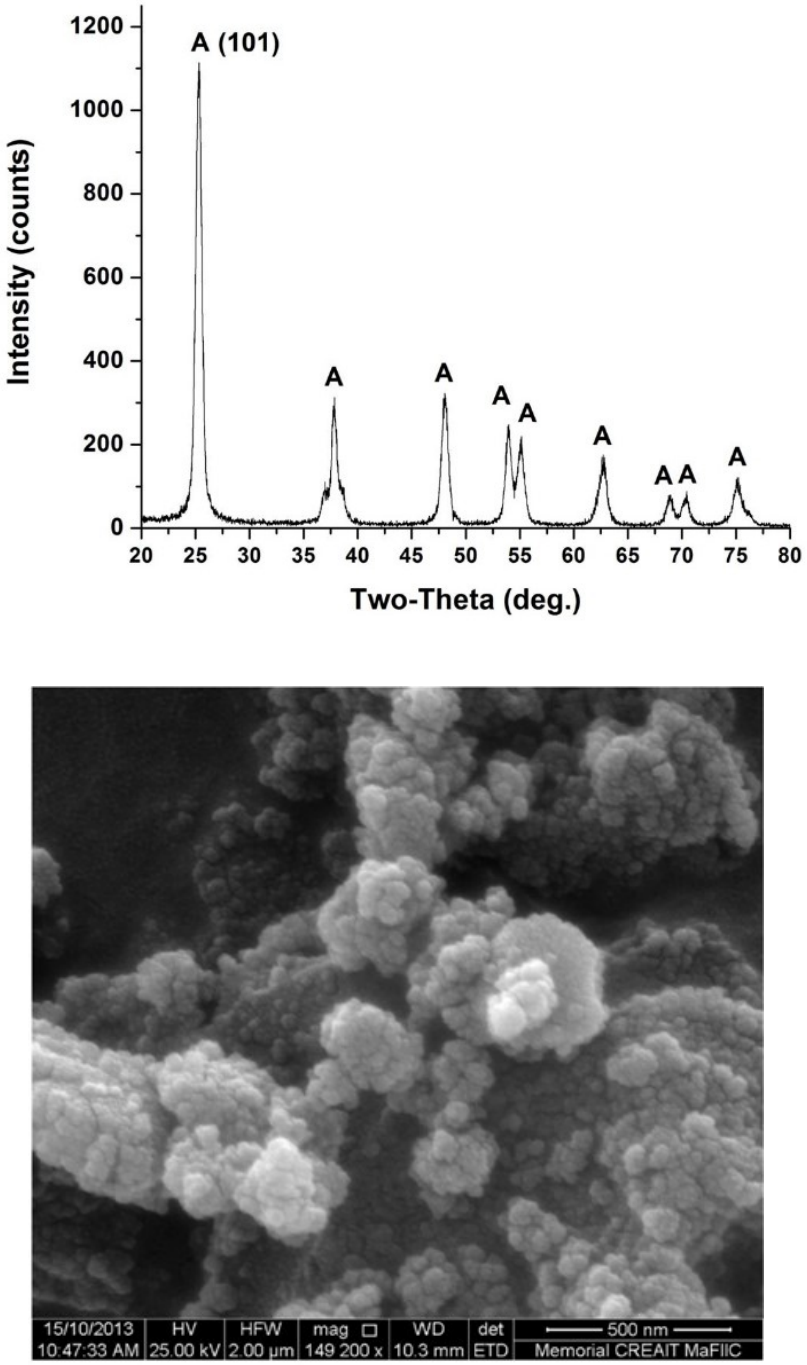

Figure 3.2 Characterization of synthesized TiO_2: XRD Spectrum (top) and SEM image (bottom)

However, when the concentration of analyte is low, the degradation performance follows the apparent-first-order kinetics (Xu et al., 2013).

$$Rate = \frac{c_t}{c_0} = e^{-kt} \quad (3.1)$$

where t is reaction time; k is the first-order reaction rate constant; c_t is the determined concentration of a reactant at time t; and c_0 is the initial concentration of the reactant.

In this study, the degradation of PAHs was modeled by the apparent-first-order kinetics. The values of k and coefficient of determination (R^2) of PAH degradation in distilled water and OPW are shown in Table 3.3.

In Run 1, the k values were between 0.0005 and 0.019 min^{-1}, with NAP and ANT having the lowest and highest k, respectively. The results agreed well with what Bertilsson and Widenfalk reported (2002), which showed that NAP was more persistent to photolytic treatment. In Run 3, the degradation efficiencies were significantly enhanced as compared to those in Run 1. All of the PAHs could be fully decomposed within 3 hours and the k values were all increased by 10~100 times. ANY, ANA, ANT and PYR were completely removed within 10 minutes. In addition, pH in both runs was reduced to around 4.5, suggesting that acids were generated.

Table 3.3 The apparent reaction rate constant k (min^{-1}) and regression R^2 in photocatalytic experiments

PAHs	Run 1		Run 2		Run 3		Run 4	
	k	R^2	*k*	R^2	*k*	R^2	*k*	R^2
NAP	0.0005	0.52	4.73×10^{-4}	0.96	0.08	0.97	6.99×10^{-4}	0.98
ANY	0.0045	0.99	0.0019	0.92	*		0.00235	0.93
ANA	0.0040	0.99	3.57×10^{-4}	0.97	*		6.85×10^{-4}	0.99
FLU	0.0047	0.99	7.39×10^{-4}	0.95	0.007	0.96	0.0013	0.99
PHE	0.0093	0.99	5.05×10^{-4}	0.88	0.14	0.99	0.0012	0.90
ANT	0.0190	0.99	0.0021	0.99	*		0.0042	0.99
FLT	0.0013	0.99	**		0.17	0.99	4.08×10^{-4}	0.48
PYR	0.0067	0.99	**		*		4.98×10^{-4}	0.70
BaA	0.0150	0.99	2.19×10^{-4}	0.87	0.24	0.99	6.07×10^{-4}	0.74
CHR	0.0043	0.97	**		0.17	0.94	4.38×10^{-4}	0.53
BbF	0.0032	0.99	**		0.02	0.98	1.67×10^{-4}	0.57
BkF	0.0036	0.98	2.82×10^{-4}	0.87	0.09	0.76	1.54×10^{-4}	0.29
BaP	0.0081	0.98	1.91×10^{-4}	0.93	0.18	0.96	3.33×10^{-4}	0.90
DBA	0.0033	0.97	**		***		3.22×10^{-4}	0.40
BPY	8.81×10^{-4}	0.97	**		***		4.03×10^{-4}	0.63
IPY	0.0014	0.98	2.46×10^{-4}	0.92	***		2.87×10^{-4}	0.22

Note: * 100% removal within 10 min;** less than 10% removal; *** not detected

Contrastingly, the values of k were significantly reduced in Run 2, which indicated that the photolysis was dramatically inhibited due to matrix effects. FLU and BaP were selected to represent low and high molecular weight PAHs, respectively. In the distilled water system, the k of FLU was 0.007 min^{-1}. It dropped to 0.0013 min^{-1} in the OPW system. However, for BaP, the constant declined from 0.18 to 3.33×10^{-4} min^{-1}, which was 541 times less. Some photo-resistant PAHs, such as FLT and BPY did not degrade in OPW.

Compared with the photolysis processes, similar results could be found in the photocatalytic processes. In Run 4, photocatalytic degradation was favored by those PAHs with low molecular weights. PAHs containing less than 4 aromatic rings had k values higher than 0.0005 min^{-1}, indicating that over 50% of them can be destructed within 24 hours. However, R^2 decreased significantly in Run 4, indicating that the OPW matrix may strongly interfere with the photooxidation of PAHs, particularly those with high molecular weights.

Another interesting finding is the observation of inconsistent trends of PAH degradation during the experiments. The irradiation processes of three representative PAHs were selected and shown in Figure 3.3. NAP, FTL and BaP represented the PAHs with low, moderate, and high molecular weights, respectively. In Run 3 (Figure 3.3), the inconsistent trends of FTL and BaP were found after 40 min, which could be caused by the inherent measurement noise at low concentration levels or the adsorption/desorption of PAHs on the catalyst surface (Hidaka et al., 2003). The same trend was found in Run 4 (Figure 3.3) where BaP had a prominent bounce at 180 min. These measurement noises

could influence the fitness of the experimental data to the kinetic model, especially when the degradation of PAHs was not significant.

3.3.3 Inorganic Ions

The dispersion of the synthesized TiO_2 nanocatalyst was measured by the change of turbidity after adding them into distilled water and OPW samples. The decrease of turbidity was observed in Run 4 (45 NTU) as compared to Run 3 (65 NTU), with flocculated catalyst settling at the bottom of the glass jar. This was indicated that the dispersion of catalyst was to some extent suppressed by the matrix of OPW. As shown in Table 3.1, the high abundance of alkaline-earth cations (Ca^{2+} and Mg^{2+}) could compress the electro static barrier of TiO_2 and promote the agglomeration of TiO_2 (Armanious et al., 2011). However, the effect of cations was not reflected in the photocatalytic degradation of PAHs in the brine sample (Figure 3.3 a, c). Interestingly, the removal rates of PAHs with lower molecular weights were accelerated.

Although it has been proved that a high concentration of chloride ion might scavenge strong radicals such as hydroxyl radical and generate weak Cl radicals (Li et al., 2006), the presence of Cl^- actually increased the degradation rate of PAHs. One reason to account for this is that brine samples with high salinity had high ionic strength which reduced the solubility of PAHs. Such a solubility decreases then accelerated the removal rate of dissolved PAHs in the aqueous phase (Katz et al., 2015). However, after the initial sharp decrease, the concentration of PAHs especially those with higher molecular weights became “stable” (Figure 3.3 b) because the PAHs salted out by high salinity were then dissolved into the system. The effect of sulfate was not observed due to a lower

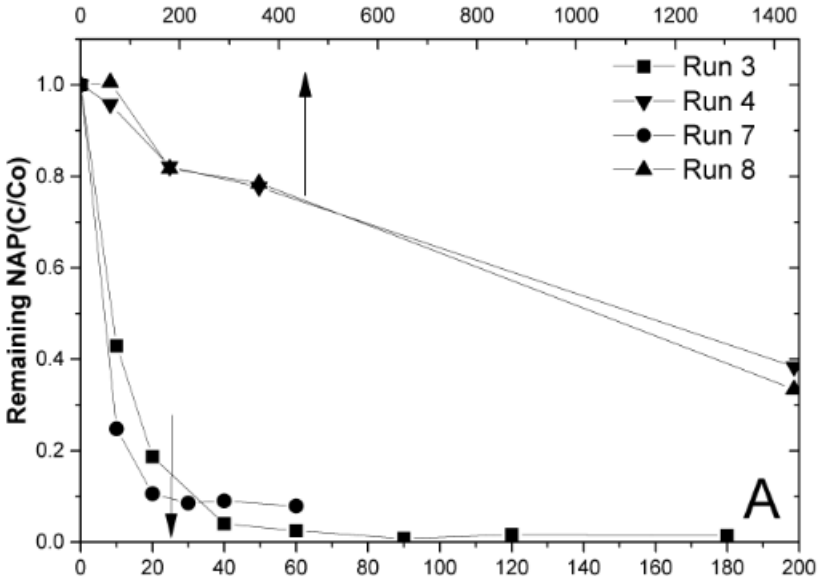
Run 3
Run 4
Run 7
Run 8
Remaining NAP(C/Co)
A

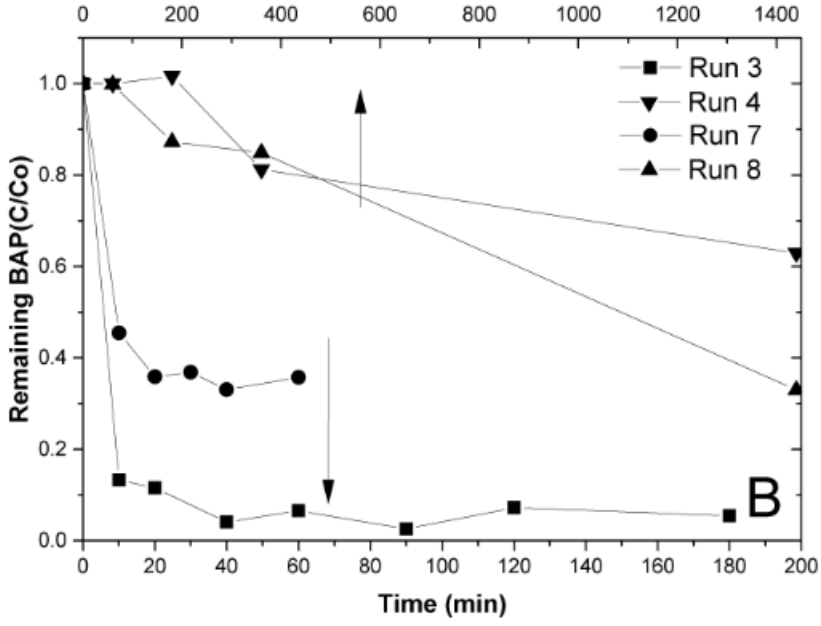
Run 3
Run 4
Run 7
Run 8
Remaining BAP(C/Co)
B
Time (min)

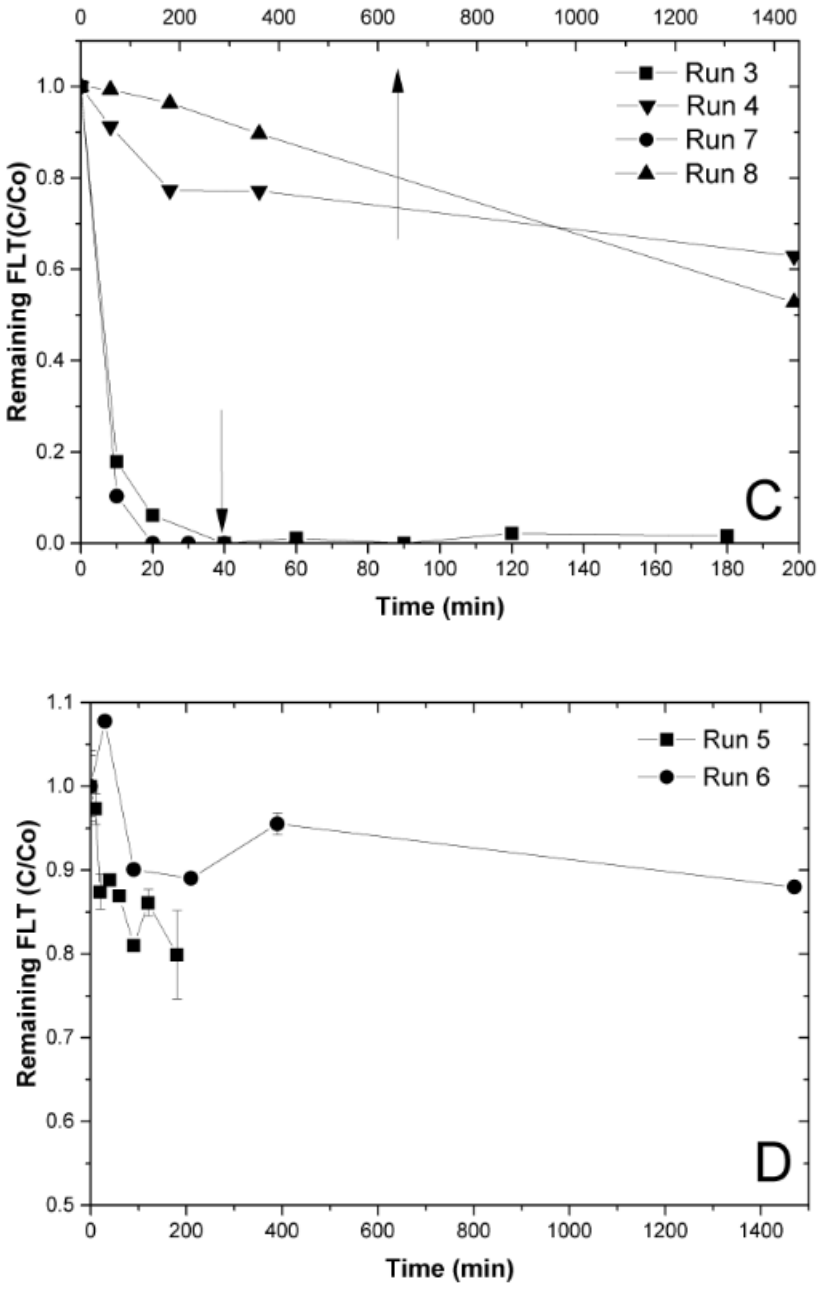

Figure 3.3 Comparison of photocatalytic degradation trends of NAP (a), FLT (b), and BAP (c) and the adsorption curve of FLT (d)in different media

concentration as compared to the threshold suggested by Wiszniowski et al. (2003).

3.3.4 Light Attenuation and Turbidity

The spectrophotometric test indicated that the average absorbance of OPW under the wavelength of 254 nm was 0.220 A/cm which means around 40% of the photons were attenuated in the system. Light intensity is a critical parameter to photolysis and photocatalysis because it is the dominating source for the excitation of the oxidative species (e.g., $OH\cdot$) and the mobile electrons on the TiO_2 surface (i.e., e^- and h^+) (Chong et al., 2010; Jing et al., 2014b). Therefore, the photo-oxidation of PAHs was significantly suppressed by the light attenuation of the matrix. The turbidity of the OPW samples was determined as 17.6 NTU, indicating a considerably large amount of insoluble particles. PAHs with high molecular weights are more likely to attach to particulate matter thus are less susceptible for remediation (Ukiwe et al., 2013). This argument was supported by the decrease ratios ($k_{run\ 1}/k_{run\ 2}$) of the corresponding PAHs (Table 3.3). The ratio for NAP was not affected by the OPW matrix, but for PAHs with high molecular weights such as ANT, BaA and BaP, the ratios were reduced from 0.1 to 0.01. Therefore, the competition between insoluble particulate matter on adsorbing PAHs could dramatically compromise the degradation of PAHs.

The degradation of PAHs of filtered OPW sample was then evaluated. The filtered residue in OPW samples was 14.4 mg/L and the chemical oxygen demand (COD) was 16.7 mg/L. After filtration, the color of OPW changed from yellowish to colorless and the light attenuation was reduced from 0.22 A/cm to 0.14 A/cm. In other words, 1/3 of light attenuation was caused by insoluble particulate matter. In addition, 67% of BaP was

degraded in filtrated sample after irradiating for 24 hours as compared with 37% of that in Run 4. On the contrary, the breakdown of NAP was not different. It suggested that inorganic matter influenced the degradation of PAHs with higher molecular weights but had less effect on the overall breakdown of PAHs.

3.3.5 Organic Compounds

Compared Run 2 with Run 4, the results showed an insignificant difference caused by applying catalyst. Further, the removal of insoluble particulate matter only enhanced the degradation of PAHs with higher molecular weights. Therefore, organic composition more likely played a key role in inhibiting the breakdown of PAHs. The major organic composition in OPW include aromatic compounds such as phenols, PAHs and their alkyl congeners and organic acids which contributed to a 0.14 A/cm of 254nm wavelength UV attenuation. It was suggested that aromatic compounds in OPW were the main species absorbing UV photons due to their abundance and UV sensitivity. In addition, the aromatic species behave similarly during the photocatalytic process: photo-adsorption on the active surface sites and similar degradation trends (Marci et al., 1995). In this case, the competition between the species and targeted PAHs could be determined by the concentration of aromatic substrate. Therefore, a high concentration of aromatic substrate could decrease the overall degradation rates including PAHs. Organic acids, on the other hand, would strongly foul the TiO_2 surface especially in acidic conditions (Katz et al., 2015), and thus reduced the photocatalytic activity. It was observed that a reduction of FLT absorbed on the TiO_2 nanoparticles in OPW compared with that in distilled water was observed (Figure 3.3d), suggesting that the surface of TiO_2 was partially occupied.

Considering the major species of organic acids in OPW were fatty acids (Orem et al., 2014) which have less fouling potential and the pH of OPW samples was neutral, their effects on the deactivation of catalyst could be limited. Therefore, the breakdown of PAHs was mainly inhibited by the competition from the aromatic substrate.

3.4 Summary

This study investigated the effects of OPW matrix on the photo-degradation of PAHs by using UV and TiO_2. The TiO_2 nanocatalyst was synthesized by a modified sol-gel method and the average particle size was around 12-17 nm. The experimental results showed that the degradation of PAHs in the distilled water samples followed the apparent-first-order kinetics and the reaction rate constants of photocatalysis were higher than those of the photolysis alone, indicating a better performance with the addition of the synthesized nanocatalyst. The photocatalytic efficiency was significantly decreased in the OPW samples, especially for PAHs with high molecular weights. The OPW matrix including salinity, insoluble particulate matter, and organic composition were then investigated individually. The results showed that the increase of ionic strength increased the removal rates of PAHs with lower molecular weights. The breakdown of PAHs with high molecular weights was more sensitive to the change of salinity and insoluble matter due to their low solubility by the "salting out" effect and the adsorptive competition of PAHs between insoluble matter and TiO_2. The organic composition was the major source leading to the attenuation of UV light. Its components especially aromatic compounds competed with PAHs thus reduced the overall efficiency of photocatalysis. Therefore, the major matrix effects of OPW were caused by the aromatic compounds. Some other

species such as alcohols, organic acids and halogens presented in OPW may also affect the photocatalytic performance. This finding points to further research opportunities on the effects of these organic species as well as halogen ions on the effectiveness of applying the photocatalysis technologies for OPW treatment.

Chapter 4 Removal of Naphthalene from Offshore Produced Water through Immobilized Nano-TiO_2 Aided Photo-oxidation[3]

[3] *The contents of this chapter are based and expanded on the following paper:*

Liu. B., Chen B., Lee, K., Zhang, B.Y., Ma, Y.C., and Jing, L. (2016) Removal of Naphthalene from Offshore Produced Water Through Immobilized Nano-TiO_2 aided photo-oxidation. Water Quality Research Journal of Canada, 51(3), 246-254. **DOI: 10.2166/wqrjc.2016.027**
Role: Bo Liu solely worked on this study and acted as the first author of this manuscript under Dr. Bing Chen and Dr. Baiyu Zhang's guidance. Most contents of this paper were written by him and further edited by the other co-authors.

4.1 Introduction

There are many concerns regarding the introduction of catalyst slurry to photocatalysis. One of the most significant disadvantages is that the aqueous suspension of catalyst in treated effluent needs to go through a solid-liquid separation step before discharge, which in turn greatly increases treatment time and cost (Byrne et al., 1998; Yahia Cherif et al., 2014). Further, the suspended catalysts are more susceptible to the water matrix. The immobilization of TiO_2 on different substrates has then been studied to control the dispersion of catalyst in the treated effluent (Behnajady et al., 2008; Chong et al., 2010). Some studies compared suspended TiO_2 and immobilized TiO_2 in terms of their performance in photocatalysis and the results indicated that fixation of catalyst can reduce its surface-active sites and limit its mass transfer potential (Matthews, 1987; Mascolo et al., 2007). However, these studies were conducted without the matrix effects of water media being considered. Limited research has been conducted to compare the performance of different catalysts in wastewater treatment (Pozzo et al., 1997; Mascolo et al., 2007). To date, the research on photocatalytic treatment of OPW by immobilized catalysts has not been well studied. The unique and complex composition of OPW may to some extent affect the photocatalytic performance of catalysts.

In order to investigate the applicability of immobilized photocatalysis in treating OPW, immobilized and suspended TiO_2 have been used as catalysts to evaluate their photocatalytic and adsorptive performance in the presence of OPW substrate. The catalysts were immobilized by a heat-attached method and further characterized by scanning electron microscope (SEM) and energy-dispersive x-ray spectroscopy (EDS).

Naphthalene was selected as the target contaminant due to its abundance in OPW. The removal of naphthalene and other organic compounds in OPW was examined. The effects of OPW substrates were discussed. The findings are expected to help develop better photocatalytic technology to improve its efficiency in treating OPW and reduce adverse effects caused by the OPW matrix.

4.2 Materials and Methods

4.2.1 Materials

Naphthalene-d_8 was purchased from Cambridge Isotopes Labs (U.S.A.) as a surrogate of naphthalene. Acetone, ethyl alcohol, dichloromethane (DCM) and concentrated hydrofluoric acid solution were purchased from Sigma-Aldrich Canada Co. Aeroxide® P25 nano-scale TiO_2 (anatase: rutile is 9:1, average particle size is around 21 nm) and sodium hydroxide were obtained from Fisher Scientific, Canada. All of the chemicals were of analytical grade. Glass microscope slides (75 × 25 mm^2) were purchased from VWR International, Canada. The laboratory tests on OPW samples were performed and the key components were identified.

4.2.2 Immobilization of Catalysts

The immobilization of catalysts on glass plates was conducted by using a heat-attached method (Yahia Cherif et al., 2014). Firstly, 0.4 g of Aeroxide® P25 was dispersed into 100 mL of ethyl alcohol. The slurry solution was sonicated by a Branson S-450D homogenizer with 100% amplitude for 30 minutes. Glass microscope slides were pre-treated with dilute hydrofluoric acid for 1 day and 0.01 $mol \cdot L^{-1}$ sodium hydroxide solution for 2 hours successively to increase the amount of OH group on the slides. After

washing with distilled water, both sides of the slides were dipped with the slurry solution and then dried at ambient temperature. After drying, the glass slides were calcinated in a muffle furnace (Thermolyne^{TM}) under 450 ^{o}C for 2 hours. The weakly attached P25 particles on glass slides were removed by rinsing with distilled water. The attaching process was duplicated to ensure the formation of a P25 film. The estimated concentration of P25 on the glass surface was around 0.8 g·m^{-2}. The surface changes of slides before and after use were examined to evaluate the fouling effect caused by OPW.

4.2.3 Irradiation Experiments

The irradiation experiments were conducted in a photocatalytic reactor (Figure 4.1). Five hundred millilitres of produced water sample were filled into a 500 mL amber bottle. Four coated glass slides or the equivalent amount of P25 powder was added in the amber bottle and the mixture was stirred for 30 minutes prior to irradiation in order to achieve equilibrium. The systems with coated glass slides and P25 powder represented the immobilized and suspended systems, respectively. Pen-ray light source (peak wavelength at 254 nm) covered with a quartz tube was then submerged in the bottle for 12 hours' irradiation. Water bath was set to keep the system at ambient temperature. Water samples were collected at 0, 0.5, 1, 1.5, 2, 3, 6 and 12 hours, respectively. The mixture was kept homogeneous by magnetic stirring. Adsorption experiments were conducted using the same apparatus as stated above. The sampling intervals for adsorption were 0, 0.25, 0.5, 1, 1.5, 2, 3, 6 and 12 hours, respectively.

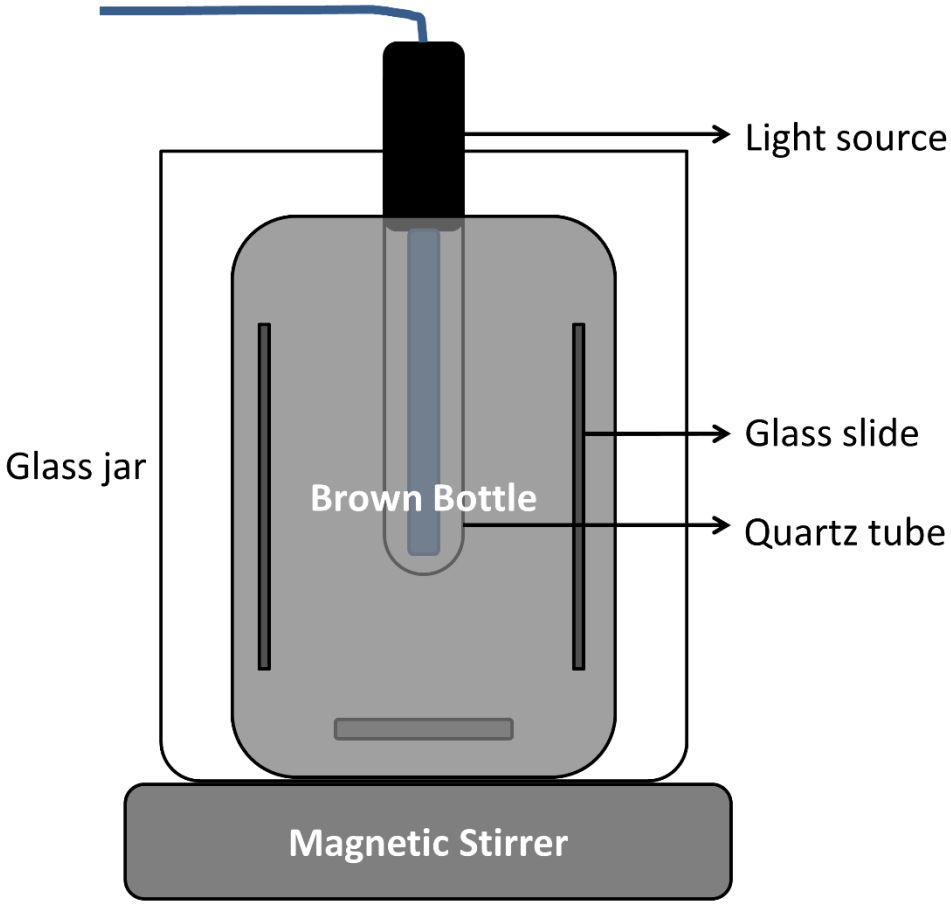

Figure 4.1 Scheme of the photocatalytic reactor

4.2.4 Analytical Methods

Liquid-liquid micro-extraction (LLME) method was established based on those reported by Zheng et al. (2015) and Jing et al. (2014b) with modifications. For the OPW samples from the immobilized system, 10 mL of water sample was spiked with 20 μg mL^{-1} naphthalene-d_8 solution and vortexed for 10 second and then extracted by 250 μL DCM for 1 minute. The mixture was centrifuged at 1,500 rpm for 5 minutes to completely separate the water layer from the organic phase. Then 100 μL of extract was transferred into a 150 μL micro-vial.

For the OPW samples collected from the suspended system, 10 mL of water sample was centrifuged at 3,000 rpm for 15 minutes. Then 5 mL of supernatant was forced to pass through a 0.2 μm syringe filter (Whatman® Spartan® RC) to remove any catalyst residue. Then 10 μg mL^{-1} naphthalene-d_8 solution was added and the solution was vortexed for 10 seconds. After that, 250 μL of DCM was added and further vortexed for 1 minute. The mixture was finally centrifuged at 1,500 rpm for 5 minutes to complete the phase separation. The extract with a volume of 100 μL was transferred into a 150 μL micro-vial.

Instrumental analysis was performed using an Agilent® 7890A/5975C gas chromatography-mass spectrometer (GC-MS) system equipped with an Agilent® 7693 autosampler. The analytes were separated by a 30 m × 0.25 mm id × 0.25 μm DB-5MS UI fused silica capillary column. The injected mode was spitless at 300 °C. A temperature ramp was set as follows: held at 65 °C for 1 minute, then raised at the rate of 4 °C min^{-1} to 110 °C and held for 5 minutes; and finally raised to 300 °C at the rate of

20 °C min^{-1}. Total ion current (TIC) chromatograms were acquired to examine the changes of organic components in OPW. The analysis of naphthalene and its surrogate was carried out in a selected-ion monitoring chromatogram (SIM). The analytical processes were triplicated. The relative standard deviations for naphthalene in the immobilized system and suspended system were 6% and 4%, respectively.

Other parameters of OPW, such as inorganic composition, pH, and turbidity, were quantified by inductively coupled plasma mass spectrometry (ICP-MS, PerkinElmer ELAN® DRCII), a pH meter (EL20, Mettler Toledo®), and a turbidity meter (VWR Scientific®, USA), respectively.

4.3 Results and Discussion

4.3.1 Characterization of Immobilized Catalyst on Glass Slides

The surface morphology of the immobilized catalyst is illustrated in Figure 4.2. It depicts the formation of a P25 film on the surface of glass slides. It also illustrates the film is non-uniformed in texture at different locations. The brighter region indicates a thicker coating, whereas the darker region indicates the thinner coating. By EDS analysis, the density of Ti element and its relative proportion in one area can be quantified. Overall, the relative proportion of Ti was 36% on the depicted surface, indicating that a considerable amount of TiO_2 has been coated onto the slides. The density of Ti element in the scan area of Figure 4.2(a) is shown in Figure 4.2(b). The higher brightness refers to a larger amount of Ti atoms in a specific area. The black indicates the absence of Ti element. Figure 4.2(b) gives It gave a clearer illustration of the TiO_2 distribution across the surface. This non-uniform texture was formed by the uneven evaporation of solvent

during the drying step of immobilization. A higher solvent evaporation rate in some areas caused the drift of P25 in other areas with a low evaporation rate, forming a catalytic film of uneven thickness.

4.3.2 Effect of Filtration on Sample Analysis

The LLME methods were suitably modified to pre-treat the samples obtained from the immobilized and suspended systems. For the suspended system, the implementation of centrifugation and filtration significantly increased the pre-treatment time (around 15 minutes) whereas the immobilized system did not need these separation steps. It was because that only a negligible amount of dispersive catalytic particles was found in the immobilized system in comparison with the suspended system. Without filtration, the overall time of sample pre-treatment was significantly shortened.

The Chromatograph of analytic samples in the different systems are further compared in Figure 4.3. The abundance was observed to decrease after filtration, which can be attributed to the retention of organics by using a syringe filter. Furthermore, some of the organic components in OPW, especially those hydrocarbons with longer retention time, “disappeared” in the spectrum after filtration. These hydrocarbons have higher hydrophobicity and are hence more attracted to the insoluble particles and other insoluble organic matters in OPW (Luo et al., 2009; Ukiwe et al., 2013). For this reason, they were separated from the solution phase through either precipitation or entrapment in the filtration membrane during the centrifugation step.

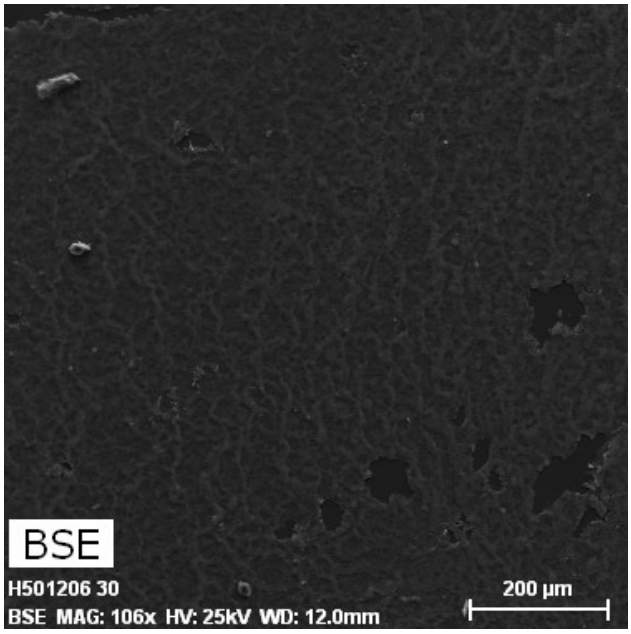

(a)

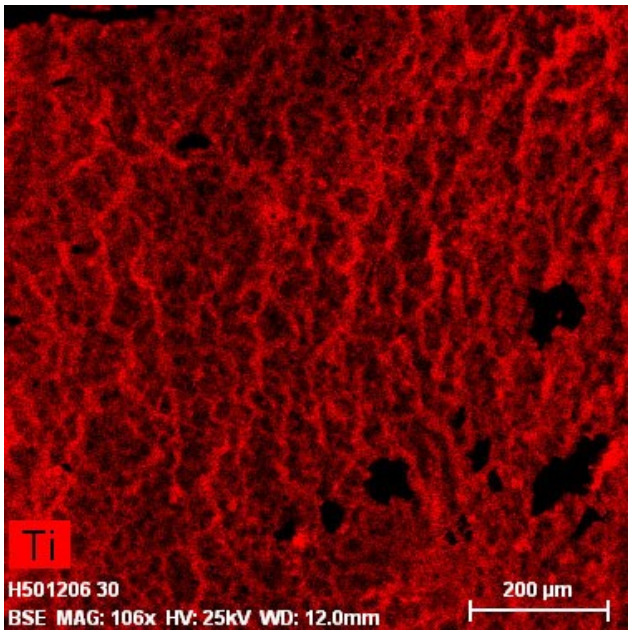

(b)

Figure 4.2 Characterization of TiO_2 coated glass slides by (a) SEM and (b) EDS

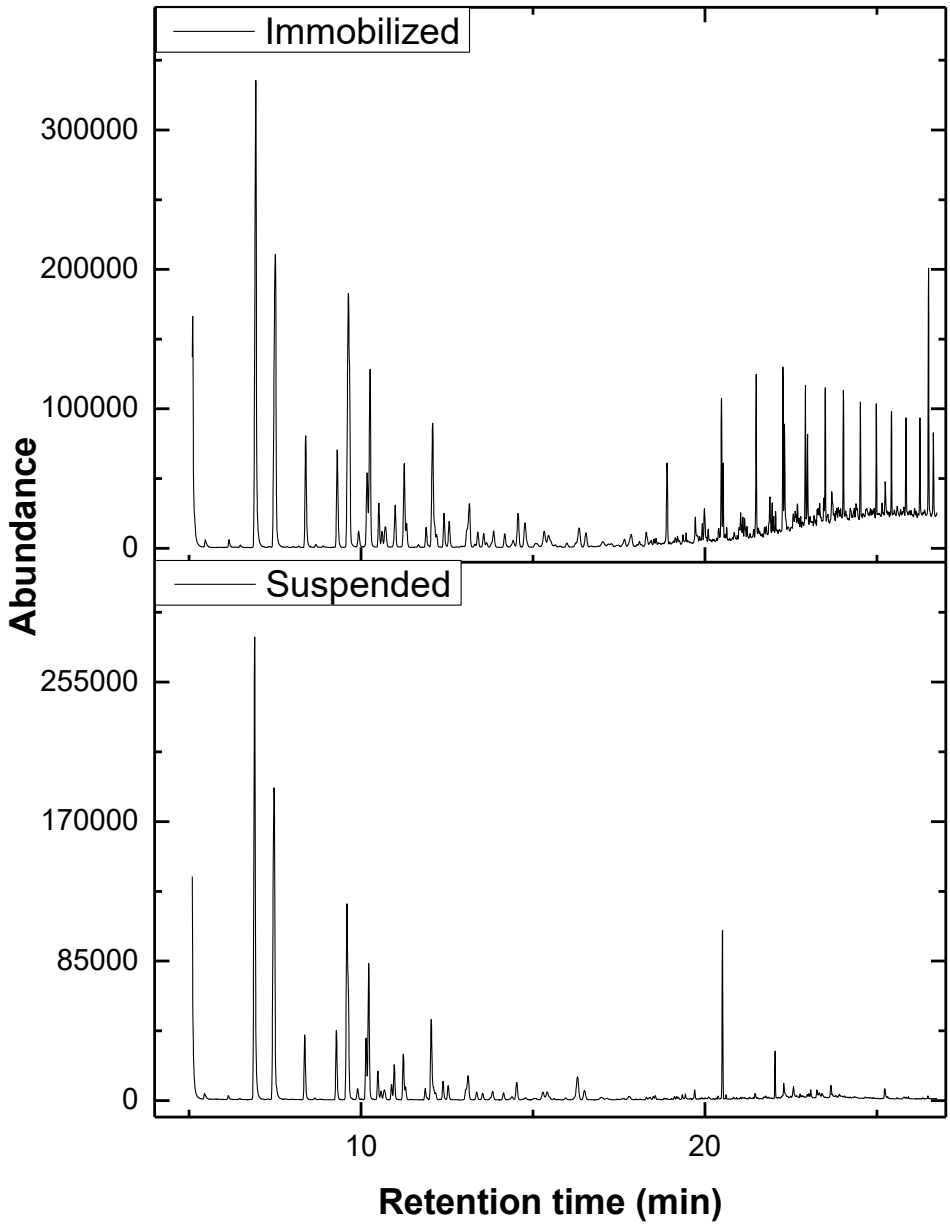

Figure 4.3 The Chromatograph of OPW samples from immobilized system and suspended system

4.3.3 Evaluation of Adsorption and Photocatalysis

The adsorption of naphthalene on TiO_2 particles is dependent upon hydrophobicity, the surface of catalyst and solution conditions (Xue et al., 2011). The concentration of naphthalene left in the solution without UV light irradiation was monitored for over 12 hours (Figure 4.4).

The kinetic data of naphthalene adsorption on TiO_2 were fitted into the pseudo first-order Lagergren equation (Gimeno et al., 2007):

$$\frac{dq_t}{dt} = K_{ads}(q_e - q_t) \quad (4.1)$$

where q_e is the amount of naphthalene adsorbed per unit mass of adsorbent at equilibrium (mg/g); q_t is the amount of naphthalene adsorbed per unit mass of adsorbent at different time (mg/g); and K_{ads} is the adsorption constant (g/mg·min^{-1}).

The changes of naphthalene concentration occurred in the first 90 minutes of adsorption appear to be irregular and inconsistent with the first-order equation in both systems. The introduction of catalysts broke the balance of naphthalene in OPW and forced a new adsorption/desorption equilibrium. As the suspended catalyst has a higher mobility in OPW, a greater fluctuation of naphthalene concentration in OPW was observed. A trend of steady decrease in naphthalene concentration was found after 90 minutes. It is believed that the naphthalene was adsorbed on the catalyst after 90 minutes. Therefore, the initial adsorption of naphthalene was assumed to commence after 90 minutes. The kinetics simulation was then conducted.

The kinetics data of adsorption were tabulated in Table 4.1. The K_{ads} value (0.0254 g/mg min) in the suspended system (P25) was much higher than that (0.00367 g/mg min) in the immobilized system (plates), which indicated a higher mass transfer rate of P25 powder compared with the coated glass plates. However, the adsorption equilibria were similar, which were 0.00353 mg/g for plate and 0.00320 mg/g for P25, indicating negligible differences of surface area between the P25 powder and the coated glass plates. The results suggest that the active sites on both catalysts were similar. This observation contradicted the result that the immobilization of catalyst could significantly reduce its surface area (Mascolo et al., 2007). It could be due to an agglomerating effect of OPW substrate to suspended TiO_2. The significant amount of alkaline-earth cations (Ca^{2+} and Mg^{2+}) could lower the electro-static barrier of TiO_2 and facilitate the agglomeration of TiO_2 (Armanious et al., 2011). In our study, the agglomeration of TiO_2 has an effect leading to the reduction of available specific surface area, which is similar to immobilization. Limited dispersion of catalyst was less influenced by alkaline-earth cations. In this case, the immobilized catalysts show more resistance to the negative effects caused by the OPW substrate.

The photocatalytic process was conducted under UV irradiation for 12 hours and the experimental results were then simulated with an apparent-first-order kinetic models (Xu et al., 2013)

$$Rate = \frac{c_t}{c_0} = e^{-kt} \qquad (4.2)$$

where t is the reaction time (min); k is the first-order reaction rate constant (min^{-1}); c_t is the determined concentration of the reactant at time t (μg/L); and c_0 is the initial concentration of the reactant(μg/L).

The photocatalytic experimental results and the simulated kinetic curves are illustrated in Figure 4.4. In the immobilized system, the regression coefficient between the simulated and experimental results was higher than 0.99, indicating a good fit. In the suspended system, an odd concentration change of naphthalene at the beginning of irradiation was noticed. The regression coefficient was therefore decreased to 0.95. Such a reduction could be caused by the inherent measurement noise at low concentration levels or the adsorption/desorption of NAP on the suspended P25 powder. The k values for the immobilized and suspended systems were 0.00305 and 0.00219 min^{-1}, respectively. The results showed a higher removal effectiveness of naphthalene by the immobilized system. The attenuation of UV light caused by the increase of turbidity significantly affected the photocatalytic efficiency as light intensity is a critical factor in photocatalysis (Jing et al., 2014b). The turbidity of OPW did not changed after introducing the immobilized catalyst. Contrastingly, it increased to 100 NTU by applying P25 powder. The increase of turbidity promoted the attenuation of UV-C, and thus reduced the overall intensity of irradiation.

Table 4.1 The comparison of different catalysts on the adsorption and photocatalysis of naphthalene

	Adsorption			Photocatalysis	
Catalysts	K_{ads} (g/mg min)	q_e (mg/g)	Regression (R^2)	k （min^{-1}）	Regression (R^2)
Plate	0.00367	0.00353	0.979	0.00305	0.995
P25	0.02543	0.00320	0.825	0.00219	0.949

4.3.4 Degradation of Organic Substrate

The degradation efficiency of different organic compounds in OPW varied. As seen from the GC chromatogram shown in Figure 4.5, the major organic components in the spectra were phenols and their alkyl congeners, aromatic hydrocarbons and aliphatic hydrocarbons. The peaks with retention time less than 15 minutes are generally due to phenols, their alkyl homologues and some of the aliphatic hydrocarbons with lower molecular weights. Most of the higher molecular weight aliphatic hydrocarbons were eluted after 15 minutes. After irradiation, most of the peaks before 15 minutes disappeared from the chromatogram, indicating an effective photo-degradation of phenols and those hydrocarbons with lower molecular weights. However, the peaks after 15 minutes showed insignificant changes. It indicated that aliphatic hydrocarbons were much more inert than aromatic hydrocarbons in photocatalysis. There could be two reasons: 1) aliphatic hydrocarbons were UV-transparent in the wavelength of 254 nm, limiting their photo-degradation (Dolinová et al., 2006; D'Auria et al., 2009); 2) the addition of hydroxyl radicals to aromatic organics in photocatalysis occurs faster than the H-abstraction of aliphatic organics (Dionysiou et al., 2016). Therefore, the presence of aliphatic hydrocarbons has limited influence on competing the UV adsorption and the radical oxidation of NAP. The negative impact of organic substrate to the photocatalytic oxidation of NAP was mainly from the aromatic organics such as phenols in OPW. It was also observed that all the organic matters were depleted after photocatalysis and filtration, suggesting great potential in treating and/or reclaiming OPW.

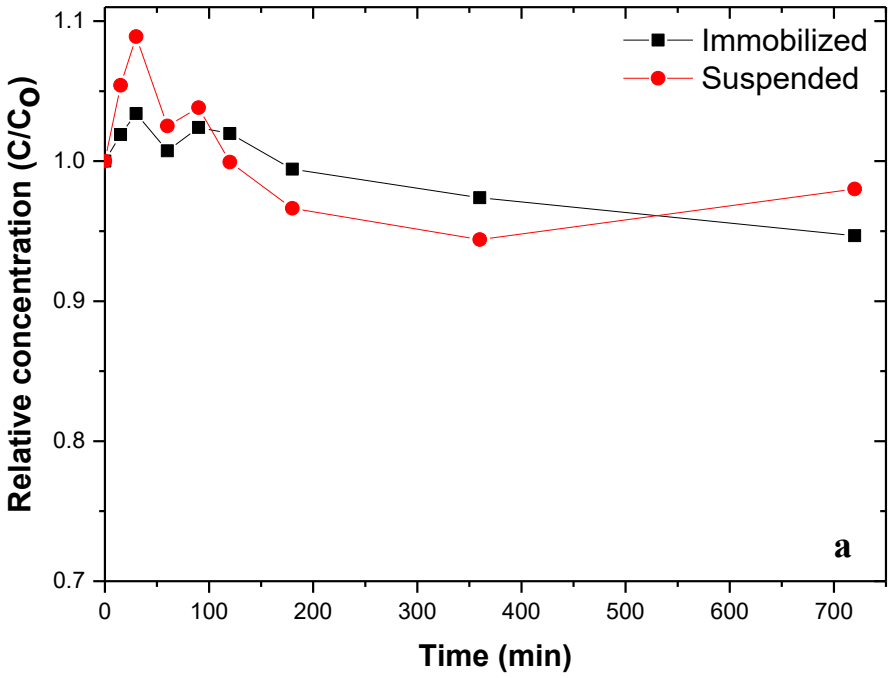

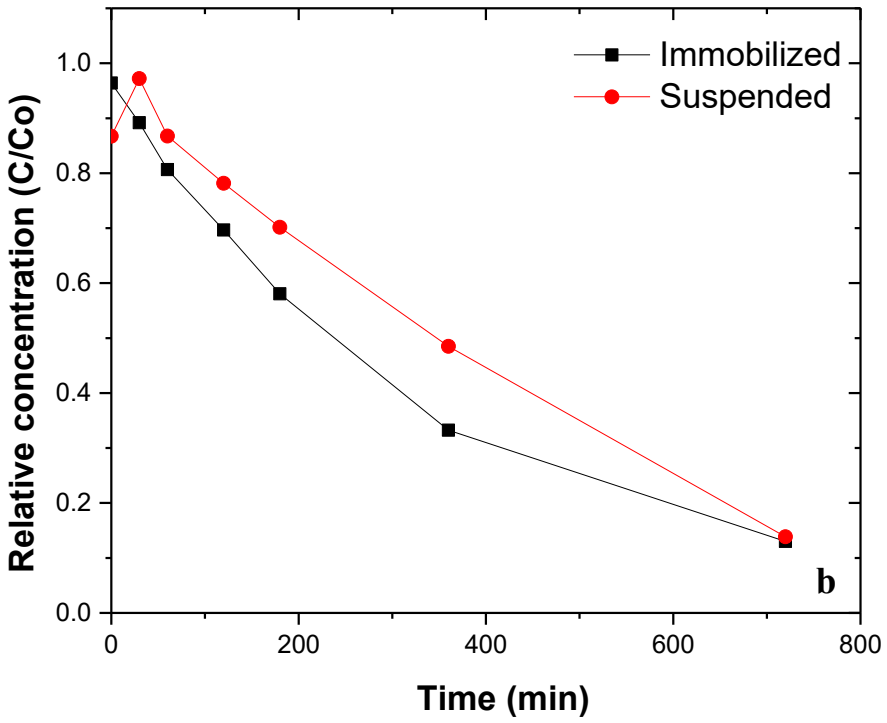

Figure 4.4 The comparison of different catalysts/systems: adsorption (a) and photocatalysis (b)

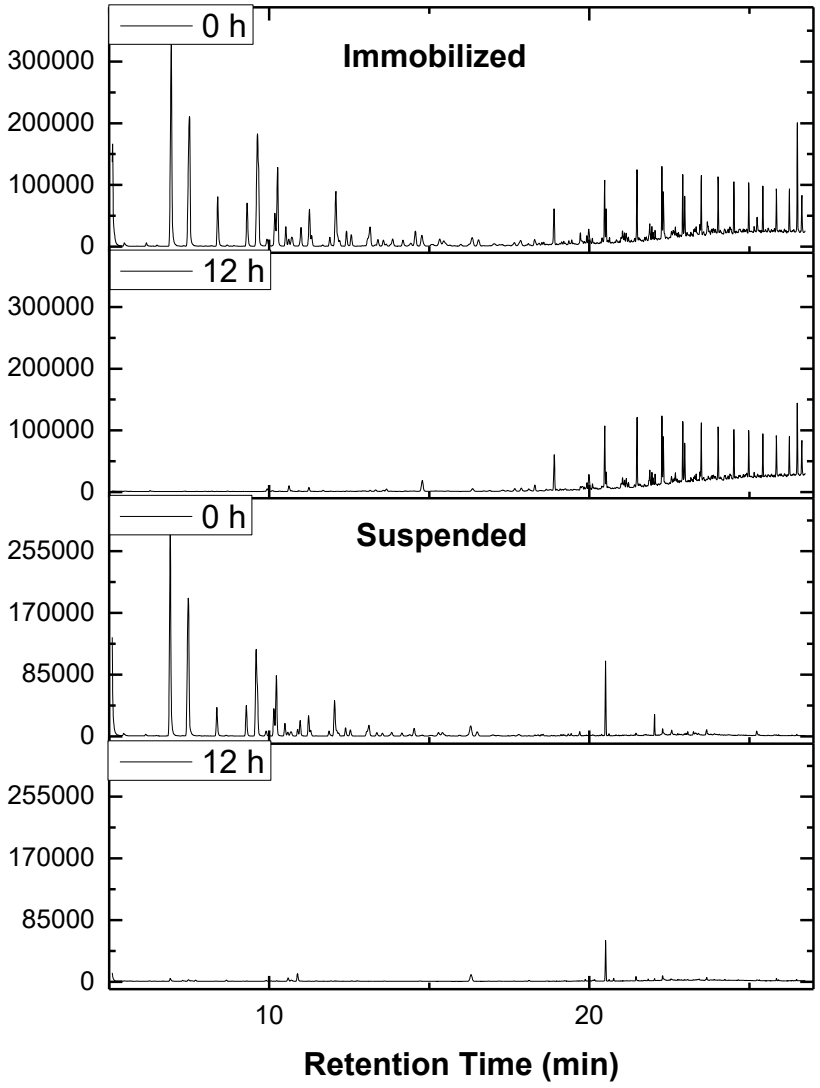

Figure 4.5 Degradation of organic components in OPW by different catalysts/systems

4.3.5 Substrate Effects of OPW on Coating Surface

The substrate of OPW was determined by ICP-MS and GC-MS analyses. The results showed that the OPW contained high salinity, high concentration of bivalent cations, and a large number of organic components (phenols, PAHs, aliphatic hydrocarbons, etc). The turbidity was around 22 NTU (Table 4.2), indicating a large amount of insoluble particular matters in the OPW.

The significant decrease of photocatalytic degradation performance with suspended catalysts was found in OPW. It was indicated that the presence of bivalent cations such as (Ca^{2+}, Mg^{2+}) would force catalyst particles to agglomerate (Armanious et al., 2011). This therefore reduced the active sites on catalyst consequently lowered the photocatalytic reaction rates of analytes. The presence of hydrophobic organic matters could also result in precipitates on the catalyst, which may further enlarge the particle size and reduce of the number of activated sites.

The surface of coated glass slides changed from white to pale yellow in color during adsorption and photocatalysis processes. The pale yellow color was similar to that of OPW, suggesting that the fouling of slides was due to the deposition of OPW substrates. The turbidity of OPW decreased from 22 NTU to 16.5 NTU after applying the coated glass slides, suggesting that the deposition of insoluble particles occurred during the experiments. The results from EDS showed no evidence for the presence of iron, which is usually in yellow color. However, the Ca/Si ratio increased from 0.234 to 0.276 after irradiation, suggesting that a slight amount of calcium was deposited on the TiO_2 film. The scaling of calcium could be attributed to the increase of temperature during

irradiation. Hydrophobic organic matter could also precipitate on the catalyst surface to reduce the number of active sites. Six peaks were shown in the FT-IR spectra (Figure 4.6). The peaks at 2,920 cm^{-1} and 2,850 cm^{-1} are due to the C-H stretching modes of alkyl groups, while the peaks at 3,391 cm^{-1}, 1,632 cm^{-1}, 1,453 cm^{-1}, and 1,106 cm^{-1} are assigned to the stretching of the O-H bond in ROH functional group, stretching of unsaturated C=C bond, C-H bending in alkanes and the stretching mode of C-O bond, respectively. Therefore, the organic substrate on the fouled glass slides included alcohols, alkanes, and aromatic organics.

Table 4.2 Background information of the OPW sample

Parameters	values	
Naphthalene	0.01	mg/L
Magnesium	83.28	mg/L
Calcium	971.08	mg/L
Iron	4.12	mg/L
Silicon	20.38	mg/L
Chlorine	17197	mg/L
Sulfur	630.92	mg/L
pH	6.86	
Turbidity	22	NTU

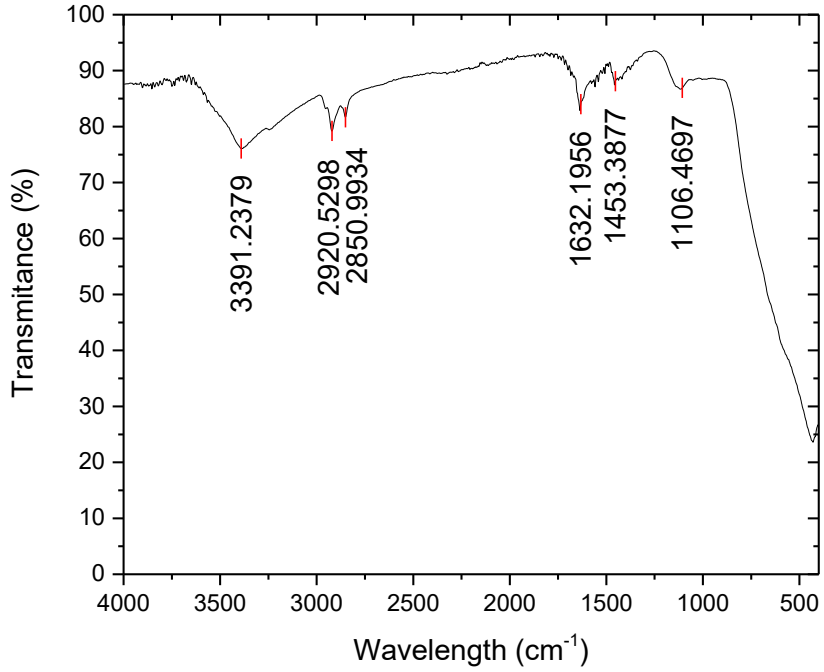

Figure 4.6 The FTIR spectra of the immobilized TiO_2 on the glass slide after photocatalysis

4.4 Summary

This study has compared the removal of naphthalene by photocatalysis using suspended TiO_2 and immobilized TiO_2 in offshore produced water. The adsorption of naphthalene on the surface of TiO_2 and the photo-degradation of naphthalene have been evaluated. Hydrocarbons with higher molecular weights were not detected in the GC analysis after filtration. This was probably caused by their higher affinity for the insoluble matters, which resulted in their removal by centrifugation and membrane filtration. The differences of adsorbed naphthalene at equilibrium indicated that the immobilized TiO_2 has an active surface area similar to as that of the suspended TiO_2 in OPW. The photodegradation efficiency of naphthalene was enhanced by immobilized TiO_2 because of the significant reduction of turbidity compared with TiO_2 powder. The degradation of other major hydrocarbons (phenols and aliphatic hydrocarbons) suggested that the abundance of aromatic organics was more likely to affect the naphthalene degradation. The fouling on the catalyst surface was occurred, which was associated with a notable color change from white to pale yellow. The reduction of turbidity in OPW, the increase in calcium element, and the identification of various organic functional groups on the coated glass slides suggested that the components on the fouling surface were made of insoluble particles, scaling and organic matters in OPW.

Chapter 5 Photocatalytic Ozonation of Offshore Produced Water by TiO_2 Nanotube Arrays Coupled with LED-UV Irradiation[4]

[4] *The contents of this chapter are based and expanded on the following manuscript:*

Liu, B., Chen, B., Zhang, B.Y., Lee, K. (2018) Photocatalytic Ozonation of Offshore Produced Water by TiO_2 Nanotube Arrays Coupled with LED-UV Irradiation. *Environmental Science and Technology*, to be submitted.

Role: Bo Liu solely worked on this study and acted as the first author of this manuscript under Dr. Bing Chen and Dr. Baiyu Zhang's guidance. Most contents of this paper were written by him and further edited by the other co-authors.

5.1 Background

Recently, many research efforts have been made to study the degradation of PAHs in produced water by AOPs, which is regarded as a promising treatment option (Corrêa et al., 2009; Neff et al., 2011; Igunnu and Chen, 2012; Jing et al., 2014b; Zheng et al., 2016). It was reported that PAHs could rapidly react with hydroxyl radicals during the AOPs. However, the degradation rate was susceptible to the strong negative effects by the produced water matrix, leading to low efficiency, high energy consumption and cost, and generation of toxic by-products (Zheng et al., 2016; Liu et al., 2016a; Liu et al., 2016b). Furthermore, it was observed that the efficiency of the single AOP method such as photocatalysis was significantly reduced in OPW mainly due to the organic competitors (e.g. phenols) and surface fouling (Liu et al., 2016a; Liu et al., 2016b). Consequently, the prolonged retention time might not meet the requirements in the field because of the high volume of OPW generated daily. Although ozone was regarded as a strong candidate due to its high reactivity to aromatic species, the harmful ozone-generated by-products were a growing concern (Haag and Hoigne, 1983; Agustina et al., 2005; Mehrjouei et al., 2015; Cochran et al., 2016; Li et al., 2017).

To help address these challenges and meet the needs, this study investigates a novel treatment method by integrating photocatalytic ozonation, TiO_2 nanotube arrays (TNAs) and UV-light-emitting diode (UV-LED). Photocatalytic ozonation has been considered as a good method for OPW treatment because it is a powerful oxidation process with high efficiency and cost-effectiveness (Beltrán et al., 2005a; Mehrjouei et al., 2015; Beltrán and Rey, 2017). TNAs are advanced nanomaterials with hollow 1D nanostructures. The

unique structures not only improve the surface area, but also increase the electron transportation rate thorough the nanotube walls (Zhao et al., 2016). Compared with conventional TiO_2 nano-particles, the applicability of TNAs is much enhanced. The UV-LED lamp as an alternative UV source for irradiation has the advantage of high illumination efficiency, low heat generation and long lifetime (Venkataramani et al., 2007; Levchuk et al., 2015; Ghosh et al., 2016; Radwan et al., 2016). Integration of these elements is expected to afford more cost-effective and feasible methods for treating OPW. This study is thus focused on the development of an integrated method and comprehensive evaluation of its applicability in treating OPW. The results would not only fill the knowledge gaps but also provide an effective and feasible alternative option to OPW treatment.

5.2 Materials and Methods

5.2.1 Materials

The standard solution of 16 PAHs (500 μg/mL) was purchased from Agilent (USA). The internal standard (IS) o-terphenyl and titanium foil (≥99.5%, 0.125 mm thickness) were purchased from Sigma-Aldrich (Canada). Aeroxide® P25 nano-scale TiO_2 (anatase: rutile is 9:1, average particle size is around 21 nm), ethylene glycol (99%), and ammonium fluoride (NH_4F, 99%) were obtained from Fisher Science (Canada). Acetone (Honeywell Burdick and Jackson, USA) and dichloromethane (Honeywell Burdick and Jackson, USA) were used for preparing stock solutions and aqueous sample extraction, respectively. Distilled water was produced on-site from a double fused-silica distillation unit. OPW samples were obtained from the local offshore platforms in the North Atlantic.

Detailed information cannot be provided here due to client confidentiality and non-disclosure. Laboratory tests on the OPW samples were performed using ICP-MS (FEI™ MLA 650F) and pH value were measured by using a pH meter (EL20, Mettler Toledo®).

5.2.2 Synthesis of TiO_2 Nanotube Arrays by Anodization

The anodization method was modified from the method introduced by Ghosh and co-workers (Ghosh et al., 2016). Ti foils were first pre-cleaned by ultrasound for 20 min in acetone, ethanol, distilled water then dried in an oven covered by aluminum foil. Then, Ti foils were placed in a PP reservoir filled with 0.15 M NH_4F ethylene glycol/water (98:2) solution and connected to a B&K Precision 1762 DC power supply. Both anode and cathode were Ti foils. TiO_2 nanotube arrays were then synthesized by a two-step method, which resulted in a high light-to-electron efficiency (Zhang et al., 2010; Momeni and Hosseini, 2014). The initial anodization was conducted for 2 hours under 60 V and a room temperature. The anode was removed and washed with distilled water and sonicated in 1 M HCl water solution for 30 minutes to remove the thin film generated in the anodization. After sonication, the anode was dried and further anodized at 60 V for 8 hours. The anode was then submerged in distilled water until the nanotube arrays were detached from the foil. The synthesis was finished by air drying and annealing of the arrays was done at 450 ^oC for 2 hours. The surface morphologies of the prepared TNA were characterized by the JEOL JSM-7100F Field-Emission SEM and Rigaku Ultima IV XRD.

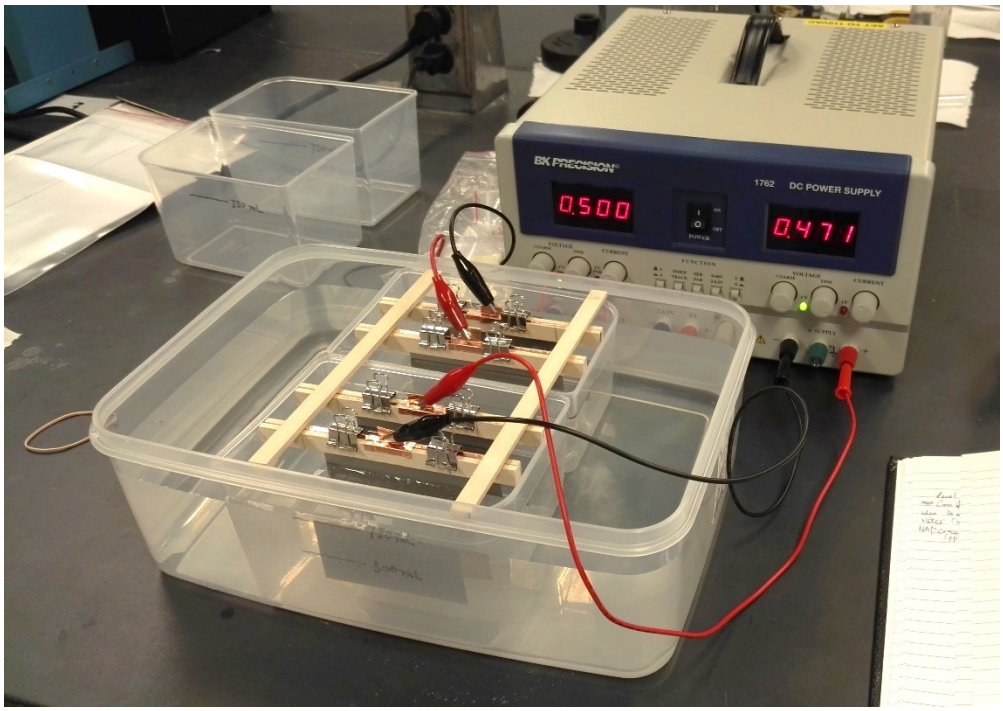

Figure 5.1 Anodization reactor

5.2.3 Degradation of PAHs during OPW by Photocatalytic Oxidation

OPW samples were first filtrated by a 1.5 μm glass-fiber membrane to remove any insoluble particle matters that may interfere the treatment process. The filtrated sample was then spiked with a solution of 16 PAHs working standard. Four hundred millilitres of fortified OPW samples and various amounts of TNA were added to a 500 mL amber bottle and stirred for 30 minutes prior to irradiation to achieve equilibrium. The bottle, in which a UV-LED light source (10 bulbs, 365 nm) covered with a borosilicate glass tube was submerged, was then irradiated for 1 hour. Light intensity was controlled by the voltage output from the DC supply. At the same time, 0.12 L/min O_2 flow carried certain amount of ozone was purged trough a dispersive tube with an average pore size of 2-5 μm. The aqueous suspension in the bottle was kept homogeneous by using a magnetic stirrer. The runs and corresponding sets of different parameters are listed in Table 5.1. The levels of ozone dose and catalyst dose were adjusted based on the previous studies (Liu et al. 2016b) to fine the maximum efficiency of the system without hindering by the side-effects such as the generation of high levels of ozone-by-products and turbidity. The UV-LED voltage was set as the working voltage recommended by the manufacturer.

Table 5.1 Experimental design of photocatalytic ozonation

Parameter	Run 1	Run 2	Run 3	Run 4	Run 5	Run 6	Run 7	Run 8	Run 9
Ozone dose (ppm)	10	0	10	10	5	15	10	10	10
Catalyst dose (g/L)	0.1	0.1	0	0	0.1	0.1	0.2	0.3	0.1
UV voltage (V)	34	34	34	0	34	34	34	34	36

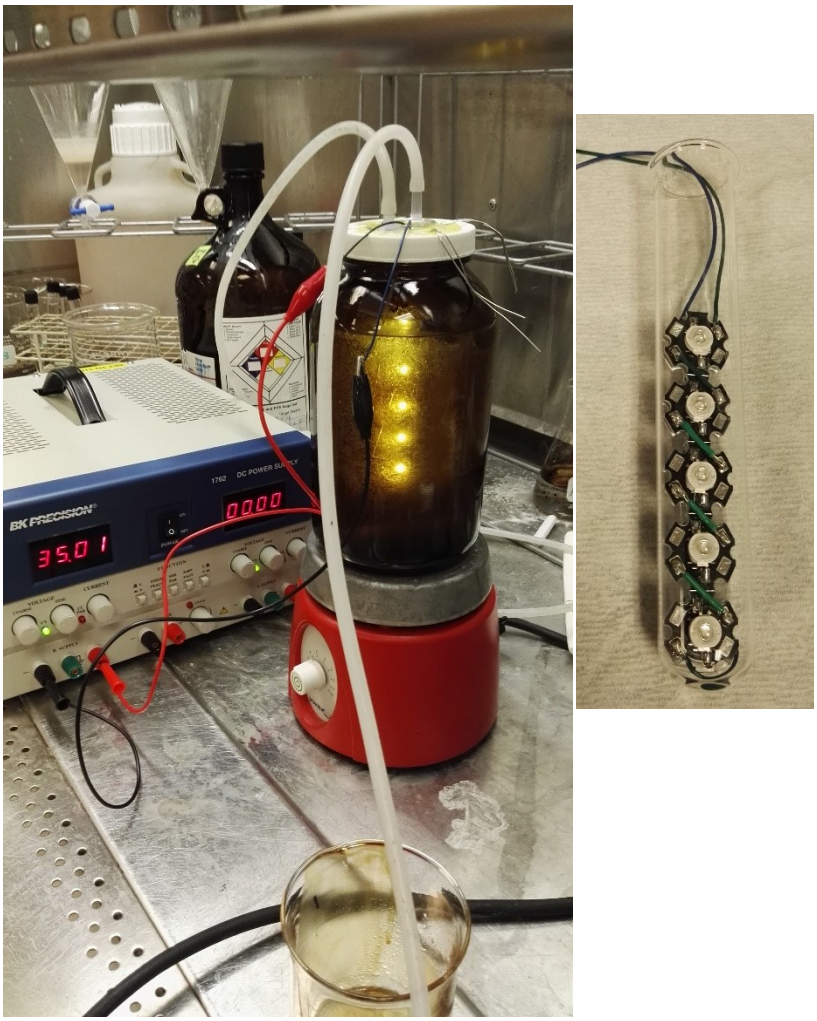

Figure 5.2 Photocatalytic ozonation reactor: amber reaction chamber, direct current supply (left) and UV-LED light (right)

5.2.4 Analytical Methods

The water samples were first pre-treated by an LLME method modified form that reported by Zheng and co-workers (Zheng et al. 2016). One milliliter of sample was collected in a 2 mL amber screw top vial and 250 µL of DCM was added. The vial was well sealed and vortexed for 1 min. Then the vial was let stand for 10 min to allow the separation of organic phase and aqueous phase to separate. Fifty microliters of organic part were transferred to a 150 µL micro-vial. 10 µL of IS was added before instrumental analysis.

After the treatment, the TNA residue was collected by filtration of OPW samples through a 0.4 µm membrane. The residue on the membrane was washed off, ambient dried and transferred in a 2 mL screw top vial. One mL of DCM was added into the vial. The mixture was vortexed for 1 min and 50 µL of it was transferred to a 150 µL micro-vial. 10 µL of IS was added before instrumental analysis.

Instrumental analysis was performed using an Agilent 7890A/5975C GC-MS equipped with an Agilent 7693 autosampler. Two nanoliters of analytes were injected to GC and separated by a 30 m × 0.25 mm id × 0.25 µm DB-5MS UI fused silica capillary columns. The injected mode was splitless at 300 °C. The temperature program used for GC-MS analysis was set as: initial temperature holds at 65 °C for 1 minute; temperature ramps from 65 to 300 °C at 4 °C/min; temperature holds at 300 °C for 1 minute. The PAH analyses were performed in the selected ion monitoring (SIM) mode with an electron energy of 70 eV. The ion-source was set at 300 °C. The method detection limit of PAHs

was 0.3 - 1 ng/L. The variance of the analytic method was 5%. The measure points of OPW samples were duplicated.

5.3 Results and Discussion

5.3.1 Characterization of TiO_2 Nanotube Array

After water washing, TNA was automatically disconnected from the Ti foil, forming a thin layer film (Figure 5.3). The film was peeled off and annealed. During the annealing process, the film was broken into small pieces which showed a yellow color (Figure 5.3). The SEM image of the TNA is shown in Figure 5.4. The top view indicates that the size of nanotube is in the range of 75~100 nm, and the tube wall thickness around 42 nm. The side view of the array indicates that the length of the tubes is within the range of 25~74 μm. The surface of tube is not as smooth as that before annealing and show some cracks. It indicates that the annealing process could damage the wall of tubes on the surface. However, the walls of inner tubes are less affected. XRD spectra (Figure 5.5) indicate that the crystal structure of TiO_2 after annealing are anatase, which has been proved to show the highest photocatalytic activity compared with other crystal forms of TiO_2 (Carp et al., 2004). The BET surface area of the catalyst is 43.12 m^2/g, which is comparable with Aeroxide® P25.

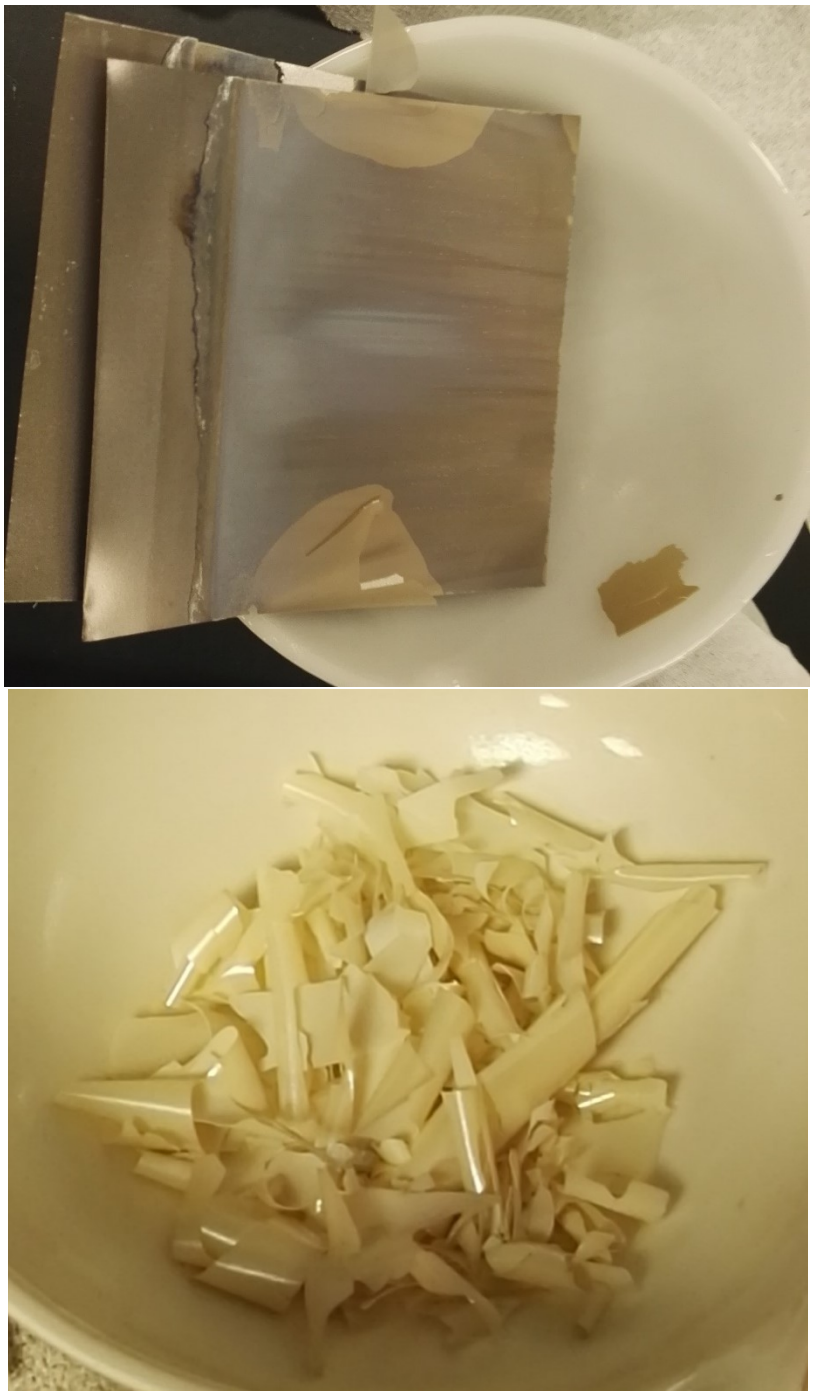

Figure 5.3 TNA film before (up) and after (down) annealing

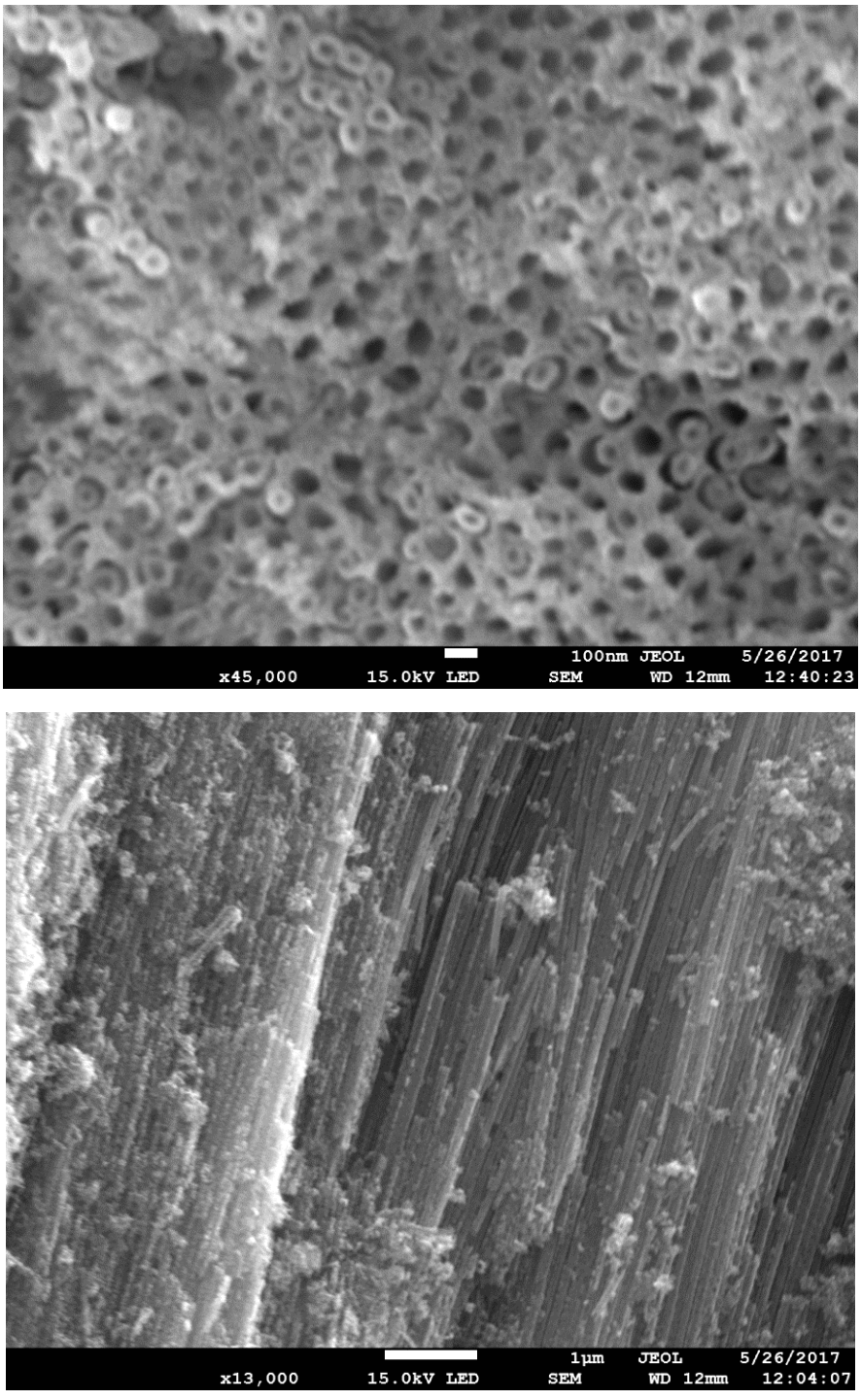

Figure 5.4 SEM image of TNA: top view (up) and side view (down)

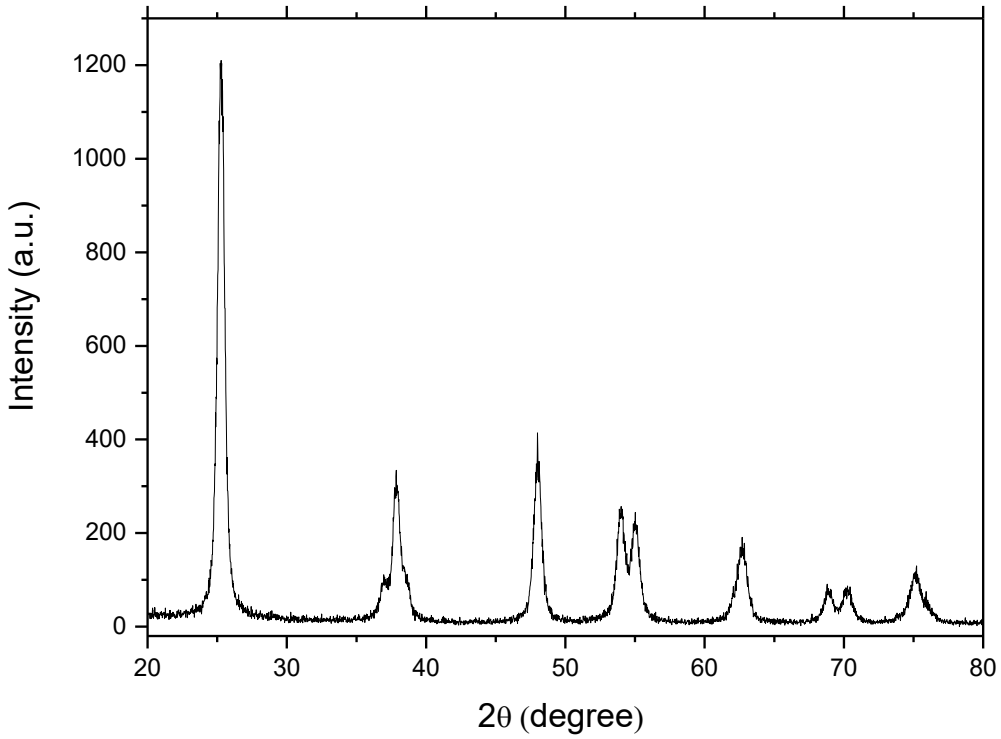

Figure 5.5 XRD spectrum of TNA

5.3.2 Characterization of OPW samples

Selected inorganic ions and other parameters were characterized. As shown in Table 5.2, the salinity of OPW is much higher than of in seawater (around 30 ppt). The major elements are sodium, potassium, chlorine, sulfur, calcium, magnesium, silicon, iron, bromine and iodine. Among which, the presence of iron, bromine and iodine would have significant effects towards the AOP processes (Chong et al., 2010; Wan and Xu, 2013; Wang et al., 2017). The pH was around neutral. The COD was not significantly changed after filtration, indicating that most of COD was from the dissolved matters in OPW. Table 5.3 lists the concentration of individual 16 PAHs in the OPW sample by GC-MS analysis. In non-spiked OPW, NAP has the highest concentration of 9.2 μg/L while PHE, BaA, BbF, BaP, BPY and IPY are less than 1 μg/L. Other organics showed in the GC chromatograph (Figure 5.6) are BETX, phenols and alkylphenols, alkyl-PAHs and alkanes, in which phenols and alkylphenols constitute the dominant components.

5.3.3 Kinetics of PAHs Degradation during Photocatalytic Oxidation

PAHs removal in the photocatalytic oxidation with different parameters was regressed with the apparent-first-order kinetics. The correlation coefficients (R^2) between the kinetic models and experimental data are higher than 0.9, indicating that the degradation of PAHs follows the apparent-first order kinetics. Therefore, the half-life times of PAHs degradation in all runs are displayed in Table 5.4 to represent the degradation efficiency in photocatalytic oxidation.

Table 5.2 Characterization of OPW

Parameters	Concentration (mg/L)
Bromine	91.1
Calcium	923
Iodine	4.23
Iron	4.49
Magnesium	70.1
Silicon	19.4
Sulfur	591
pH	7.68
Salinity	40 ppt
COD	390
DOC	55.37

Table 5.3 Concentration of PAHs in raw OPW and spiked OPW

PAHs	Raw OPW µg/L	Spiked OPW µg/L
NAP	9.20	10.20
ANY	0.00	1.00
ANA	0.00	1.00
FLU	0.00	1.00
PHE	0.76	1.76
ANT	0.00	1.00
FLT	0.00	1.00
PYR	0.00	1.00
BaA	0.84	1.84
CHR	0.00	1.00
BbF	0.25	1.25
BkF	0.00	1.00
BaP	0.12	1.12
DBA	0.00	1.00
BPY	0.04	1.04
IPY	0.10	1.10

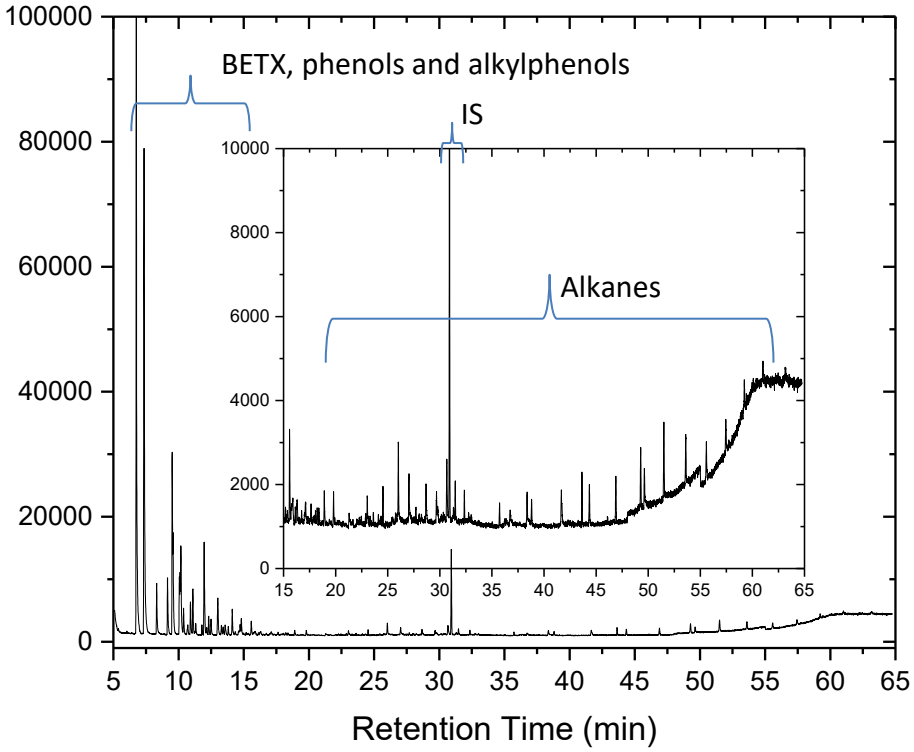

Figure 5.6 GC chromatograph of OPW

Table 5.4 The comparison of ozonation and integrated ozonation and photocatalysis on PAHs degradation (half-life time)

$t_{1/2}$ (min)	Run 1	Run 2	Run 3	Run 4	Run 5	Run 6	Run 7	Run 8	Run 9
NAP	10.77	51.54	12.41	9.15	15.70	4.04	7.63	9.28	9.68
ANY	1.90	89.90	2.73	2.08	2.15	1.60	*	*	1.18
ANA	4.76	72.50	5.08	2.95	6.25	1.81	2.46	3.30	2.78
FLU	15.92	101.19	17.49	18.48	15.71	8.76	11.04	14.96	11.78
PHE	11.56	297.49	10.73	9.90	19.98	5.73	9.39	12.01	10.29
ANT	*	22.79	3.62	2.22	4.14	1.79	2.59	2.19	2.12
FLT	12.10	90.37	12.20	10.94	18.70	7.06	12.27	12.18	11.08
PYR	8.26	93.54	8.54	7.78	12.60	4.28	9.06	9.44	8.13
BaA	7.16	34.71	6.68	5.31	9.66	*	4.70	6.18	5.79
CHR	10.49	56.26	9.80	8.62	18.02	4.83	9.42	10.70	12.54
BbF	14.65	27.78	15.01	13.80	16.86	8.80	13.28	14.83	14.55
BkF	11.03	31.29	13.00	8.69	13.53	5.43	9.62	9.80	9.83
BaP	5.53	12.59	4.12	4.27	6.74	*	2.98	4.31	4.44
DBA	9.65	31.71	11.58	8.10	13.81	4.28	8.19	9.48	12.15
BPY	13.14	35.10	13.17	10.92	22.21	6.41	8.81	13.77	20.78
IPY	8.69	27.14	8.94	8.03	14.93	4.80	7.63	9.60	11.34

Note: Runs 1 and 5-9 were UV-LED/TNA/ozonation, Run 2 was UV-LED/TNA, Run 3 was UV-LED/ozonation, and Run 4 was ozonation.

*completed degraded within 10 minutes.

5.3.4 Effect of Catalyst Dose

Before conducting the photocatalytic oxidation, the spiked OPW samples were first mixed with TNA for 30 min to reach adsorption equilibrium. The adsorption rates of PAHs on TNA are showed in Figure 5.7. In general, the affinity of PAH and TNA is weak as the average value of each adsorbed PAH is less than 20%, and the PAH with a higher molecular weight had a higher rate compared with that with a lower molecular weight. This could be due to the low solubility of PAH with a high molecular weight, which is more likely deposit on the surface of the catalysts.

Addition of catalysts can significantly increase the generation of hydroxyl radicals in AOPs (Agustina et al., 2005; Ni et al., 2007; Mehrjouei et al., 2015). Consequently, the degradation of PAHs in photocatalytic oxidation can be significantly enhanced. In this study, 0 g/L, 0.1 g/L, 0.2 g/L and 0.3 g/L of TNA were selected. The results are shown in Figure 5.8. As reported previously (Liu et al., 2016b), the introduction of catalyst enhanced the degradation of PAHs in OPW. Comparing the two levels of 0 g/L and 0.1 g/L, for example, the residue of NAP at 10 min decreases from 91% to 77%. Almost all the PAHs especially the ones with high molecular weights were fully removed within 1 hour of reaction. This result confirms a positive effect of the introduced catalyst on the AOPs systems in degrading PAHs. The removal of PAHs is further enhanced by the increase of catalyst dose. When the catalyst dose is increased to 0.2 g/L, the maximum removal rate is achieved. However, the removal rate was observed to decrease when the system was overdosed. For example, the half-life times of NAP with catalyst doses of 0 g/L, 0.1 g/L, 0.2 g/L and 0.3 g/L were determined to be 12.41 min, 10.77 min, 7.63 min

and 9.28 min, respectively. It indicates catalyst dose that catalyst dose is the limit factor when the TNA concentration is less than 0.2 g/L. Whereas the addition of TNA exceeded 0.2 g/L, the turbidity of water sample increases, causing the attenuation of UV-A light intensity, consequently leads to the decrease of overall removal rate. Therefore, for this experiment, the optimum dose of TNA is 0.2 g/L.

The evaluation of PAH residues on TNA after treatment can help to understand the removal of total PAHs and the desorption behavior of PAHs on TNA. The presence of insoluble matters in OPW would interfere the analytical results of PAHs in the filtrate (insoluble matters and TNA) after treatment. It was found that the filtrate of OPW contributed only a small amount of COD and had limited effect on the overall degradation of PAHs (Liu et al., 2016b). Therefore, the OPW samples were filtrated prior to the photocatalytic ozonation to minimize the effect of insoluble matters.

The PAH residue absorbed on TNA and remained in the OPW sample after photocatalytic ozonation are illustrated in Figure 5.9 and Figure 5.10 respectively. In general, the partition of PAHs in OPW sample and on the TNA surface should be a constant at equilibrium stage, which means that the PAH residues absorbed on TNA should correlate to the concentration of PAHs in OPW samples. As the removal efficiency increasing, PAHs especially for those with high molecular weights were still detected on TNA after treatment, even when their concentrations in OPW samples were lower than the detection limit.

The photocatalytic ozonation is a 2-stage treatment process, which involves the adsorption followed by the oxidation. PAHs showed fast adsorption/deposition on TNA in the adsorption stage. In the oxidation stage, the introduction of ozone started to oxidize the PAHs both in OPW and on the TNA surface. The oxidation of PAHs was overwhelmed by the dynamic exchange of PAHs between adsorption and desorption, and the degradation in OPW had a much higher rate than that on the TNA surface due to a higher mass flux rate. Therefore, the concentration of PAHs in OPW decreased to an undetectable level, whereas PAH residues still existed on the TNA surface. The solubility of PAHs plays an important role during this process. PAHs with high molecular weights (> 3 rings) are less soluble than those with lower molecular weights (Pearlman et al., 1984), and thus are more likely to be deposited/absorbed onto the TNA surface and less prone to re-dissolving in water. It can be confirmed by comparing with the PAHs with low molecular weights (e.g., NAP, ANY and ANA), the amounts of which adsorbed on TNA are negligible no matter how their high concentrations are in the water phase.

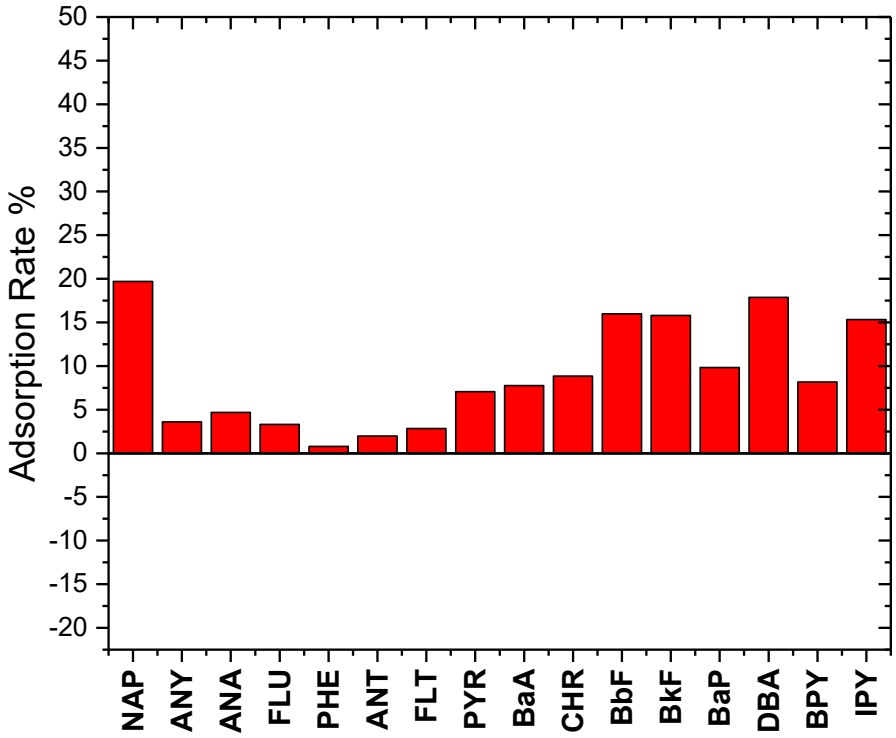

Figure 5.7 Adsorption rates of PAHs on TNA before photo-oxidation

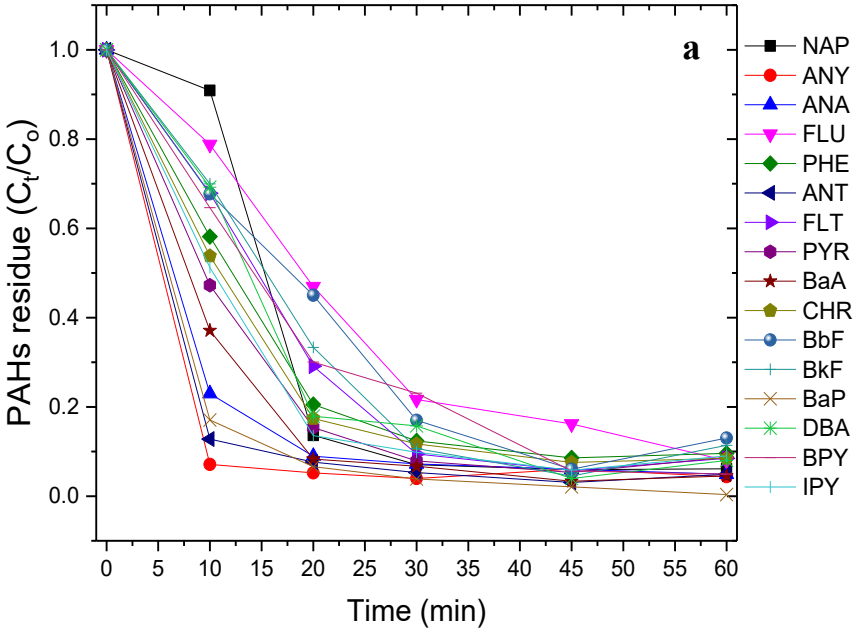
a
PAHs residue (C_t/C_o)
Time (min)
NAP
ANY
ANA
FLU
PHE
ANT
FLT
PYR
BaA
CHR
BbF
BkF
BaP
DBA
BPY
IPY

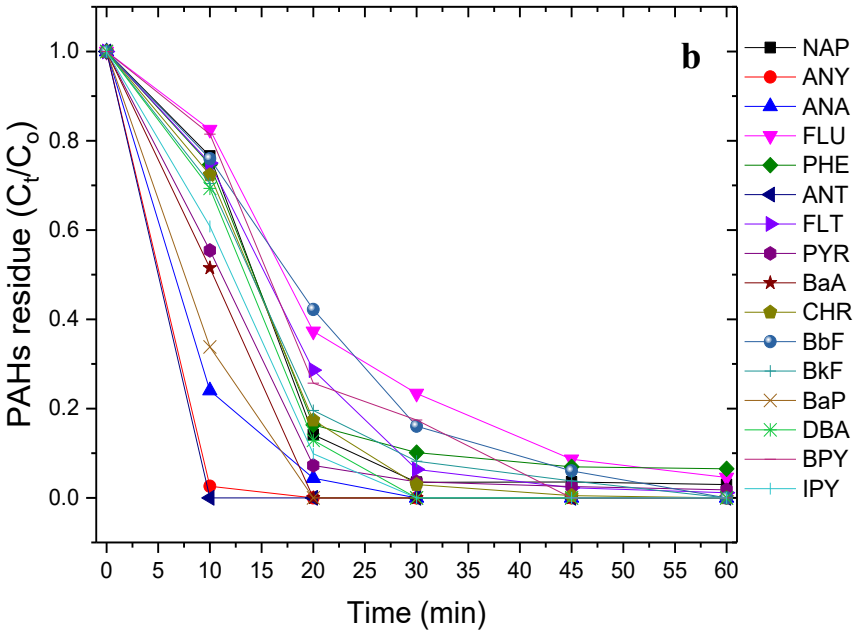
b
PAHs residue (C_t/C_o)
Time (min)
NAP
ANY
ANA
FLU
PHE
ANT
FLT
PYR
BaA
CHR
BbF
BkF
BaP
DBA
BPY
IPY

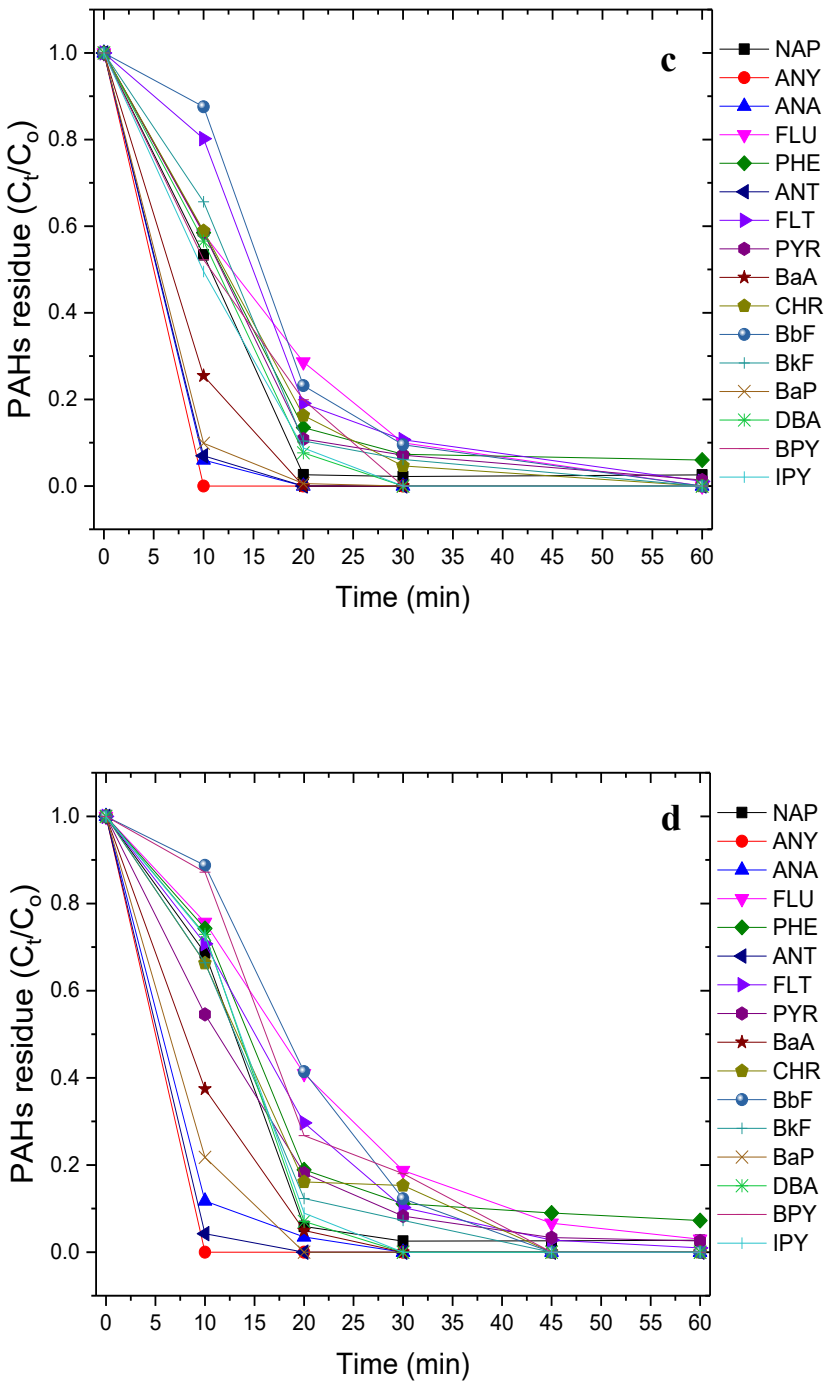

Figure 5.8 Effect of catalyst dose to photocatalytic ozonation at TNA concentration of 0 g/L (a), 0.1 g/L (b), 0.2 g/L (c) and 0.3 g/L (d).

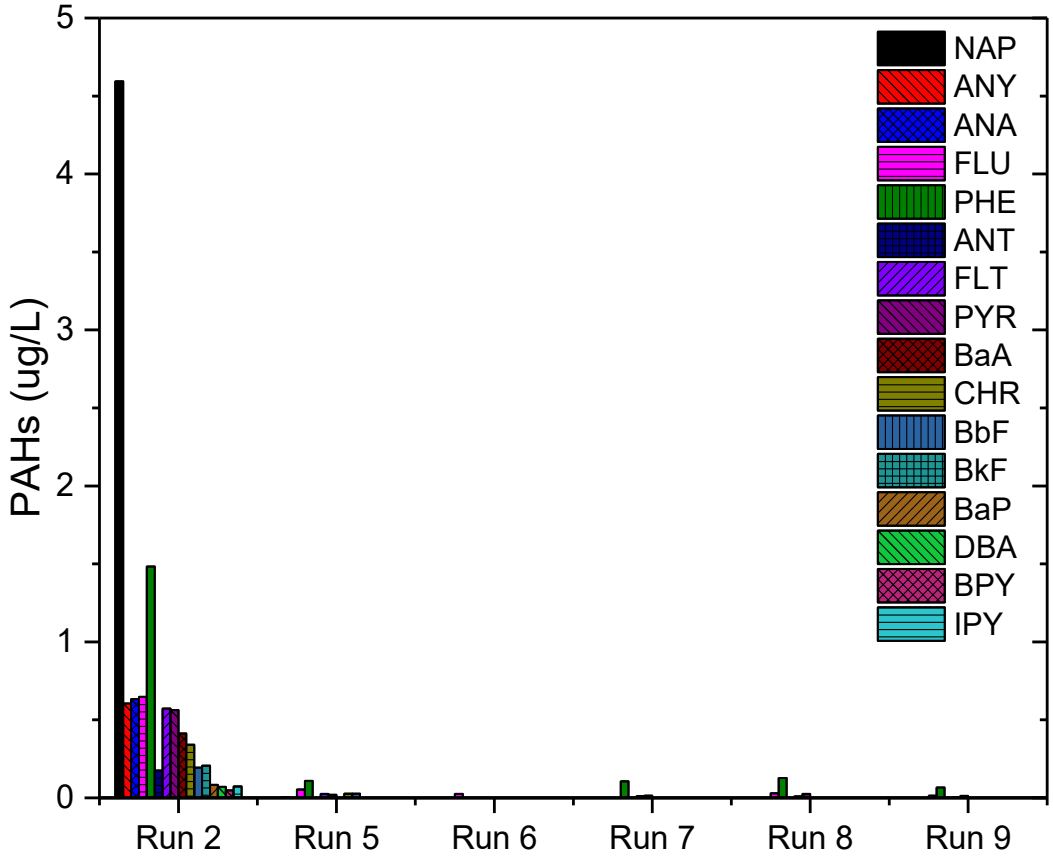

Figure 5.9 PAH residues in OPW sample after 1 hour photocatalytic ozonation. (no catalyst was added in Runs 3 and 4)

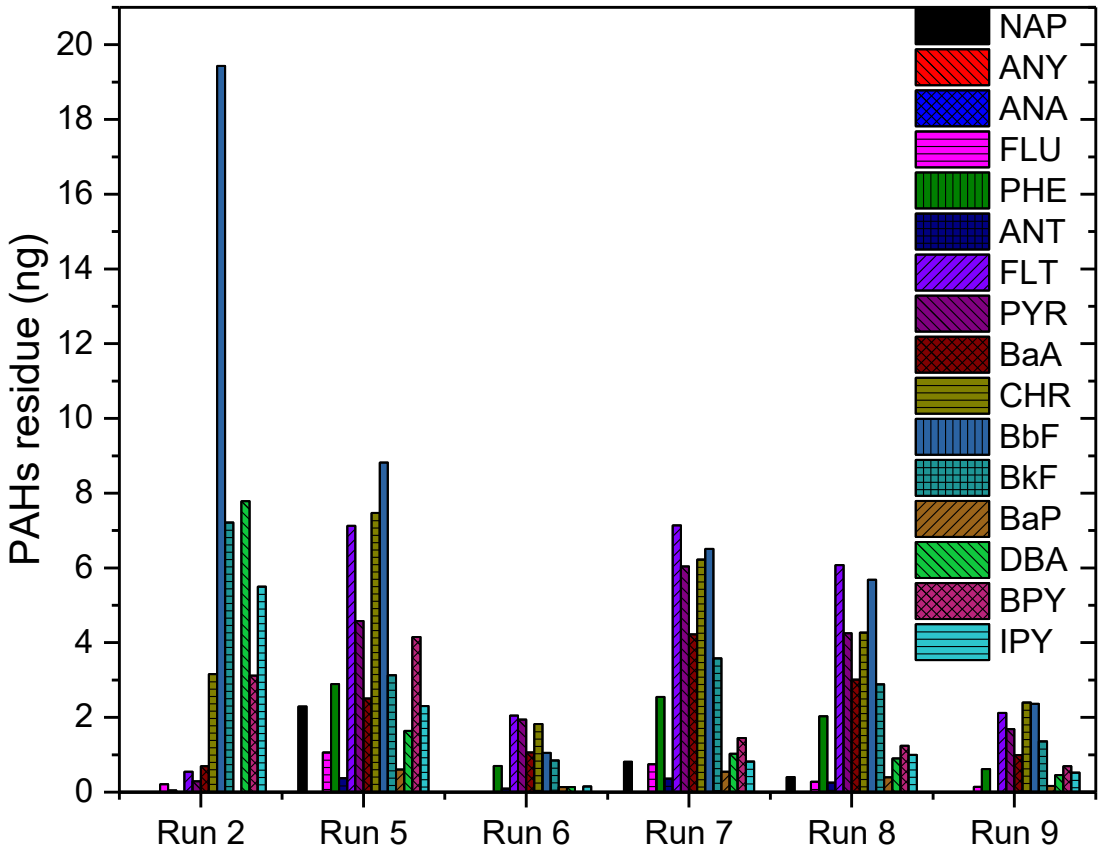

Figure 5.10 PAHs residues on TNA after 1 hour photocatalytic ozonation. (no catalyst was added in Runs 3 and 4)

The relationships between the catalyst dose and PAH residues was observed to as follows: 1) when the initial concentration of PAHs was fixed, the addition of more catalyst increased the total adsorbed PAHs but decreased the uptake per mass of catalyst; 2) the catalyst dose affected the degradation rate of PAHs thus changed the total concentrations of remaining PAHs in water and the residues on catalyst surface. Analysis of the residues on catalyst with different catalytic doses showed that 0.3 g/L has a low level of total PAHs. It indicates that the increase in catalytic dose could slowly promote the degradation of PAHs attached to the catalyst surface.

5.3.5 Effect of Light Intensity

The light flux of UV-LED was measured by a ferrioxalate actinometer using the equation as follows.

$$I = \Delta n/(10^{-3} \cdot \emptyset \cdot V \cdot t) \quad (5.1)$$

where the unit of I is the light flux (Einstein/L/s); Δn is the ferrous iron photo-generated (mole); $\emptyset$ is the quantum yield and 1.21 was used (Kuhn et al., 2004); V is the irradiated volume (mL); and t is the irradiation time (s).

For example, when the working voltage of UV-LED was 35 V, the light flux was 2.56×10^{-5} Einstein/s. The light intensity of UV-LED under different forward currents was detected by a UVP intensity meter with a 365nm radiometer sensor. The result (Figure 5.11) showed that the natural logarithm of light intensity has a linear relationship to the natural logarithm of DC current with a regression coefficient (R^2) of 0.997. At 35 V, the forward current was 0.39 Amp, and the light intensity of UV-LED was 7.88 mw/cm^2. To

compare these with the results form actinometer, mw/cm^2 need to be converted to Einstein/s by applying a coefficient 3.26 ×10^{-6} Einstein/s/(mw/cm^2). At 34 V and 36 V, the forward currents were 0.224 Amp and 0.48 Amp, respectively. Correspondingly, the light flux was 1.38 × 10^{-5} Einstein/s and 3.23 × 10^{-5} Einstein/s, respectively.

UV-A enhanced ozonation has been studied by many researchers and proved to have a higher degradation efficiency compared with ozonation only (Beltran et al., 1995; Pengyi et al., 2003; Agustina et al., 2005; Beltrán and Rey, 2017). It was demonstrated that UV-A could increase the generation of hydroxyl radicals by irradiating OH^- and ozone. However, the kinetics in this study suggest a process more complicated than those previously reported. For example, as shown in Figure 5.12 (a) and (b), the half-life time of NAP was increased from 9.15 min under ozonation to 12.4 min under UV+ozonation. At 10 min, the concentrations of PAHs by UV assisted ozonation were higher than those by ozonation, leading to the decreasing slopes of PAH degradation in the range of 0 to 10 min. The reduction of these slopes has a dominant effect on the reduction of the reaction rate constants of the apparent-first order kinetics. However, the removal rate of PAHs after 20 min was increased, implying that the generation of oxidative radicals (hydroxyl radical etc.) was increased in the presence of UV.

A similar trend was observed in photocatalytic ozonation as well. The UV irradiation did not promote the degradation of PAHs in the first 20 min. Then the increase of light intensity exerted a positive effect on the reduction of the PAH residues both in the OPW samples and on the TNA surface.

In other studies, enhancement of UV-A in photocatalytic ozonation was reported and most of them were done by using the distilled water matrix (Beltrán et al., 2005b; Yıldırım et al., 2011), which did not have such a complex composition as OPW. Meanwhile, the wavelength of irradiation light could also contribute to the influence on the removal rate. The previous studies on the removal of PAHs in OPW by UV-C enhanced ozonation also showed the enhancement of UV-C treatment efficiency during the whole period (Rubio-Clemente et al., 2014). Therefore, the decrease of PAHs removal rate at the early stage should be attributed to the matrix of OPW.

The mechanism of UV-C enhanced ozonation has been well studied and described below (Rubio-Clemente et al., 2014):

$$O_3 + H_2O \xrightarrow{h\nu} 2HO\cdot + O_2 \rightarrow H_2O_2 + O_2 \qquad (5.2)$$

$$H_2O_2 \xrightarrow{h\nu} 2HO\cdot \qquad (5.3)$$

The generated hydroxyl radical has a higher oxidation power than ozone and a much higher reaction rate with the target compounds such as PAHs (Hoigne and Bader, 1976; De et al., 1999; Cheng et al., 2016). UV-A was poorly absorbed by both ozone and H_2O_2. The generation of hydroxyl radical is thus limited compared to the process occurring under UV-C irradiation, in which causes the insignificant enhancement on the removal of PAHs (Beltrán et al., 2005b) .

In addition, the OPW contains an abundance of halides which could significantly interfere the oxidation of organics in AOP system. Iodide for example, can react with both ozone and hydroxyl radical to produce less oxidative species:

$$I^- + O_3 \rightarrow IO^- + O_2 \quad (5.4)$$

$$IO^- + I^- + 2H^+ \rightarrow I_2 + H_2O \ (5.5)$$

$$I_2 + I^- \rightarrow I_3^- \ (5.6)$$

$$I^- + HO\cdot \rightarrow I\cdot + HO^- \ (5.7)$$

I_3^- and I_2 strongly absorb on UV and visible light, especially the molar absorptivity of UV-A by I_3^- can reach as high as 25,800 $M^{-1}cm^{-1}$ (Wan and Xu, 2013).

$$I_3^- \xrightarrow{h\nu} [I_3^-]^* \rightarrow I_2^{-\cdot} + I^{\cdot} \ (5.8)$$

The generated radicals have been recognized as a strong reagent to react with ozone, therefore, there is a continuous deduction of ozone under the UV-A irradiation.

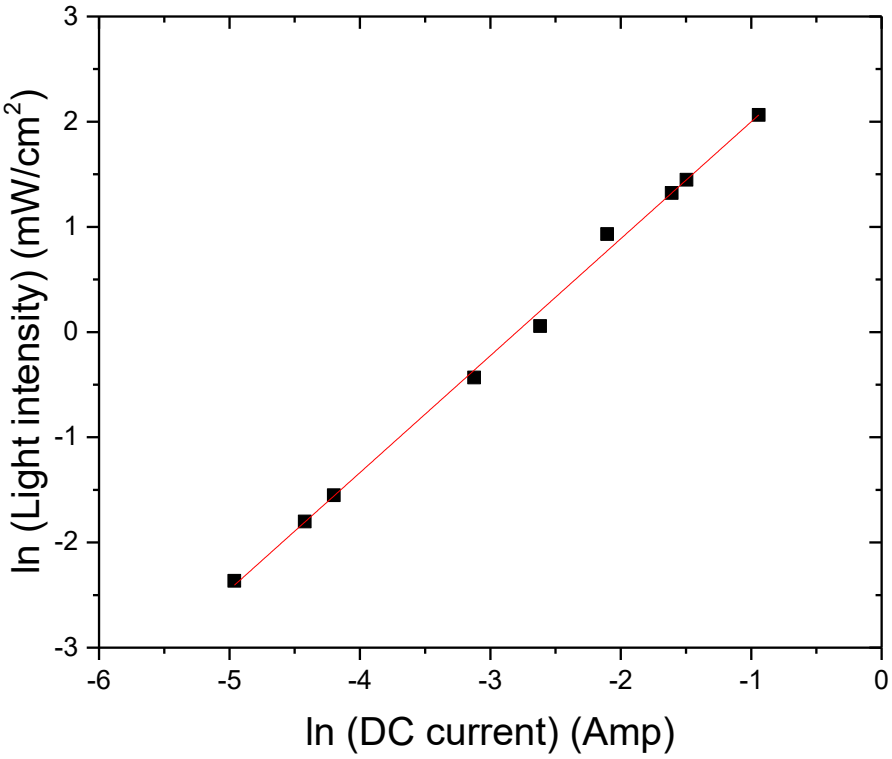

Figure 5.11 Linear regression of ln(light intensity) and ln(DC current)

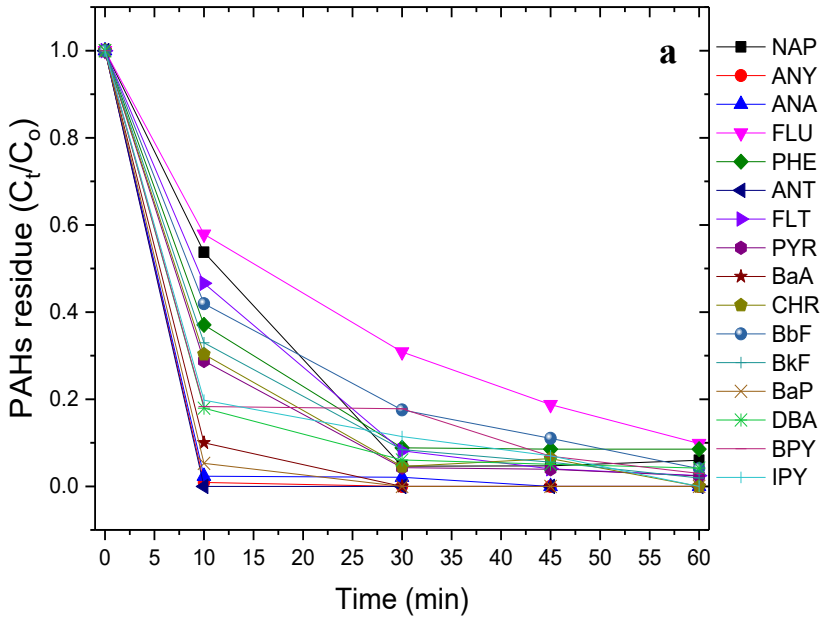
a
PAHs residue (C_t/C_o)
Time (min)
NAP
ANY
ANA
FLU
PHE
ANT
FLT
PYR
BaA
CHR
BbF
BkF
BaP
DBA
BPY
IPY

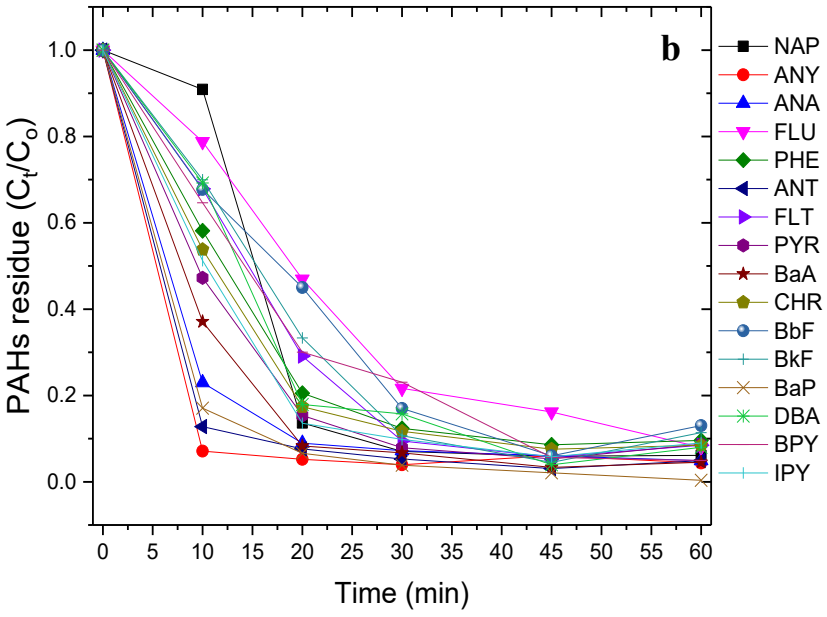
b
PAHs residue (C_t/C_o)
Time (min)
NAP
ANY
ANA
FLU
PHE
ANT
FLT
PYR
BaA
CHR
BbF
BkF
BaP
DBA
BPY
IPY

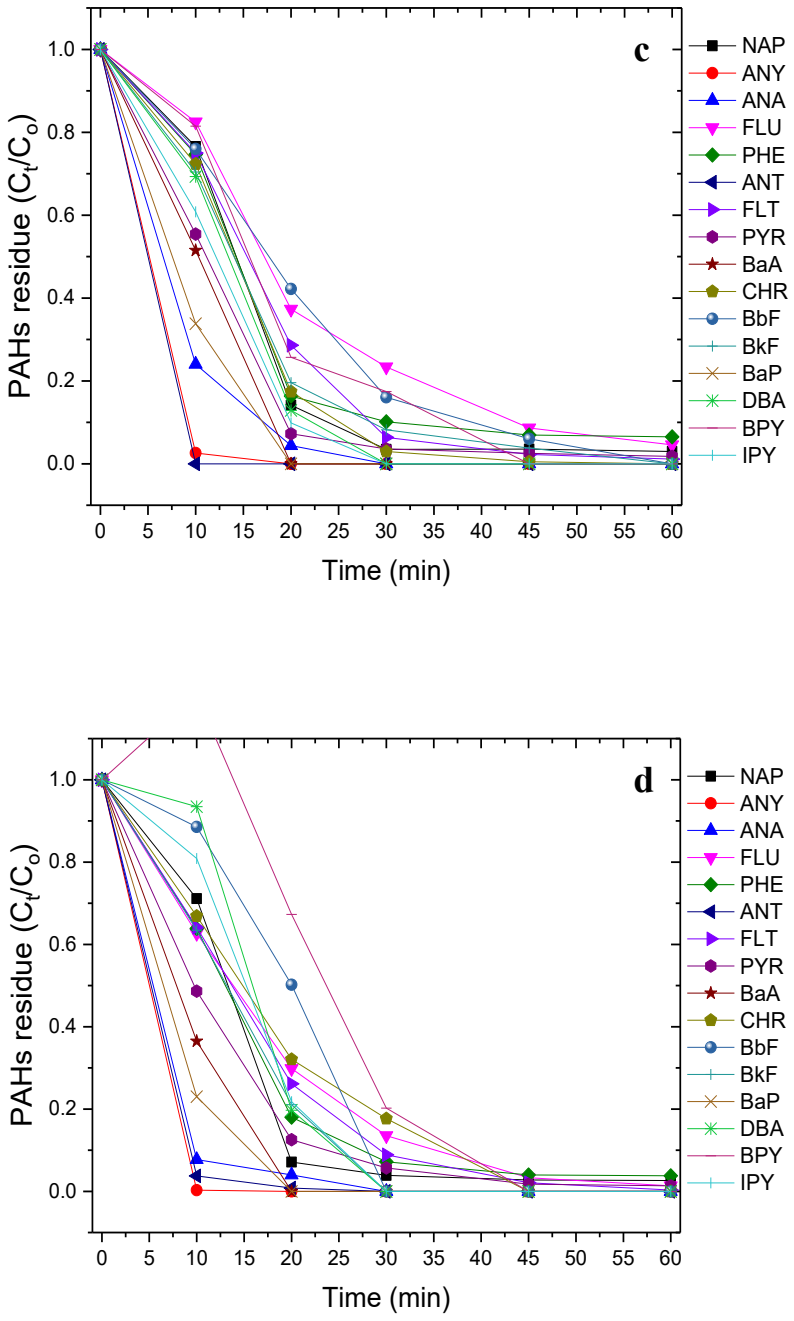

Figure 5.12 Effect of light intensity to ozonation at 0 Einstein/s (a) and 1.38×10^{-5} Einstein/s (b) and photocatalytic ozonation at 1.38×10^{-5} Einstein/s (c) and 3.23×10^{-5} Einstein/s (d).

5.3.6 Effect of Ozone Dose

The ozone dose is a dominant factor in the photocatalytic ozonation process.

Figure 5.13 indicates that the direct reaction between O_3 and PAHs would be significant. The ozone doses from 0-15 ppm have been tested. Strong enhancement on the degradation rates of PAHs was observed in the cases where ozone was used: the half-life times of PAHs with ozone was reduced to 2-63% compared with the reaction without ozone. The PAHs with low molecular weights (< 4 rings) are more vulnerable to ozonation. The average enhancement on the removal rates of these PAHs ranges from 3 to 40 times, in which NAP has the lowest rate and ANY the highest. For PAHs with 4 rings (FLT, PYR, BaA and CHR), the enhancement of degradation was less, only in the range of 3-7 times. Relatively weak enhancement on removal rates was found for the PAHs with the number of rings more than 4, ranging from 1 to 2 times. A possible reason for this could be that PAHs have relatively low solubility which reduces their mobility and result in low contact rate with ozone.

Phenols present in the system are the greatest competitor to PAHs in the photocatalytic degradation process, since they can react both ozone and hydroxyl radicals efficiently (Figure 5.14). The concentration of phenols was slightly changed during photocatalysis, compared with a clear decrease of PAHs, especially for those with higher molecular weights. Addition of ozone significantly accelerated the degradation of phenols, resulting the complete degradation of phenols within 10 min. Comparing the degradation of PAHs in the same run, photocatalytic ozonation showed a stronger preference for degrading phenols. It is probably because phenols have higher solubility and hence more

opportunities to react with ozone. The degradation of PAHs was also accelerated by ozone but in a lower degree in comparison with that of phenols. The key reason is that the synergetic effect of ozone and photocatalysis leads to more hydroxyl radicals being generated, which enhance degradation of organics (Mehrjouei et al., 2015). Therefore, most of PAHs in the OPW sample were removed by more than 90% within 20 min at the ozone dose of 15 ppm.

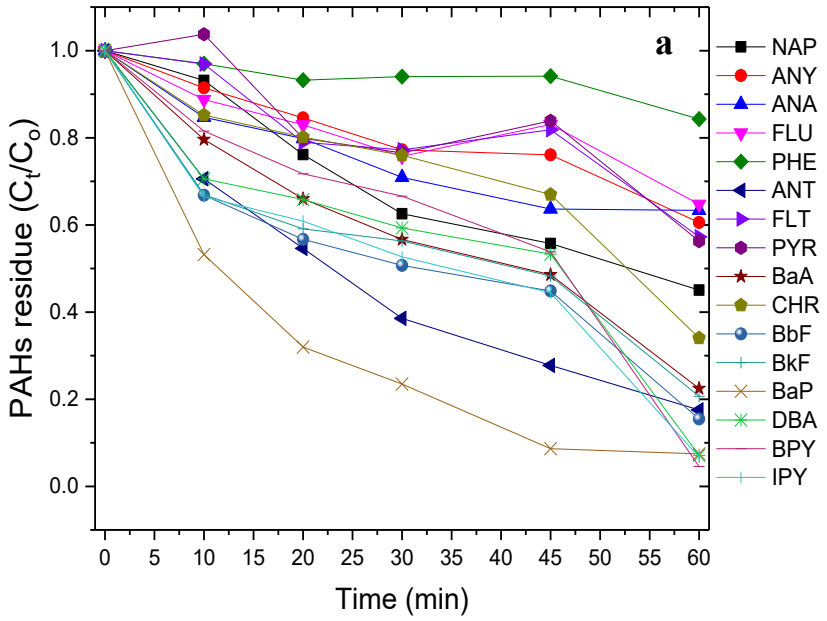
a
PAHs residue (C_t/C_o)
Time (min)
NAP
ANY
ANA
FLU
PHE
ANT
FLT
PYR
BaA
CHR
BbF
BkF
BaP
DBA
BPY
IPY

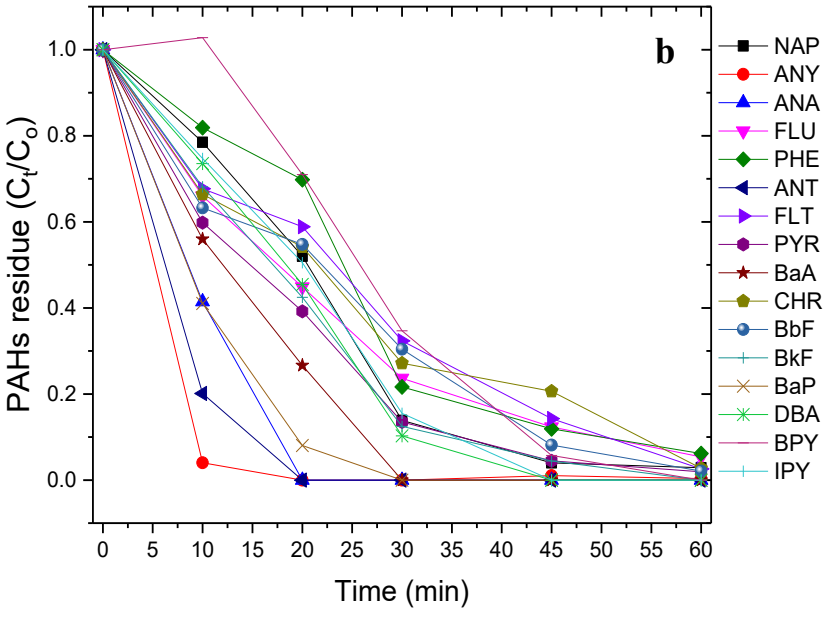
b
PAHs residue (C_t/C_o)
Time (min)
NAP
ANY
ANA
FLU
PHE
ANT
FLT
PYR
BaA
CHR
BbF
BkF
BaP
DBA
BPY
IPY

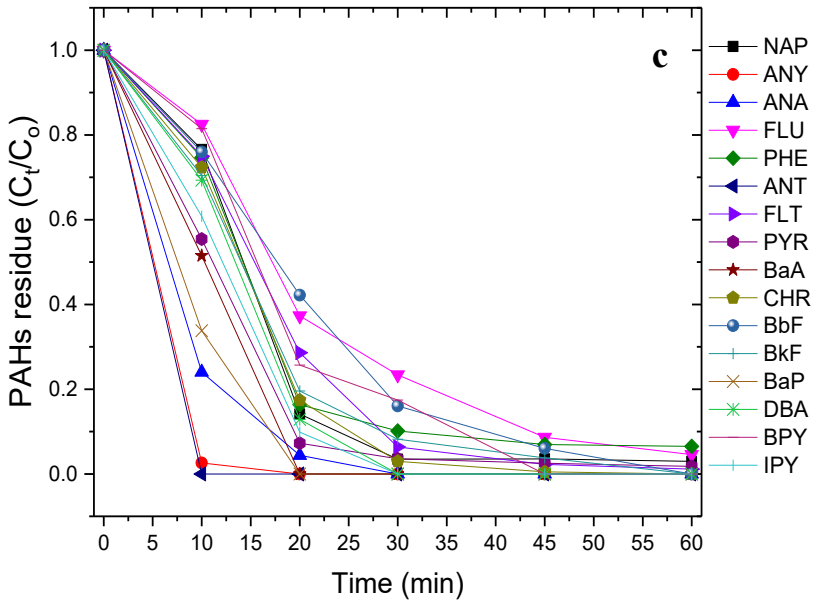

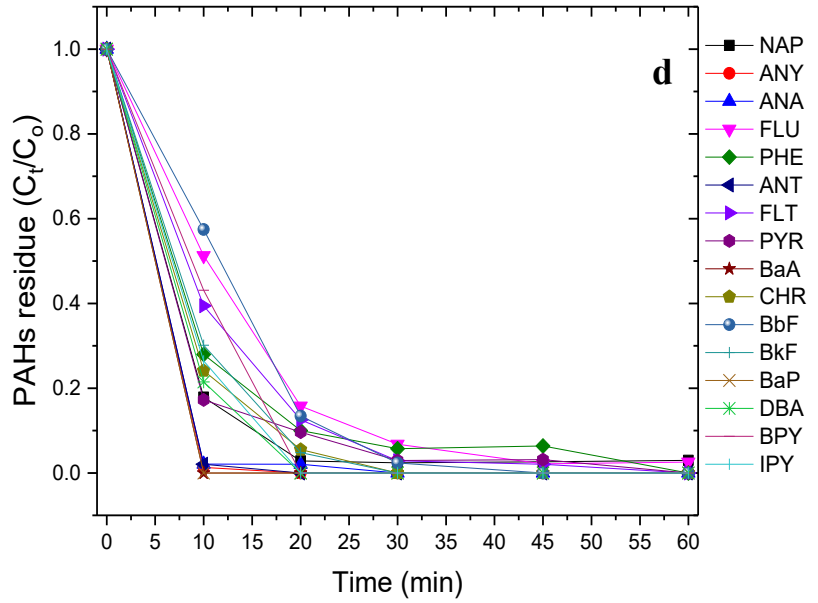

Figure 5.13 Effect of ozone dose to photocatalytic ozonation at 0 ppm (a), 5 ppm (b), 10 ppm (c) and 15 ppm (d).

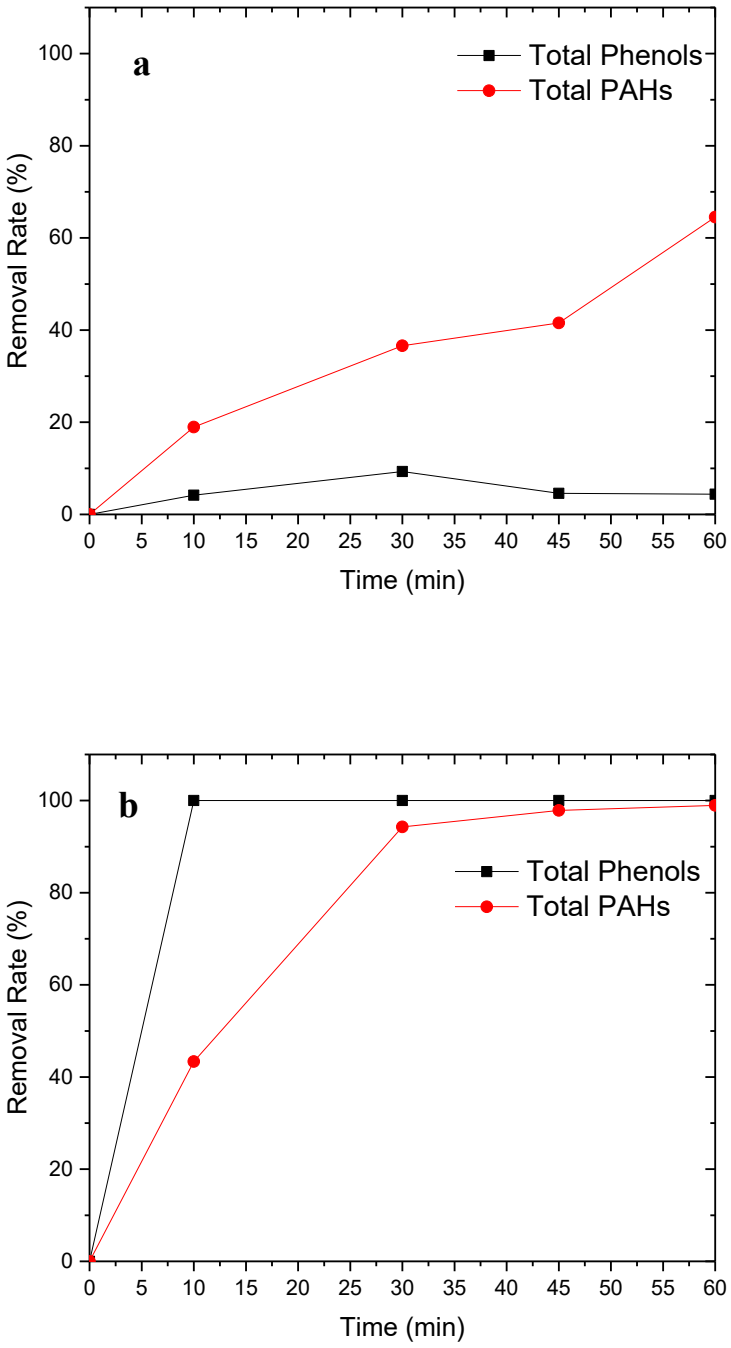

Figure 5.14 Degradation of PAHs and phenols a) without ozone and b) with ozone

5.4 Summary

In this chapter, a novel method that integrates photocatalytic ozonation, UV-LED and TNA was developed. Through its application to OPW treatment, comprehensive evaluation was conducted on the kinetics of PAHs degradation and the effects of catalyst dose, light intensity and ozone dose.

The experimental results agreed with the the apparent-first-order kinetics. The half-life times of PAHs in most of runs were less than 20 min, proving that the proposed photocatalytic ozonation method is highly efficient in degrading the PAHs in OPW.

The TNA catalyst shows the advantage of easy handling without scarifying its surface area. The surface area of TNA is comparable to that of the commercial TiO_2 nano-particles (e.g. Aeroxide® P25). By introducing TNA, the adsorption and degradation rates of PAHs with high molecular weights were found to be greater than those with low molecular weights, indicating that the oxidation of these PAHs more likely happens on the catalyst surface. Increasing catalyst dose could cause the degradation rate to increase at the early stage and later to decrease mainly due to the increase of turbidity. The optimal catalyst dose was determined at 0.2 g/L for the studied system.

The light intensity has a negative effect on the treatment system when using UV-A as the light source, which accelerates the generation of iodine radicals. The radical acts a strong ozone scavenger thus significantly reduces the concentration of ozone in the system. The removal rates could be consequently reduced especially on which the ozone dose is a limiting factor.

The increase of ozone dose promotes in the photocatalytic ozonation of PAHs. It was found that ozonation was more effective in removing the aromatic compounds with relatively high water solubility, such as PAHs with less rings and phenols. Further, ozone favors to the phenol oxidation. In this case, the process might be more economically efficient if a higher dose of ozone is applied in the system at the beginning to remove phenols, which are competitors to PAHs in photocatalytic degradation. After removal of phenols, the dose of ozone can be lowered and coupled with photocatalysis to save the cost treatment.

Chapter 6 Degradation Pathways, Toxicity and Biodegradability of Offshore Produced Water Treated by Photocatalytic Ozonation[5]

[5] *The contents of this chapter are based and expanded on the following manuscript:*

Liu, B., Chen, B., Zhang, B.Y., Lee, K. (2018) Photocatalytic Ozonation of Offshore Produced Water by TiO_2 Nanotube Arrays Coupled with LED-UV Irradiation. *Environmental Science and Technology*, to be submitted.
Role: Bo Liu solely worked on this study and acted as the first author of this manuscript under Dr. Bing Chen and Dr. Baiyu Zhang's guidance. Most contents of this paper were written by him and further edited by the other co-authors.

6.1 Background

The effectiveness and the applicability of photocatalytic ozonation were determined not only by the degradation of target contaminants, but also by their impacts on the reduction of toxicity to the marine ecosystem and on the improvement of biodegradability. Some studies have reported that the oxygenated aromatics (e.g., hydroquinone, oxy-PAHs) generated during the AOPs might increase the toxicity of effluent (de Torres-Socías et al., 2013; Enguita and Leitao, 2013; Erjavec et al., 2016). Further, the introduction of ozone could increase the acute toxicity and mutagenic activity of treated water if halogen ions were present (Von Gunten, 2003; Huang et al., 2009). Therefore, it is important to examine the change of OPW composition during the photocatalytic ozonation process and the corresponding toxicity, which would help optimize the process to ensure both the efficacy of hazardous matter removal and the diminishment of secondary pollutants. In this chapter, the intermediates generated during the photocatalytic ozonation and their correlated toxicity were investigated. Further, the changes of the biodegradability of OPW with/without photocatalytic ozonation were evaluated.

6.2 Materials and Methods

6.2.1 Materials

The standard solution 16 PAHs (500 μg/mL) was purchased from Agilent (USA). The internal standard (IS) o-terphenyl and titanium foil (≥99.5%, 0.125 mm thickness) were purchased from Sigma-Aldrich (Canada). Acetone (Honeywell Burdick and Jackson, USA) and dichloromethane (Honeywell Burdick and Jackson, USA) were used for preparing stock solutions and aqueous sample extraction. The nutrients including

potassium dihydrogen orthophosphate, dipotassium hydrogen orthophosphate, disodium hydrogen orthophosphate dihydrate, ammonium chloride, calcium chloride, magnesium sulfate and iron (III) chloride hexahydrate were purchased from Sigma-Aldrich (Canada). Distilled water was produced on-site from a double fused-silica distillation unit. Seawater was obtained from a harbor in the Newfoundland offshore. OPW samples were obtained from the local offshore platforms in the North Atlantic. Detailed information cannot be provided here due to client confidentiality and non-disclosure.

6.2.2 Photocatalytic Ozonation of OPW

The experimental conditions for the photocatalytic ozonation of OPW were the same as those described in Chapter 5 (Table 5.1).

6.2.3 Analysis of Intermediates

The analysis of water samples was conducted following the methods introduced in Chapter 5. The intermediates formed during catalytic degradation reactions were identified by GC-MS using the Agilent ChemStation software. The relative concentration of each individual intermediate was determined by the ratio between the peak area of intermediate relative to that of IS.

6.2.4 Toxicity and Biodegradability Tests

Microtox® toxicity test was undertaken to evaluate the acute toxicity of raw and treated OPW samples. Samples were evaluated by a 4-level dilution method recommended by the manual. The median effective concentration (EC_{50}) of treated/untreated produced water samples (% V/V) to *Vibrio Fisheri* were used as the indicators. The readings at 5

min and 15 min were recorded and calculated. Biodegradability tests included a 5-day close-bottle biodegradation oxygen demand (BOD) test and a 28-day biodegradability test by recording the oxygen uptake rate (OUR) from AER-208 Aerobic/Anaerobic respirometer. The two tests were based on the Organization for Economic Co-operation and Development (OECD) Method 306 (OECD, 1992).

6.3 Results and Discussion

6.3.1 Degradation Pathways and Intermediates

The degradation of organics in OPW reduces the COD and dissolved organic carbon (DOC) (Figure 6.1). However, the removal of both COD and DOC was relatively slow compared with the degradation of PAHs. In the degradation of PAHs, the intermediates formed were and analyzed detected by GC-MS. The formation of catechol, hydroquinone and benzoquinone indicates the pathways of degradation involve oxidation steps. Generally, the oxidation of aromatic compounds was through the electrophilic substitution. For example, the benzene was oxidized into phenols and then catechol, hydroquinone and *p*-benzoquinone etc. (Huang and Shu, 1995; Beltrán et al., 2005a). Then the aromatic ring was broken to form ketone, aldehyde and carboxyl acids (Huang and Shu, 1995). PAHs degrade through a similar pathway (Yao et al., 1998; Von Gunten, 2003; Beltrán et al., 2005b): OH substitution, ring cleavage and release of ketone, aldehyde and carboxylic acids. By this path, PAHs could lose the rings and be transformed into simpler organic compounds. In the OPW, however, due to the relatively low concentration of PAHs, the peaks of the oxy-PAHs in GC-MS results were not as obvious as those of the intermediates generated from phenols.

Figure 6.2 shows the change of intermediates in Run 1 over time. Many iodized intermediates were observed at 10 min. It indicates that the iodide in OPW plays an important role at this stage. The generated iodine radical completed with the ozone and hydroxyl radical to substitute the H atom on aromatic rings. It therefore altered the oxidation pathways (Figure 6.3). All the intermediates with aromatic rings were further depleted. The formation of iodoform and dibromo-pentane was also observed. At this stage, the cleavage of aromatic rings formed ketones, aldehydes and carboxylic acids. The appearance of iodoform may suggest the presence of ketones, aldehydes, carboxylic acids and alcohols, which could react with iodine and form iodoform as a main product.

A clearer trend was observed at relatively low ozone dose (Figure 6.4): H atom substitution at the first 10 min, then ring cleavage and haloform reaction at 20 min, and the concentration of iodoform reached its peak at 30 min. After 30 min, iodide was oxidized into iodate, which is less reactive and would not compete with ozone and hydroxyl radicals.

Bromine radicals were clearly involved in free-radical chain reactions during the treatment as the formation of brominated short-chain hydrocarbons (e.g. dibromo-pentane) at 30 min.

$$R - H + 2\,Br \cdot\!\rightarrow R - Br + HBr \qquad (6.1)$$

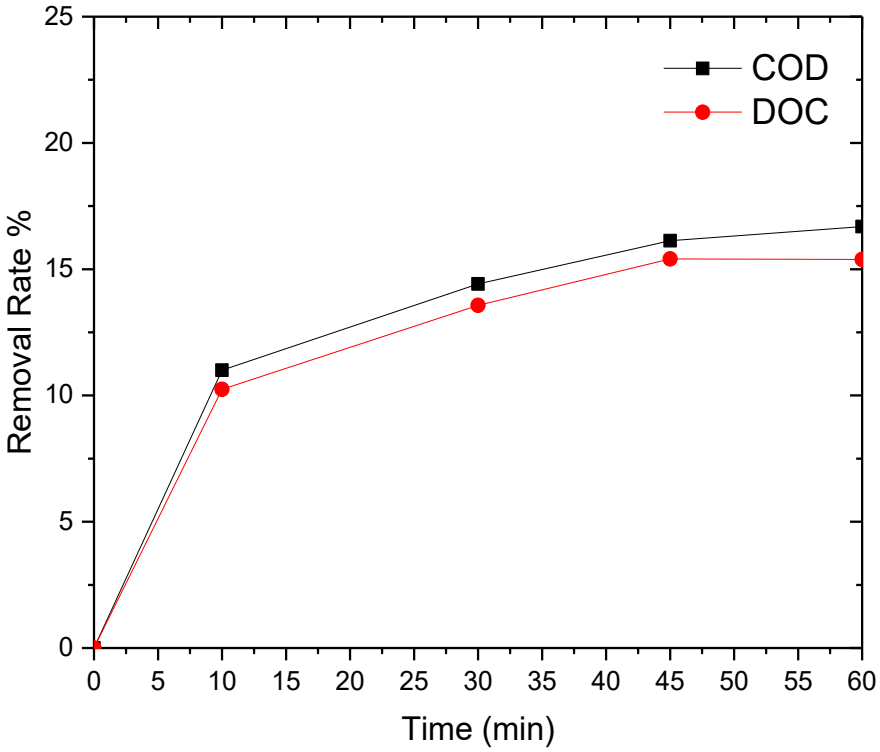

Figure 6.1 Change of COD and DOC during the photocatalytic ozonation (Run 5)

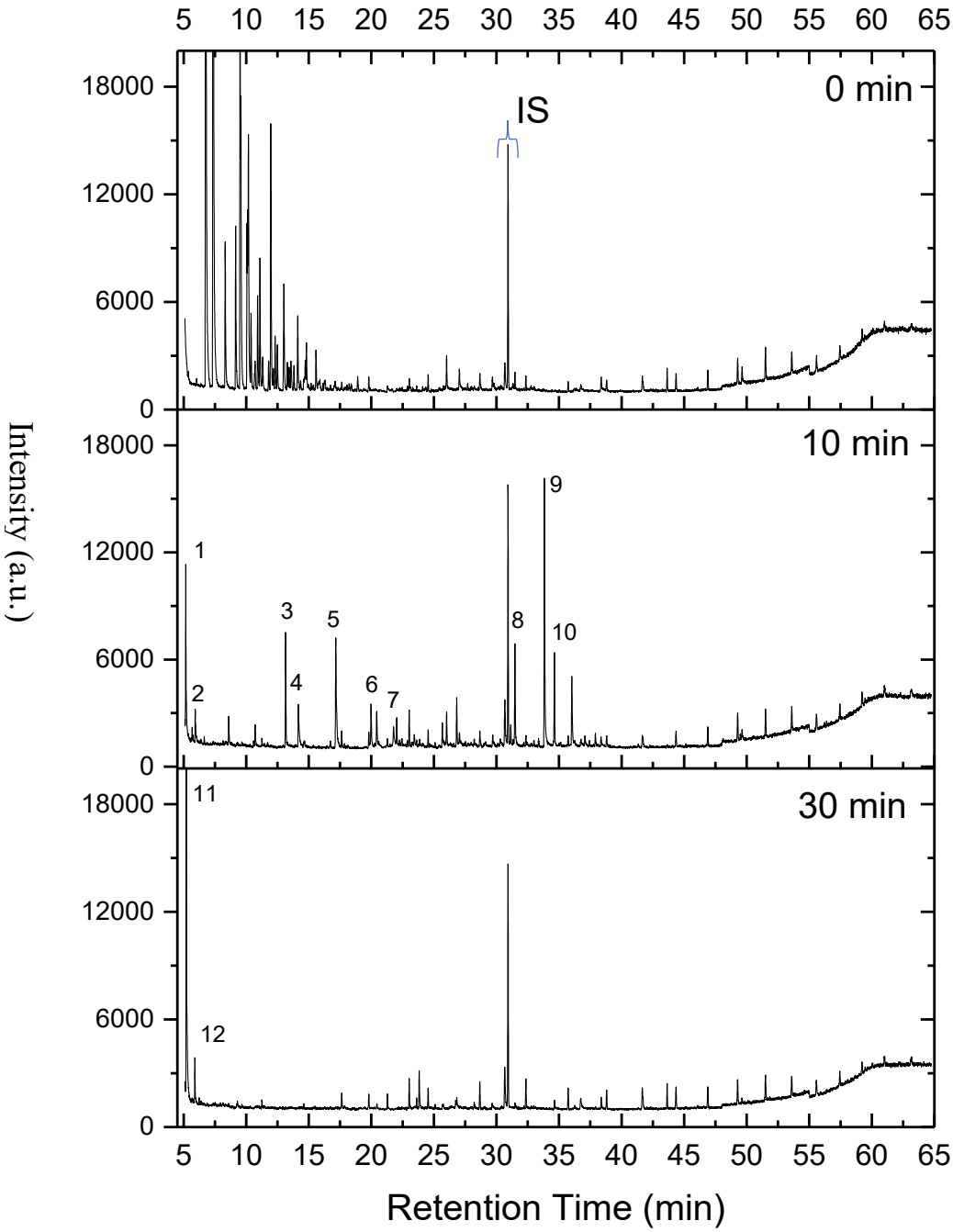

Figure 6.2 Detection of intermediates during photocatalytic ozonation 1) alkanol, 2) alkyl q-benzoquinone, 3) triiodomethane, 4) 2 iodo-4 methyl phenol, 5) 2-iodo-1-methoxy-4-methyl-benzene, 6) 4-methyl benzoic methyl ester, 7) 1,3-benzenediol, 4-iodo, 8) benzoic acid, 3,5 bis(1,1-dimethylethyl)-4-hydroxy-,methyl ester, 9) 2,6-diiodohydroquinone, 10) phenol, 2,4,6-triiodo, 11) dibromo pentane and 12) tribromomethane

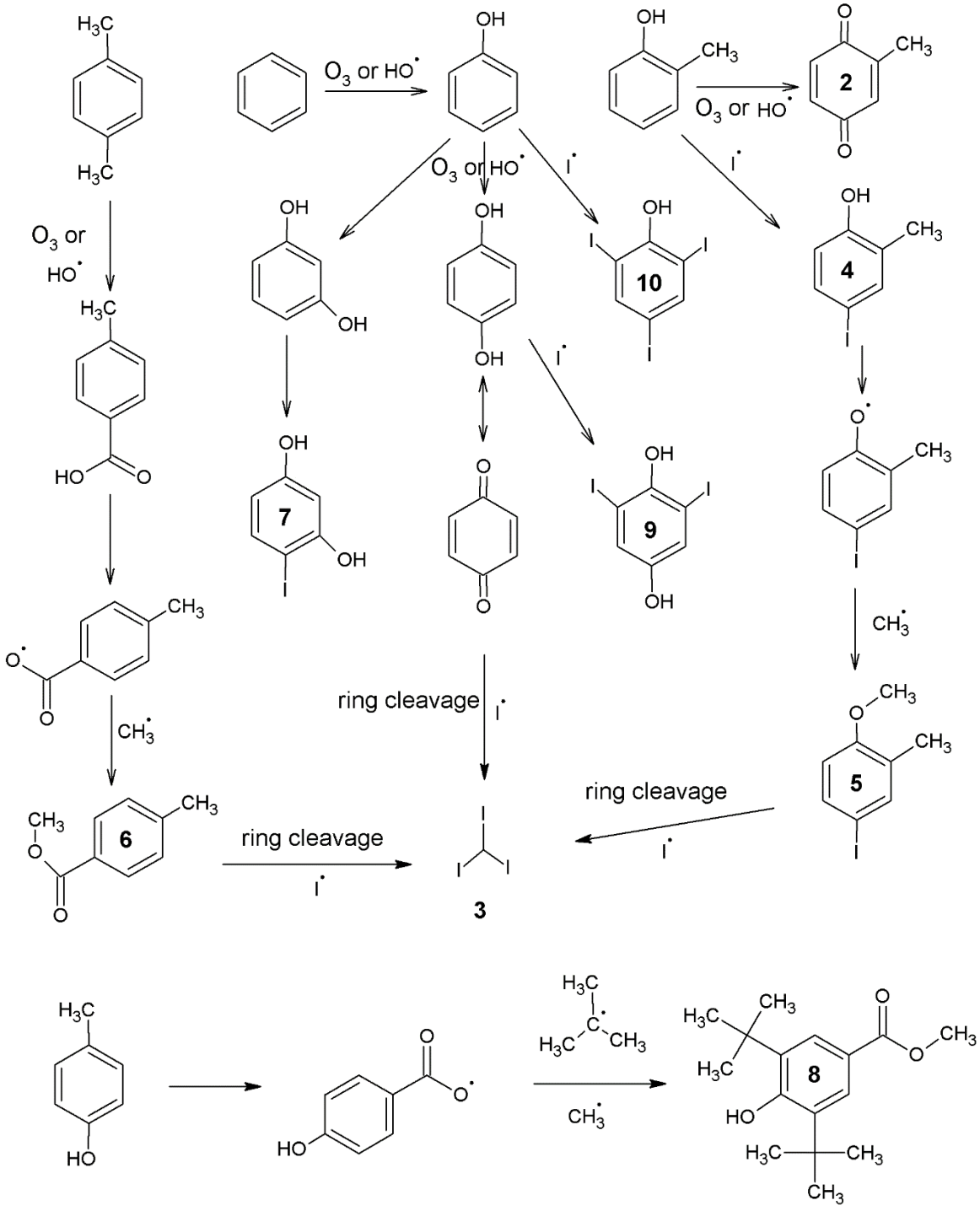

Figure 6.3 Proposed degradation pathways of aromatic compounds and their intermediates in OPW at 10 min photocatalytic ozonation

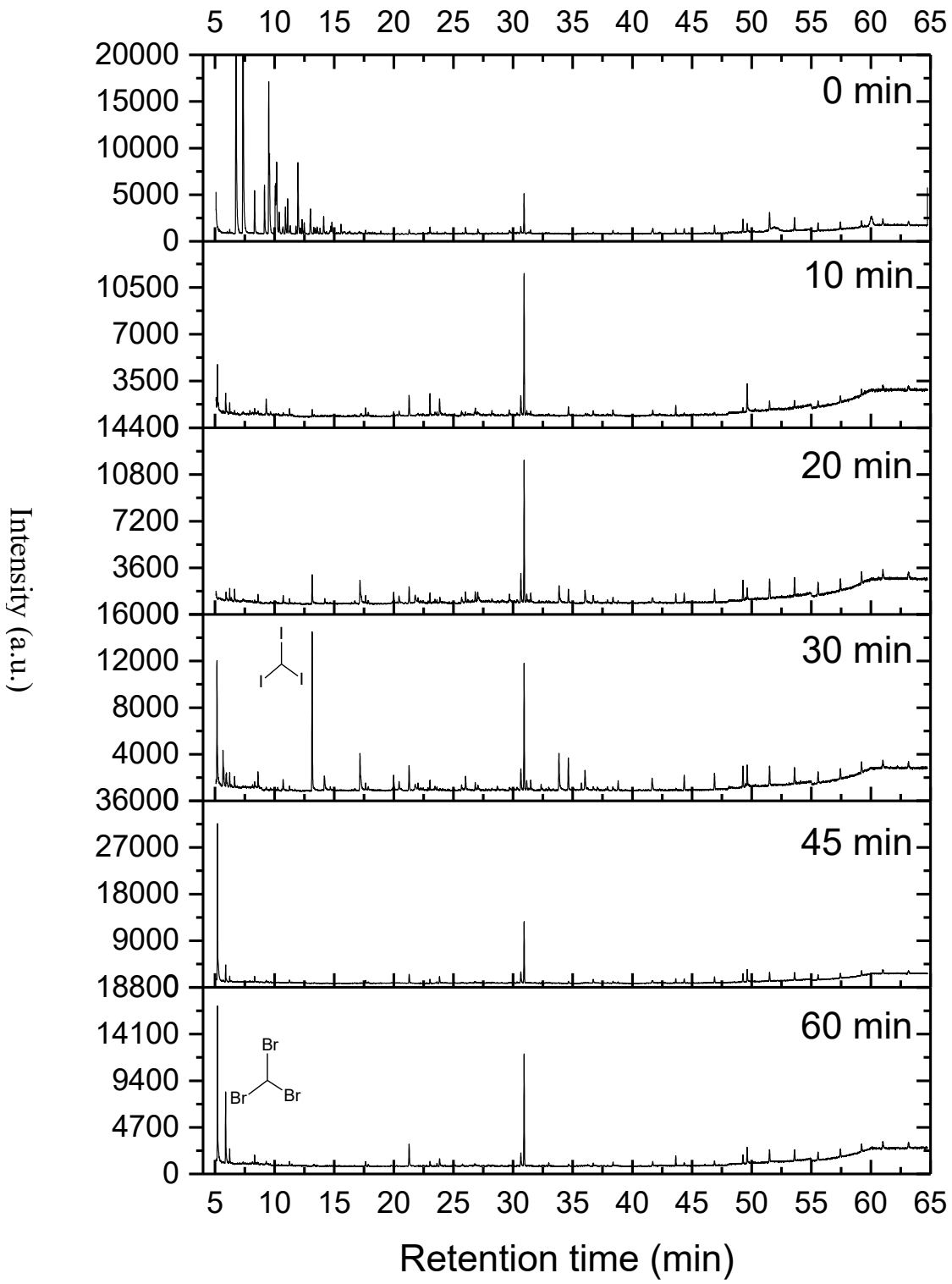
Intensity (a.u.)
Retention time (min)
0 min
10 min
20 min
30 min
45 min
60 min
Br
Br
Br
I
I
I

Figure 6.4 Generation of intermediates in low ozone dose (Run 5)

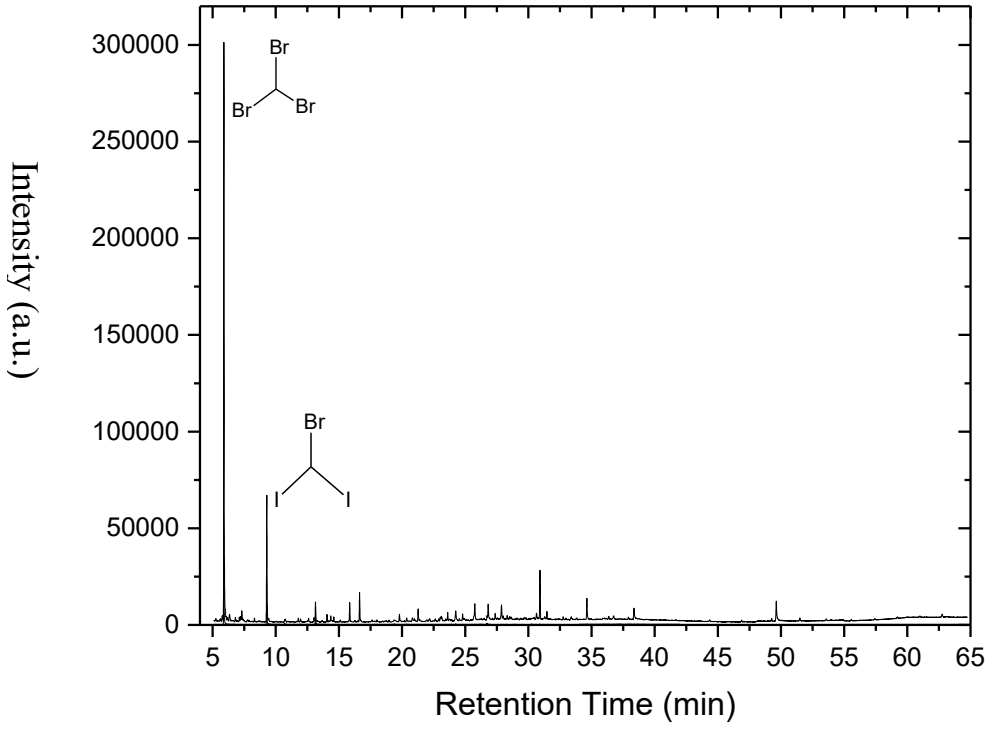

Figure 6.5 Intermediates of treated OPW after settling in 1-2 days

Conversion of brominated by-products was observed in treated OPW samples after settling in 1-2 days (Figure 6.5). The ultimate products of ozonated bromide and iodide were bromates and iodates respectively, which can be widely found in the treated water (Haag and Hoigne, 1983; Huang et al., 2009). Further transformation was proposed, which involves the breakdown of hydrocarbon chain and the generation of simpler products. As shown in Figure 6.5, dibromo pentane was depleted, leading to the generation of bromodiiodomethane and a significant increase in bromoform formation.

6.3.2 Toxicity

The toxicity of PAHs and phenols in the environment has been well studied (Johnsen et al., 1994; Elias-Samlalsingh and Agard, 2004; Nweke and Okpokwasili, 2010; Camus et al., 2015). The PAHs with 1-3 rings have an acute toxicity to the biota and the high molecular weight PAHs are carcinogenic and mutagenic due to their genotoxicity (Gupta et al., 2015). Phenols could damage the cytoplasmic membrane of microorganisms, leading to cell death and inhibition of their activity of biodegradation, especially at a high concentration (Nweke and Okpokwasili, 2010). Well et al. (1997) investigated the toxicity of the individual compounds in produced water and showed that most of PAHs have an EC_{50} lower than 1 mg/L. Phenols with less toxicity (EC_{50} = 15.1 mg/L) also play as a major contributor due to their high concentrations in OPW. Therefore, the toxicity level of untreated OPW is strongly related to the concentrations of PAHs and phenols in it.

To examine if the acute toxicity of OPW can be reduced by removing the PAHs and phenols in it, the toxicity change of OPW was monitored during and after the

photocatalytic oxidation in this study. The results are shown in Table 6.1 and Figure 6.6. The introduction of ozone could significantly reduce the acute toxicity of OPW: at EC_{50} (5 min), the dilution rate of OPW samples is increased from 3% to 50% on average. Run 1 shows the highest rate of 57%. However, the EC_{50} of the single ozonation process is around 46%, indicating UV-A and photocatalysis could further reduce the acute toxicity. The relative concentrations of OBPs in freshly treated OPW samples are also listed in Table 6.1. The levels of dibromopentane were increased from 4.84 (Run 5) to 18.8 (Run 6) where the ozone dose was increased from 5 ppm to 15 ppm. Without irradiation (Run 4), the relative concentration of dibromo-pentane reached as high as 28.97. It suggests that UV-A (or UV-A photocatalysis) is able to control the generation of OBPs. The levels of bromoform under different configurations did not show a clear relation to the operational factors. One of the most controversial results was that the highest concentration of bromoform was observed at the lowest ozone dose. In the degradation trend in Run 1 (Figure 6.7), the relative concentration of bromoform was first increased to 0.6 then decreased. This trend could be attenuated by applying lower ozone dose and the bromoform at 60 min might be still in its peak.

Table 6.1 Microtox® acute toxicity analysis of raw and treated OPW samples

Sample	Relative concentration				EC_{50} (%)	
	PAHs	Phenols	Dibromo-pentane	Bromoform	5 min	15 min
Raw	0.73	18.2	0	0	3.03	4.89
Run 1	0.01	0	7.33	0.37	57.08	65.94
Run 2	0.26	17.4	0	0	6.83	8.41
Run 3	0.05	0	18.79	0	51.78	57.09
Run 4	0.03	0	28.97	0	45.68	48.07
Run 5	0.01	0	4.84	2.40	51.45	50.24
Run 6	0.01	0	18.8	0	27.73[1]	27.96[1]
Run 7	0.01	0	15.05	0	52.15	50.25
Run 8	0.01	0	11.88	0.42	54.61	52.4
Run 9	0.01	0	12.24	0.45	52.75	52.56

Note: the low values were caused by the insufficient activation of the bacteria before the test.

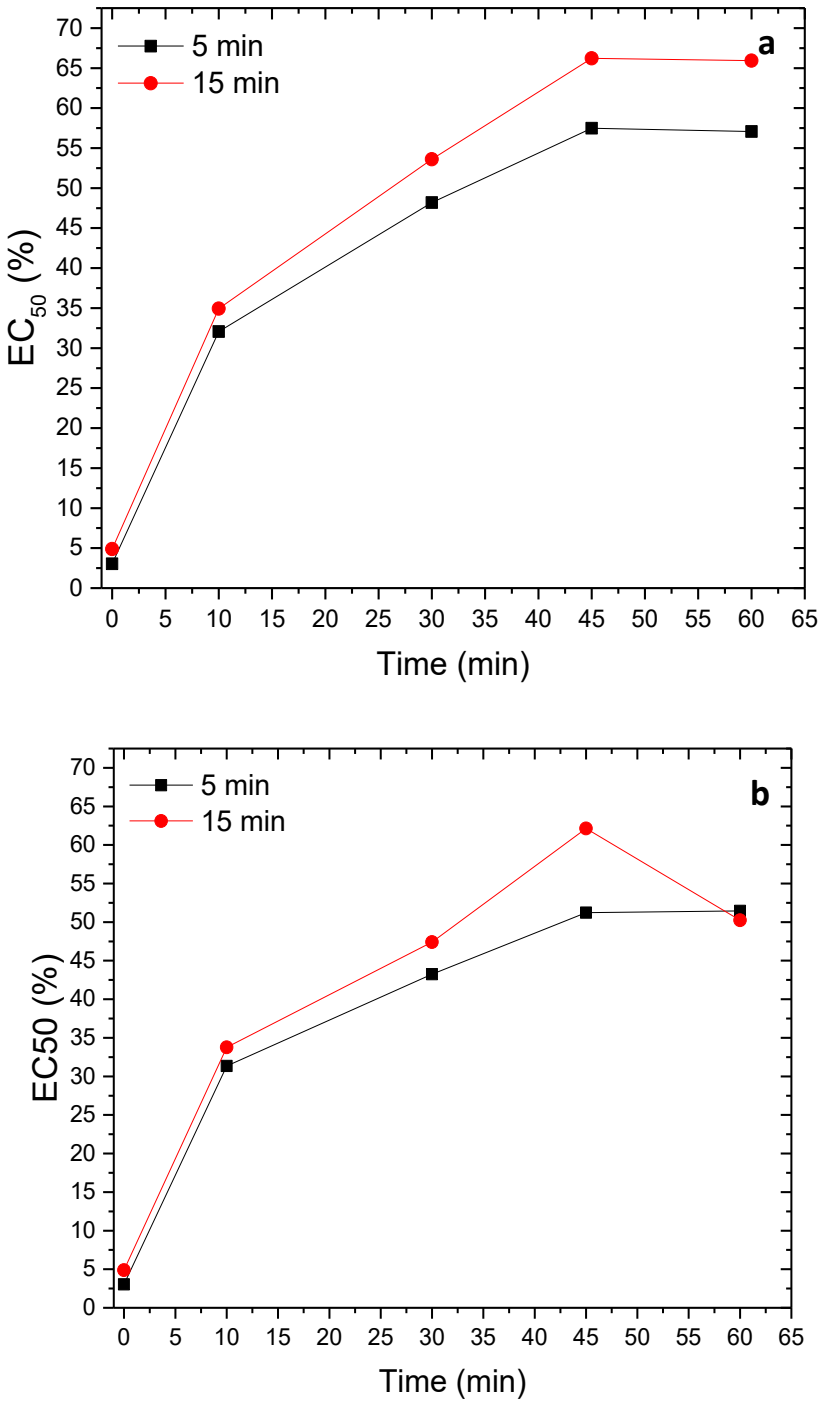

Figure 6.6 Toxicity reduction during the photocatalytic ozonation at different ozone dose of a) 10 ppm and b) 5 ppm

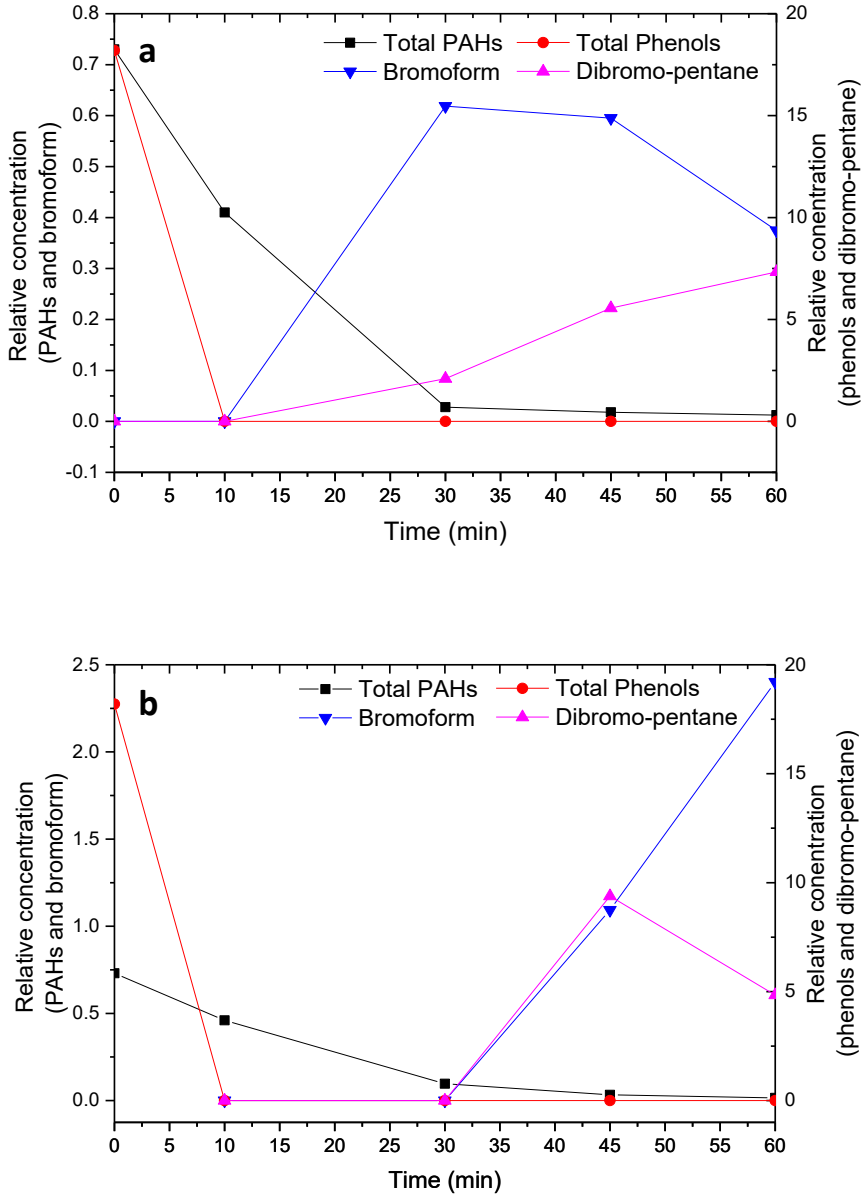

Figure 6.7 The change of relative concentrations of selected four toxicants during the photocatalytic ozonation: a) Run 1 and b) Run 5.

Figure 6.6 shows the gradual decrease of acute toxicity during the photocatalytic ozonation at different ozone doses. The EC_{50} (5 min) of 10-min treated OPW samples increased tenfold from 3% to around 30%. The similar dilution rate was found in the processes with different ozone doses. The intermediates such as benzoquinone, iodinated bezoquinone and methyl benzoic methyl ester are irritating to animal eyes and respiratory system (Enguita and Leitao, 2013), but data show that their presence do not significantly contribute to the acute toxicity. In this period, the most significant change in the OPW composition was the depletion of phenols and the reduction of PAHs. The reduction rate of toxicity was slightly higher with higher ozone dose, which may suggest faster degradation of PAHs and conversion of intermediates.

On the other hand, the introduction of ozone into the wastewater treatment process can produce ozonated by-products (OBPs), especially when high concentrations of bromide and iodide are present in the water. These OBPs such as bromoform can also be a key contributor to the toxicity of treated effluent (Huang et al., 2009).

To further understand and quantify the roles of OPW composition in acute toxicity, a multivariable regression analysis was employed. The multivariable regression model applied to acute toxicity was:

$$Y = \alpha_1 X_1 + \alpha_2 X_2 + \alpha_1 X_1 + \alpha_1 X_1 + \beta \qquad (6.2)$$

The relative concentrations (the ratios of peak area between the target compounds and internal standard) of total PAHs, total phenols, dibromo-pentane and bromoform were recorded and selected as independent variables, and EC_{50} (5 min) was the dependent one.

The selection of dibromo-pentane and bromoform was due to their high concentrations in the treated effluents. The equation of multivariable regression is expressed as follows:

$$EC_{50}\% = -28.05[\text{total PAHs}] - 1.72[\text{total phenols}] + 0.095[\text{dibromopentane}] + 2.66[\text{bromoform}] + 49.76 \quad (6.3)$$

The predicted vs. order plot depicted (Figure 6.8) the difference of predicted data from simulated equation to the experimental data. It can be observed that the model has a good fitness and the adjusted R-square is 0.87. The intercept of the equation could be the combined toxicity caused by other substrates in OPW.

Total PAHs has the largest coefficient of 28.05 and total phenols is 1.72. The toxicity coefficient of PAHs and phenols determined here is close to that reported in the literatures (Wells et al., 1997). In raw OPW, the relative concentrations of PAHs and phenols are 0.73 and 18.2 respectively. In sum, the toxicity contribution of total PAHs is 20.48% and the toxicity contribution of total phenols 31.30%. In this case, phenols are suggested as the most toxic component in OPW. This model shows a great potential in predicting the toxicity of OPW when the concentrations of PAHs and phenols are known. The model further suggests that OBPs have positive effects on the reduction of toxicity, which contradicts to the conclusions drawn from other studies, that is, the increase of both mutagenicity and acute toxicity would cause the production of brominated by-products during ozonation (Huang et al., 2009; WHO, 2017). The significances (p-value) of bromoform and dibromo-pentane in the model are then 0.63 and 0.46 respectively, indicating that the contribution of these two variables to the model are insignificant.

Therefore, the variation of the model is mainly controlled by total PAHs and total phenols.

To amplify the toxicities of OBPs in OPW, a two-variable regression analysis focusing on dibromo-pentane and bromoform was employed. In this case, only the experimental data with negligible levels of PAHs, and phenols were selected. The regression was done through the following equation:

$$EC_{50}\% = -0.56[\text{dibromopentane}] - 3.14[\text{bromoform}] + 61.79 \quad (6.4)$$

Compared with the four-variable model and the two-variable model (Figure 6.8 and Figure 6.9), the residues between observed data and simulated data are reduced from ± 10 to ± 1. The regression coefficient for this model is increased to 0.93. The p-values are reduced to 5.2×10^{-3} for bromoform and 7.6×10^{-4} for dibromo-pentane. As a result, the toxic effect of OPBs can be revealed and amplified by removing the effect of total PAHs and total phenols.

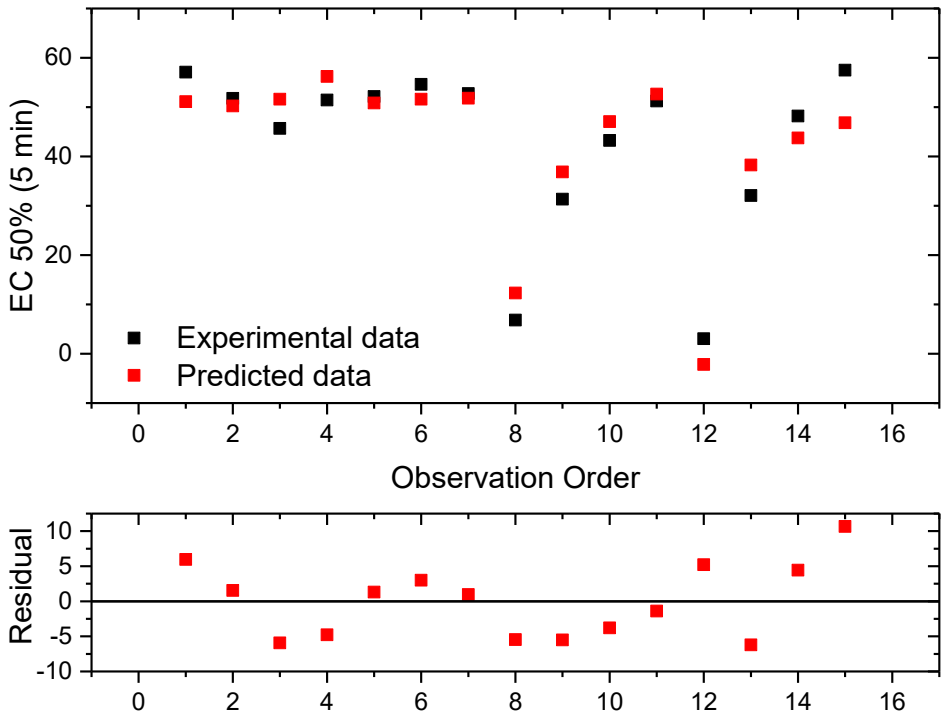

Figure 6.8 Residuals vs. Order plot based on total PAHs, total phenols, dibromo-pentane and tribromomethane as independent variables

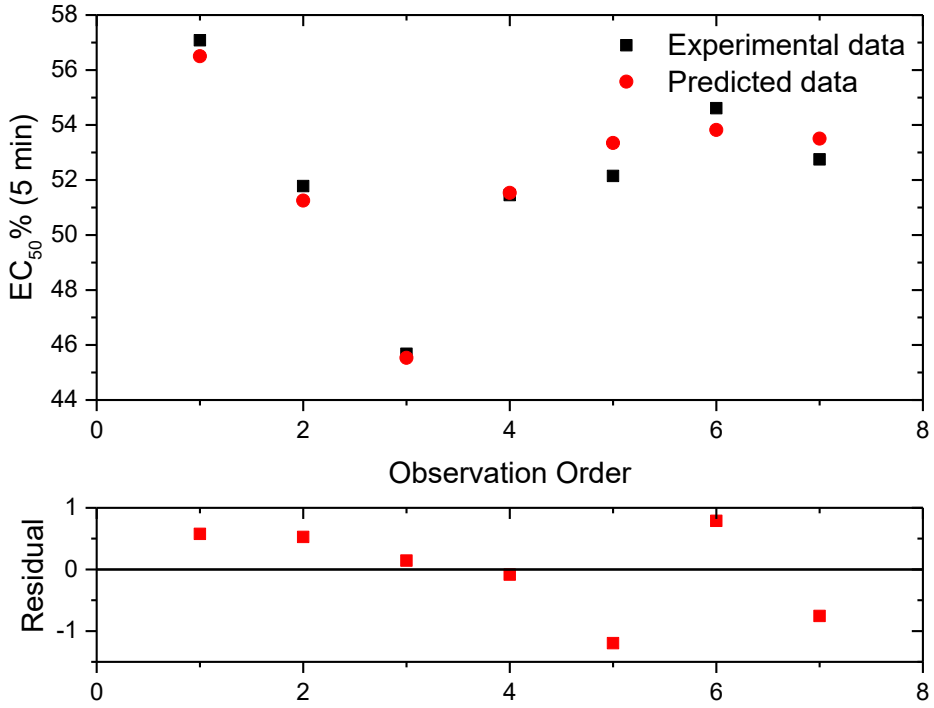

Figure 6.9 Residuals vs. Order plot based on dibromo-pentane and tribromomethane as independent variables

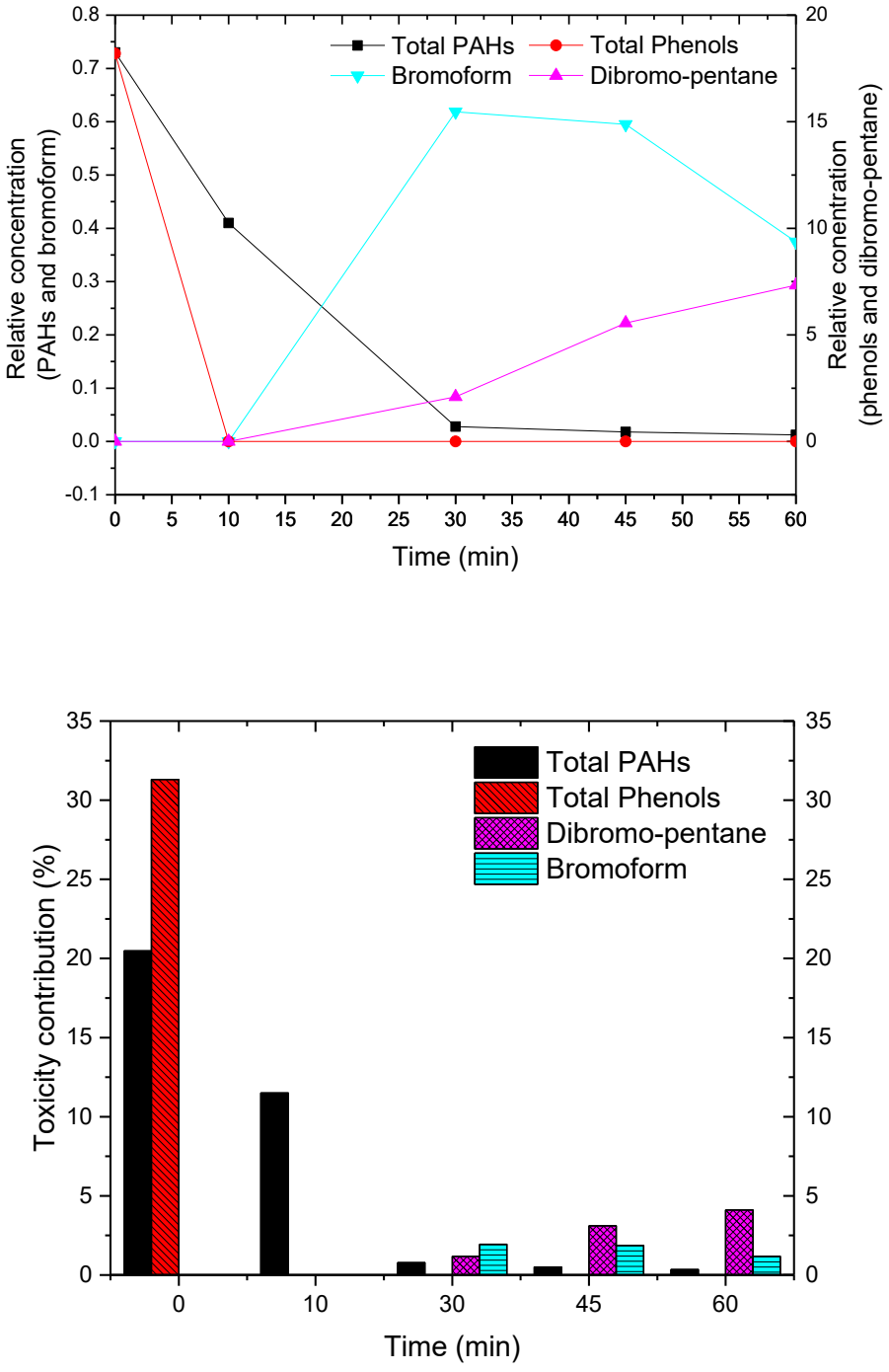

Figure 6.10 Acute toxicity contribution of selected toxicants during the photocatalytic ozonation (Run 1)

By combining the relative concentration of different toxicant and their acute toxicity coefficients obtained from two models, the contributions of different toxicants to the acute toxicity during photocatalytic ozonation process can be evaluated. In Figure 6.10, the treatment process could be divided into two periods: pre-30-min and post-30-min. In the pre-30-min period, the acute toxicity is mainly caused by the aromatic compounds, whereas in the post-30-min period the OBPs are considered as the major toxicants. The configuration of photocatalytic ozonation might be adjusted to further reduce or at least not to increase the toxicity. The treatment therefore is suggested to stop at the 30 min. The developed models could therefore provide a useful tool to evaluate the toxicity and monitor the performance of AOPs during treatment.

6.3.3 Biodegradability

The biodegradability was evaluated by the BOD bottle test (5 days) and the respirometer test (28 days). Based on the standard method for the biodegradability test in seawater (OECD, 1992), the OPW was diluted 10 times with the local seawater and, with the addition of pH buffer and nitrogen-based nutrients. The seawater used was obtained from the local harbour in Newfoundland offshore. The bacteria such as *Alcanivorax*, *Cycloclasticus, Rhodococcus, and Bacillus* were commonly found in the region and capable of decomposing the hydrocarbon species in oily wastewater (Yakimov et al., 2007; Cai et al., 2015). The seawater sample was aged for several days prior to the BOD tests to remove all biodegradable matter that would interfere.

The results of the BOD bottle test were displayed in Figure 6.11. It was observed that the BOD_5/COD ratio of the OPW samples was increased from 20% (Raw) to 29.25% (Run 6)

after photocatalytic ozonation. The oxygen consumptions for all the samples were from 58 mg/L to 69 mg/L, which were not as significant as the change of BOD_5/COD ratio. Since the BOD bottle test is a closed bottle method, the access to fresh oxygen is thus limited. The reduction of oxygen in bottles could reduce the aerobic degradation rate. When DO is decreased to a critical level, the aerobic degradation stops. In the bottle, the DO values of all the OPW samples after 5-day biodegradation were lower than 2 mg/L, restricting further oxygen consumption by aerobic process. The major differences among the runs are the concentration of COD in untreated OPW (389.5 mg/L) and in treated OPW (ranging from 335.8 mg/L to 268.6 mg/L). The untreated OPW has a higher COD value and thus a lower BOD/COD ratio.

The high DO consumption of raw OPW sample might also suggest that the biological process is not significantly affected by the acute toxicity of OPW. The seawater was sampled at a local harbour, which was a small commercial dock with some fishing and shipping activities. Sub-milligram level of phenols was also found in the seawater samples. In this case, the seawater sample was probably previously exposed to oil leaks (although no pollution event was reported previously), leading to the existence of oil-degrading bacteria. If so, such bacteria could degrade the hydrocarbons in the OPW even the toxicity level was relatively high.

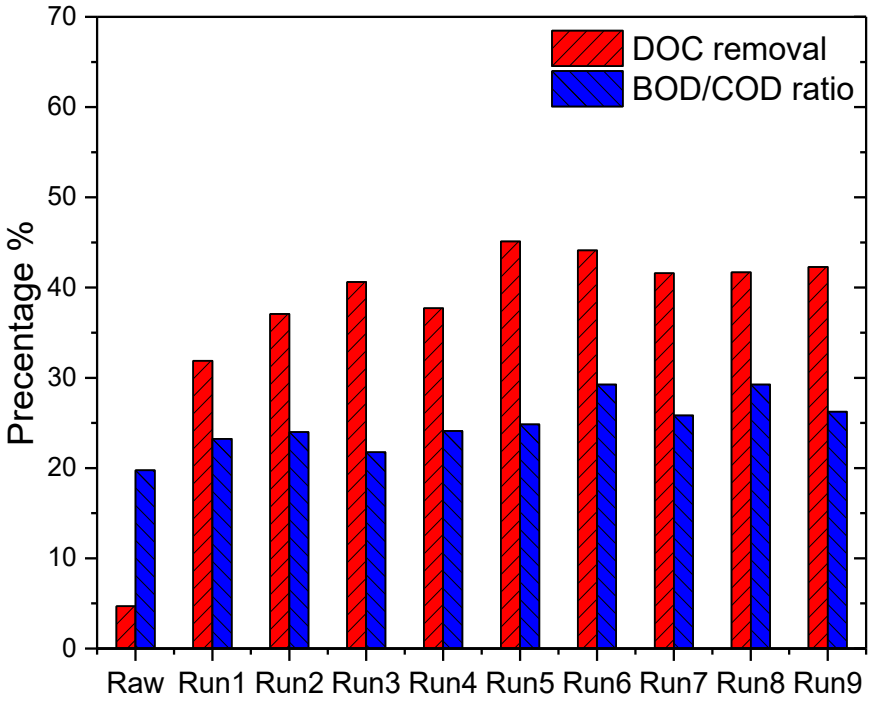

Figure 6.11 The BOD_5/COD ratios and the DOC removal rates of treated/untreated OPW samples in 5-day biodegradation

The OPW samples in the biodegradation test were further diluted to 10%. The acute toxicity of diluted solution was consequently reduced. Therefore, the inhibition effect of PAHs and phenols was diminished compared to the acute toxicity tests. However, the BOD interference by the other factors should also be considered. For example, the consumption of oxygen might be interfered by the inorganic oxidation within the system, dissolved oxygen could be captured by the sulfur/sulfite and ferrous ions in the raw OPW, leading to a high oxygen consumption. In the treated OPW samples, these reductive species were either oxidized by oxygen (photocatalysis) or ozone (photocatalytic ozonation), the consumption of dissolved oxygen by inorganic species was minimized. The interference by reductive inorganic species gave an overestimated oxygen demand, and thus further diminished the apparent BOD enhancement of the photocatalytic ozonation in the OPW samples.

It has been proved that the biodegradability of treated OPW can be significantly improved. In Figure 6.11, the limited deduction of DOC (5%) is observed in biodegradation of the raw OPW sample. Meanwhile, the DOC removal rates in the treated OPW samples are significantly increased to 31.9% - 45.11%. It indicates that the photocatalytic ozonation has a strong effect on increasing the biodegradability of the OPW composition: the less biodegradable organics, such as PAHs and phenols, can be broken down into the readily biodegradable matters, including ketones, aldehydes, carboxylic acids, alcohols, and esters. The biodegradability of the OPW is thus enhanced by the photocatalytic ozonation.

The biodegradation of the OPW samples was further studied by the respirometer tests. The oxygen demands during the biological process were monitored (Figure 6.12). The aged seawater used as a control showed negligible oxygen consumption. The background interference was thus eliminated. The BOD of raw OPW sample and treated OPW sample (Run 5) was generally contributed by two parts: carbonaceous biochemical oxygen demand (CBOD) and nitrogenous biochemical oxygen demand (NBOD). The CBOD was dominant within 6 days of degradation and the growth of NBOD started at 7-8 days.

Initially, a delay in the oxygen uptake occurred in both raw/treated OPW sample, showing a lag phase of microorganism growth (shown in the insert figure in Figure 6.12). The oxygen uptake by the raw OPW sample was slightly higher than that by the treated OPW sample, probably because of the reductive inorganic compounds. The impact of OPW toxicity on the biodegradation could be reflected by the increase of the lag time. In the study, the lag time for the treated OPW was slightly shorter than the raw OPW, indicating the acute toxicity of OPW had a limited inhibition to the aerobic degradation, which was similar to the BOD bottle test.

The growth of oxygen uptake started at the 37^{th} hour. A higher oxygen uptake rate (OUR) was observed in the treated OPW sample, indicating a higher biodegradability. On the fifth day, the oxygen uptakes by the raw OPW sample and the treated OPW sample were 7.7 mg and 10.9 mg, respectively. The OURs of both the untreated and treated OPW samples in the respirometer test were higher than that in the BOD bottle test. In the respirometer test, the bottles were connected to an oxygen source. By continuous stirring, the DO in the OPW samples were kept saturated. In this situation, the level of DO was

not a limiting factor to the aerobic degradation. Table 6.2 shows the BOD/COD ratios of raw/treated OPW samples in the two different tests. In the fifth day, the BOD_5/COD ratios in the respirometer test was higher than those in the close-bottle BOD test indicating a higher oxygen consumption. The BOD_5/COD ratio of produced water was increased to 169% after treatment.

A second exponential growth of OUR was observed around the 7^{th} day and the nitrification was started. At this stage, the OURs of the two OPW samples were increased with a similar rate, which might imply that the similar amount of ammonia and nitrogenous organics in both samples. The increase of the OURs were stopped on the 15^{th} day, showing the completion of biodegradation. The BOD/COD ratios were 45.58% and 84.87% for the raw OPW sample and the treated OPW sample, respectively, after the 28-day period. This indicated the important value of photocatalytic ozonation in treating OPW leading to a more biodegradable effluent, which could be further treated by follow-up biological treatment.

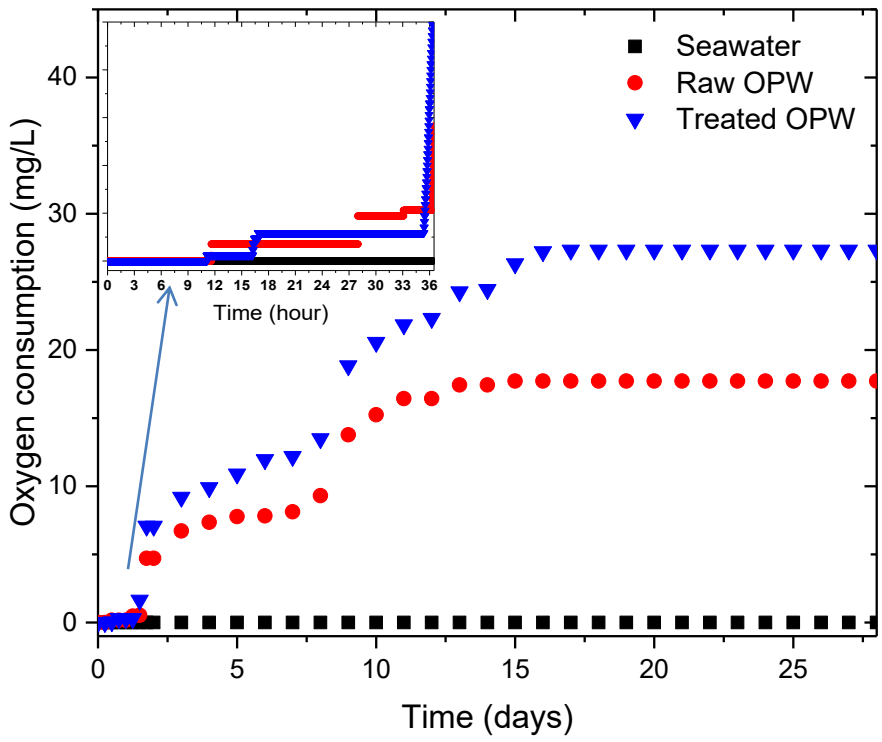

Figure 6.12 Oxygen consumption of OPW samples during biodegradation monitored by respirometer

Table 6.2 The comparison on the BOD/COD ratio of raw/treated OPW samples in different biodegradation tests

Biodegradation time (day)	BOD/COD ratio (%)			
	Bottle Test		Respirometer Test	
	Raw OPW	Treated OPW	Raw OPW	Treated OPW
0	0	0	0	0
5	19.75	24.84	19.99	33.84
28	-	-	45.58	84.87

The chromatographs of the raw OPW sample measured during biodegradation are presented in Figure 6.13. The most significant change is the depletion of phenol in 5 days. The C1-C3 alkylphenols were however not degraded. The total phenols were decreased from 18.2 to 14.7 in the 5-day biodegradation with a removal rate of 80.8%. The phenols were still detectable after 28 days. For the treated OPW (Run 5, Figure 6.14), PAHs and phenols were depleted, but the relative concentration of bromoform was 10.87. Bromoform in the treated OPW sample showed a much faster degradation rate, in which the removal could reach as high as 97% within 5 days. The results indicate that the bromoform could be rapidly degraded by bacteria in seawater. It might be explained by that the depletion rate of bromoform is much faster than that of the other THMs and the brominated THMs have a medium toxicity through a bioactivation pathway (WHO, 2017). Further degradation of bromoform was slowed down during 5-28 days compared with its fast depletion in 5 days with a removal rate of 74% (compared to its relative concentration on the 5^{th} day). The removal of alkyl phenols is also important due to its toxicity to the marine species including the interruption of redox states and reproductive system (Hasselberg et al., 2004; Meier et al., 2007). The depletion of such phenols in the photocatalytic ozonation leads to significant reduction of the chronic toxicity.

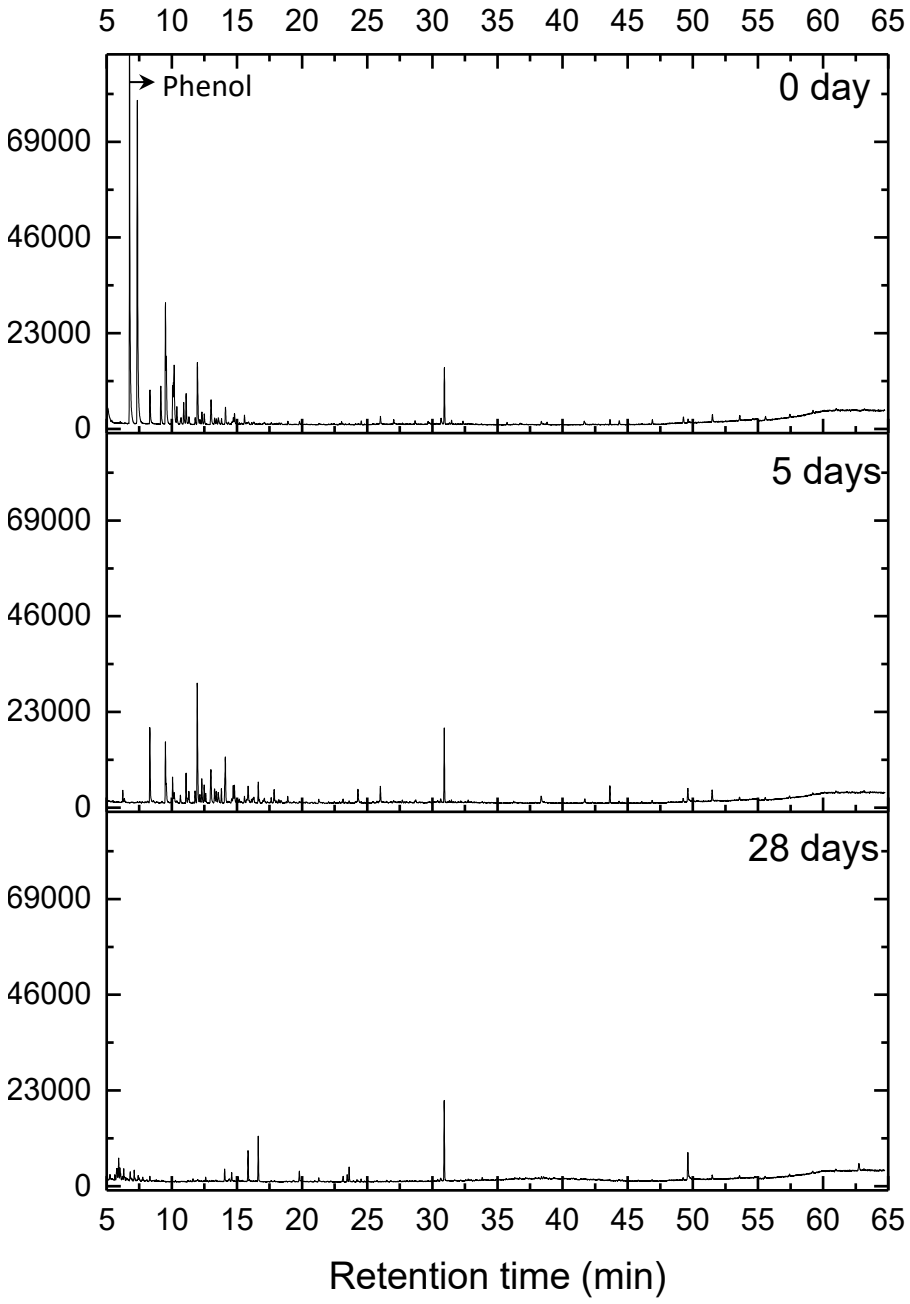

Figure 6.13 Chromatographs of raw OPW in 28-day biodegradation

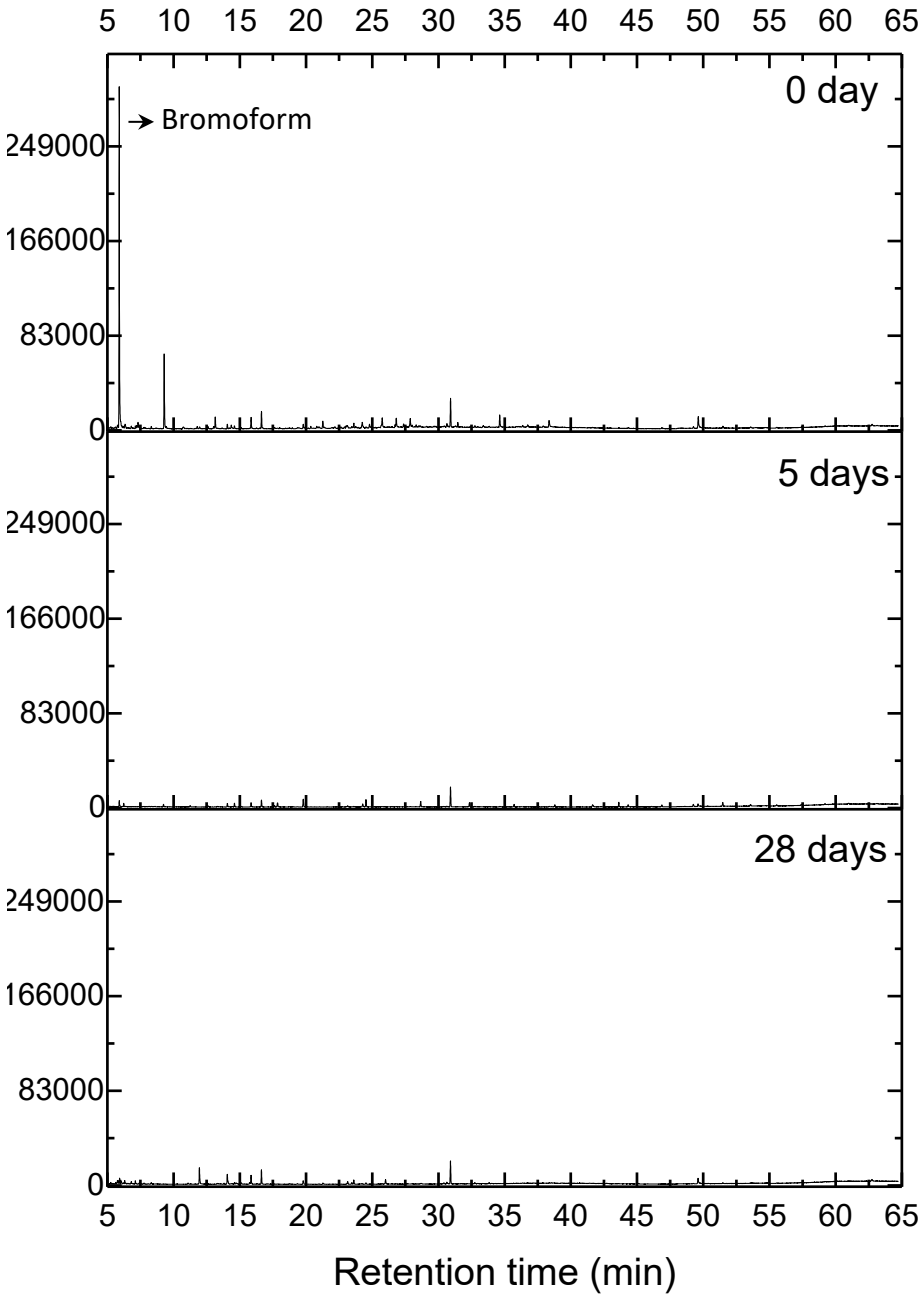

Figure 6.14 Chromatographs of treated OPW (Run 1) in 28-day biodegradation

6.4 Summary

In this chapter, an in-depth evaluation was conducted on the intermediates and degradation pathways of the organics in OPW during photocatalytic ozonation, and their effects on the toxicity and biodegradability of OPW effluent.

The intermediates formed during photocatalytic ozonation were identified by GC-MS analysis. Intermediates such as iodized phenols and phenolic esters were found after 10 mins of treatment, following by the formation of iodoform after 20-30 mins, brominated by-products (e.g., dibromo-pentane and bromoform) after 30 mins, and bromodiiodomethane and bromoform by the end of the treatment. It indicates that the presence of halogen ions could significantly alter the oxidation pathways of aromatic compounds at several stages. At the beginning of the photocatalytic ozonation, the iodine radical substituted the hydrogen atom on the aromatic rings forming iodized phenols and phenolic esters. Then the products of aromatic ring cleavage reacted with iodine radicals to form iodoform. Further, bromine radical dominated the process and the conversion of brominated by-products were occurred.

The Microtox® acute toxicity test proved a continuous decrease in the acute toxicity (EC_{50}) of treated OPW. The contributions of four toxicants (e.g., PAHs, phenols, dibromo-pentane and bromoform) to the overall toxicity of OPW were analyzed by a proposed multivariable regression model based on the experimental data. The results indicate that total PAHs was linked to a highest toxicity coefficient in the OPW but phenols contributed most significantly to acute toxicity due to their relatively high concentrations. OBPs were also observed to be much less toxic than PAHs and phenols.

It is suggested that the photocatalytic ozonation would be better stopped at 30 min, otherwise the toxicity might be increased due to the increasing amount of OBPs.

The enhancement of biodegradability was verified in the both close-bottle BOD test (5 days) and the respirometry test (28 days). The slight reduction of the lag phase of microorganism growth in treated OPW shows that the acute toxicity is irrelevant to the growth of bacteria in the seawater. However, photocatalytic ozonation could transform the less biodegradable compounds to more biodegradable compounds. The BOD/COD ratio of treated OPW was doubled 84.87% after 28 days, which meant that the treated OPW could be readily biodegraded in biological process. The results also illustrate that OBPs degrade much faster than phenols, having the limited negative effects on photocatalytic ozonation. It demonstrates that the OPW after treatment by photocatalytic ozonation is ready to be discharged into the ocean or subjected to a follow-up biological treatment if needed.

Chapter 7 Conclusions and Recommendations

7.1 Summary

The increasing generation and discharge of OPW, a typical offshore oily wastewater, has raised many concerns due to its chronic toxicity to the marine environment. The soluble organic content in produced water, especially polycyclic aromatic hydrocarbons (PAHs), have high toxicity but cannot be effectively removed by the existing treatment approaches. Removal of petroleum hydrocarbons by nano-TiO_2 photocatalytic oxidation has been proved as a promising technology to address the increasing demand of OPW treatment. However, the efficacy of this method could be significantly hindered due to the complexity of OPW composition. The matrix effect of OPW on photocatalysis had not been well investigated prior to this work. In particular, an in-depth study on the matrix effect of OPW on catalyst surface was desired. In addition, the current technologies in treating oily wastewater, including OPW, based on photocatalytic oxidation are still facing difficulties in terms of low efficacy, long processing time, or high energy consumption. Methods using advanced catalysts, lowing energy light sources and combining other AOPs technologies can potentially increase effectiveness, but they are still not matured yet and await further exploration. Further, the pathways of intermediates generated during photocatalytic oxidation, the toxicity and the biodegradability of treated OPW remain unknown in the literature.

To help fill the knowledge gaps and improve the current industrial practices, this research is aimed at 1) understanding the behaviors of the key components in OPW during photocatalytic oxidation; 2) investigating the matrix effects of OPW on various catalysts (e.g., suspended TiO_2 and immobilized TiO_2); 3) evaluating and optimizing a novel

method that integrates UV-light-emitted diode (UV-LED)/TiO_2 nanotube array (TNA)/ozonation treatment process for OPW treatment; and 4) analyzing the intermediates formed during the integrated photocatalytic oxidation treatment and their contributions to the overall toxicity and biodegradability of the treated OPW effluent.

To understand the mechanism of photocatalytic oxidation that removes PAHs from OPW, the effects of water matrix were studied by comparing the performance of TiO_2 induced photocatalysis in both distilled water and OPW samples. In OPW, the degradation rates of PAHs were found to dramatically decreased, and the photocatalysis was deactivated. The photocatalytic degradation of PAHs with high molecular weights was more sensitive to the variations of salinity and the presence of insoluble matter due to their low water solubility. The overall degradation of PAHs was strongly affected by the organic composition in OPW particularly the aromatic compounds. These compounds act as UV-light absorbers and hence compete with PAHs in photodegradation. Due to their abundance in OPW, these species can exert the most significant effect on the photocatalytic degradation of PAHs.

In order to increase the applicability of photocatalytic oxidation in treating OPW, immobilized nano-TiO_2 catalysts were introduced into the UV irradiation system. The performance of this method on the degradation of naphthalene in OPW was evaluated by experiments along with the impact analysis of nano-TiO_2 adsorption capacity. The results of adsorption analysis show that immobilization and agglomeration reduce the surface area of catalyst in a similar degree. The photocatalytic reaction rate constants in the suspended and immobilized systems were 0.00219 min^{-1} and 0.00305 min^{-1}, respectively,

indicating that the immobilized catalyst gives a better performance in photo-oxidation of OPW. The fouling of catalyst surface during the irradiation process is caused by the deposition of insoluble particles and organic matters, and the scaling of calcium. The immobilization of catalysts is more resistant to the substrate effects of OPW, suggesting a promising way of treating OPW.

To improve the efficiency and reduce the treatment time and the energy consumption, the combination of UV-LED/TNA photocatalysis and ozonation was conducted and comprehensively evaluated. Prior to photocatalytic degradation, the adsorption tests showed that the catalyst has a higher adsorption rate for PAHs with higher molecular weights. Oxidation results in an overall improvement in PAHs degradation in the integrated system, in which the half-life times of all PAHs could be reduced to less than 10 mins. By evaluating different parameters, the best catalyst dose was determined as 0.2 g/L. Light intensity has a negative effect on degradation rate due to the generation of iodine radical, which acts as a strong ozone scavenger to significantly reduce of ozone concentration in the system. The increase of ozone dose promotes the photocatalytic ozonation of PAHs. It was found that the direct ozonation favors to degrade aromatic organic matters with high mobility. The hydroxyl radical oxidation is much inhibited, which was observed near the surface.

The investigation on the influence of photocatalytic oxidation on the toxicity and the biodegradability of the treated OPW was further conducted. The compositional changes of OPW during the treatment were examined by GC-MS analysis. Many oxygenated and iodized intermediates were observed. Despite oxidation, other transformations of

aromatic compounds by iodization were found to give iodized by-products within 10 min. At this stage, the iodine radical substituted the hydrogen atom on the aromatic rings. The formation iodoform was observed during 20-30 mins of treatment, suggesting reactions between the products of the aromatic ring cleavage. After 30 mins, bromine radical was involved in the free-radical chain reactions leading to the formation of brominated short-chain hydrocarbons. The results show that iodine radical and bromine radical play active roles at different stages of the photocatalytic oxidation.

The acute toxicity tests by Microtox® revealed a continuous decrease of acute toxicity (EC_{50}), as the dilution rate of OPW was increased from 3% to 57%. The contribution of four representative toxicants (PAHs, phenols, dibromo-pentane and bromoform) to the overall toxicity of OPW was further analyzed by two proposed multivariable regression models under different scenarios. The coefficients of the toxicity effects were found to decrease following the order of PAHs >> bromoform > phenols >> dibromo-pentane. The evaluation of toxicity contribution based on the models would be helpful to identify the end-point of treatment. The recommended photocatalytic ozonation duration is 30-min based the experimental result.

Improved biodegradability was found in both close-bottle test (5 days) and respirometry test (28 days). The transformation of less biodegradable compounds to more biodegradable ones by photocatalytic ozonation was a key reason for the improvement. The BOD_{28}/COD ratio of OPW was doubled up to more that 80% after photocatalytic ozonation, which demonstrates the value of photocatalytic oxidation in terms of promoting the follow-up biological treatment. The degradation rates of bromoform in

both close-bottle test and respirometry tests are much faster than those of phenols, indicating that the OPW after treated by photocatalytic ozonation has much less impact on marine environments.

7.2 Research Contributions

The major research contributions of this work can be summarized in the following aspects:

1) Evaluation of the key matrix effects of OPW on the photocatalytic oxidation of PAHs

   The major matrix effects on photocatalytic oxidation, such as inhibitions caused by alkaline-earth cation, the insoluble particle matter and the competitive organics were revealed. The results can not only fill the knowledge gaps but also help to develop a better strategy to overcome the difficulties in the application of photocatalytic oxidation for treating OPW and other oily wastewater with similar composition. For example, filtration before photocatalytic oxidation would significantly reduce the competitive adsorption of contaminant and increase the degradation efficiency.

2) Development of a series of TiO_2 enhanced photocatalytic oxidation method for treating OPW

   Different TiO_2-based nano-catalysts significantly affect the performance in degrading PAHs in OPW. The immobilized TiO_2 not only reduce the loss of catalyst in the treatment system but also improve the efficiency in degrading PAHs. The study here provides a scientific support for better design and operation of photocatalytic

oxidation systems for OPW treatment and helps the finding of catalysts and systems that more tolerance and stable.

3) Examination of the synergic effect of adsorption and photocatalysis in OPW treatment

   The adsorption tests for the removal of PAHs indicated that higher molecular weight PAHs show greater affinity for the catalyst. Disproportional desorption causes these PAHs to remain on the catalyst surface. The behaviour further leads to a higher removal rate in the complex matrix system in comparison with the PAHs with lower molecular weights due to the surface reaction of photocatalysis. Revealing such a synergic effect could help understand the interactive mechanisms of adsorption and photo-oxidation. The gained knowledge will also facilitate the improvement of the oxidation-based OPW treatment in practice.

4) Development a novel UV-LED/TNA/ozonation method for OPW treatment

   The integrated photocatalytic process combines the advantages of low energy cost, catalyst activity and durability, and high oxidation rate. This method achieves a significant enhancement of PAHs degradation in OPW. By evaluating the effects of catalyst dose, ozone dose and light intensity, their roles in oxidation processes were revealed. Based on the findings, the photocatalytic ozonation process can be adjusted to achieve the optimum performance in OPW treatment.

5) Revealing the behaviours and mechanisms of halogen species during the photocatalytic ozonation process

The interference of halogen to the photocatalytic ozonation was found to be amplified by the UV-A irradiation. The roles various halogen species played on the different stages were therefore identified by the intermediate analysis. The finding can improve the understanding of the alternative fates and pathways of aromatic organics during AOP processes and further help the practical design and operation by reducing the generation of by-products with less environmental impact.

6) Development of new multi variable regression models to evaluate and predict the contributions of OPW composition to toxicity

   Identification and evaluations of the most toxic components during the treatment of OPW resulted in two multivariable regression models under different scenarios. The coefficients of toxicity effects were found to decrease following the order of PAHs >> bromoform > phenols >> dibromo-pentane. The acute toxicity of OPW during the treatment thus can be predicted in a quantitative manner. It can provide a useful tool to help find the optimal treatment that achieves both effectiveness of photocatalytic treatment and low toxicity of the treated effluent.

7.3 Recommendations for Future Work

1) The research on enhanced photocatalysis of oily wastewater treatment is in a pressing need. More efforts particularly on validation testing by pilot-scale systems and field trials should be made in the future. To further increase the applicability, more catalysts with long durability should be evaluated. System simulation and

optimization can be conducted to maximize the efficiency and performance of photocatalytic treatment of OPW.

2) The presence of organic acids in OPW would have a strong quenching effect on hydroxyl radical to dramatically reduce the efficiency of COD and DOC removal in the photocatalytic process. Therefore, the behaviour of organic acids in the photocatalytic oxidation process should be further investigated.
3) In this research, the toxicity model considers the key toxicants in the raw/treated OPW. There is still a need to more accurately examine the toxicity profile by taking more components in the OPW into consideration. Further research could also focus on the interactive contributions of different components to acute toxicity. The chronic toxicity of OPW and treated effluent should be evaluated as well.
4) The significant improvement on OPW biodegradability by photocatalytic ozonation strongly suggests that implementation of the developed technology followed by biological treatment would further increase the mineralization rate. In a sense, this could deliver a promising treatment option for the treatment of oily wastewater. Further study may focus on the optimization of such combined technologies and evaluation their feasibility in real application.
5) The durability of catalysts could be further investigated. Studies on surface fouling, the efficiency of multi-runs and replacing time would be helpful to the application of photocatalysis in practice.

7.4 Selected Publications

Referred Journal Articles

Liu, B., Chen, B., & Zhang, B. (2017). Oily Wastewater Treatment by Nano-TiO_2-Induced Photocatalysis: Seeking more efficient and feasible solutions. *IEEE Nanotechnology Magazine*, *11*(3), 4-15.

Liu. B., Chen B., Lee, K., Zhang, B.Y., Ma, Y.C., and Jing, L. (2016) Removal of Naphthalene from Offshore Produced Water Through Immobilized Nano-TiO_2 aided photo-oxidation. *Water Quality Research Journal of Canada*, *51(3)*, 246-254.

Liu. B., Zhang, B.Y., Chen, B., Jing, L., Zhang, H. and Lee, K. (2016) Photocatalytic Degradation of Polycyclic Aromatic Hydrocarbons (PAHs) in Offshore Produced Water (OPW): the Effects of Water Matrix. *Journal of Environmental Engineering*, *142(11)*: 04016054

Zheng, J., Chen, B., Thanyamanta, W., Hawboldt, K., Zhang, B., & **Liu, B.** (2016). Offshore produced water management: A review of current practice and challenges in harsh/Arctic environments. *Marine pollution bulletin*, *104*(1), 7-19.

Zhang, H., Zhang, B., and **Liu, B.** (2016). Integrated Nano-zero valent iron and biosurfactant-aided Remediation of PCB-Contaminated Soil. *Applied and Environmental Soil Science*, *2016*.

Zheng, J.S., **Liu, B.**, Ping, J., Chen, B., Wu, H.J. and Zhang, B.Y. (2015) Vortex- and Shaker-Assisted Liquid–Liquid Microextraction (VSA-LLME) Coupled with Gas Chromatography and Mass Spectrometry (GC-MS) for Analysis of 16 Polycyclic Aromatic Hydrocarbons (PAHs) in Offshore Produced Water. *Water Air and Soil Pollution, 226(9)*, 318-331.

Jing, L., Chen, B., Zhang, B., Zheng, J., and **Liu, B.** (2014). Naphthalene degradation in seawater by UV irradiation: the effects of fluence rate, salinity, temperature and initial concentration. *Marine pollution bulletin*, *81*(1), 149-156.

Conference Proceedings

Liu, B., Chen, B., Lee, K., Zhang, B.Y., Ma, Y.C., and Jing, L. (2014) Photocatalytic degradation of naphthalene in offshore produced water: comparison of immobilized and suspended TiO_2. Proceedings of The International Conference on Marine and Freshwater Environments (iMFE), August 06-08, St. John's, Canada. WWT1300: 1-8.

Liu. B., Zheng, J.S., Chen, B., and Zhang, B.Y. (2013) A Preliminary Study on Nano-catalyst Enhanced Heterogeneous Photo-degradation of Polycyclic Aromatic Hydrocarbons (PAHs) in Produced Water. Proceedings of the 36th AMOP Technical Seminar on Environmental Contamination and Response June 4 to 6

Zheng, J.S., **Liu, B.**, Ping, J., Zhang, B.Y., Lee, K., Chen, B., and Cai, Q.H., (2012) Two Analytical Methods for Real-time Monitoring of Polycyclic Aromatic Hydrocarbons in Oil Contaminated Seawater. Proceedings of the 35th AMOP Technical Seminar on Environmental Contamination and Response June 5 to 7

Ping, J., Chen, B., Zheng, J.S., and **Liu, B.** (2011) A modified analytical method for testing trace polycyclic aromatic hydrocarbons in produced water using GC/MS. The 64th Canadian Water Resources Association (CWRA) National Conference, June 27-30, St. John's, Canada

Liu, B., Ping, J., Zheng. J.S., Zhang, B.Y. and Chen, B. (2011) A Review of Mechanisms and Photoproducts of Polycyclic Aromatic Hydrocarbons (PAHs) Photo-oxidations. Proceedings of the 64th Canadian Water Resources Association National Conference, June 27 to 30, 2011, St. John's NL Canada

Ping, J., Chen, B., Zheng, J.S., **Liu, B.,** and Zhang, B.Y. (2011) A Preliminary Study on the Ultraviolet Irradiation Effect on Degradation of Polycyclic Aromatic Hydrocarbons in Offshore Produced Water. Proceedings of the 10th Specialized Conference on Small Water and Wastewater Treatment Systems of International Water Association (IWA), April 18-22, Venice, Italy.

References

Agustina, T. E., Ang, H., & Vareek, V. (2005). A review of synergistic effect of photocatalysis and ozonation on wastewater treatment. *Journal of Photochemistry and Photobiology C: Photochemistry Reviews, 6*(4), 264-273.

Ahmed, S., Rasul, M. G., Martens, W. N., Brown, R., Hashib, M. A. (2011). Advances in heterogeneous photocatalytic degradation of phenols and dyes in wastewater: A review. *Water, Air and Soil Pollution, 215*(1-4), 3-29.

Alizadeh Fard, M., Aminzadeh, B., & Vahidi, H. (2013). Degradation of petroleum aromatic hydrocarbons using TiO_2 nanopowder film. *Environmental Technology (United Kingdom), 34*(9), 1183-1190.

An, C., Huang, G., Yao, Y., & Zhao, S. (2017). Emerging usage of electrocoagulation technology for oil removal from wastewater: A review. *Science of the Total Environment, 579*, 537-556.

Armanious, A., Özkan, A., Sohmen, U., & Gulyas, H. (2011). Inorganic greywater matrix impact on photocatalytic oxidation: Does flocculation of TiO_2 nanoparticles impair process efficiency? *Water Science and Technology, 63*(12), 2808-2813.

Asselin, M., Drogui, P., Brar, S. K., Benmoussa, H., & Blais, J. (2008). Organics removal in oily bilgewater by electrocoagulation process. *Journal of Hazardous Materials, 151*(2-3), 446-455.

Athanasekou, C. P., Moustakas, N. G., Morales-Torres, S., Pastrana-Martínez, L. M., Figueiredo, J. L., Faria, J. L., . . . Falaras, P. (2015). Ceramic photocatalytic membranes for water filtration under UV and visible light. *Applied Catalysis B: Environmental, 178*, 12-19.

Behnajady, M. A., Modirshahla, N., Mirzamohammady, M., Vahid, B., & Behnajady, B. (2008). Increasing photoactivity of titanium dioxide immobilized on glass plate with optimization of heat attachment method parameters. *Journal of Hazardous Materials, 160*(2), 508-513.

Beltran, F. J., Ovejero, G., Garcia-Araya, J. F., & Rivas, J. (1995). Oxidation of polynuclear aromatic hydrocarbons in water. 2. UV radiation and ozonation in the presence of UV radiation. *Industrial & Engineering Chemistry Research, 34*(5), 1607-1615.

Beltrán, F. J., & Rey, A. (2017). Solar or UVA-visible photocatalytic ozonation of water contaminants. *Molecules, 22*(7), 1177.

Beltrán, F. J., Rivas, F. J., & Gimeno, O. (2005a). Comparison between photocatalytic ozonation and other oxidation processes for the removal of phenols from water. *Journal of Chemical Technology and Biotechnology, 80*(9), 973-984.

Beltrán, F. J., Rivas, F. J., Gimeno, O., & Carbajo, M. (2005b). Photocatalytic enhanced oxidation of fluorene in water with ozone. comparison with other chemical oxidation methods. *Industrial & Engineering Chemistry Research, 44*(10), 3419-3425.

Berry, R. J., & Mueller, M. R. (1994). Photocatalytic decomposition of crude oil slicks using TiO_2 on a floating substrate. *Microchemical Journal, 50*(1), 28-32.

Bertilsson, S., & Widenfalk, A. (2002). Photochemical degradation of PAHs in freshwaters and their impact on bacterial growth–influence of water chemistry. *Hydrobiologia, 469*(1), 23-32.

Brame, J. A., Hong, S. W., Lee, J., Lee, S. H., & Alvarez, P. J. J. (2013). Photocatalytic pre-treatment with food-grade TiO_2 increases the bioavailability and bioremediation potential of weathered oil from the deepwater horizon oil spill in the gulf of mexico. *Chemosphere, 90*(8), 2315-2319.

Brendehaug, J., Johnsen, S., Bryne, K., Gjøse, A., Eide, T., & Aamot, E. (1992). Toxicity testing and chemical characterization of produced water—a preliminary study. *Produced water* (pp. 245-256). New York: Springer.

Byrne, J., Eggins, B., Brown, N., McKinney, B., & Rouse, M. (1998). Immobilisation of TiO_2 powder for the treatment of polluted water. *Applied Catalysis B: Environmental, 17*(1), 25-36.

Cai, Q., Zhang, B., Chen, B., Song, X., Zhu, Z., & Cao, T. (2015). Screening of biosurfactant-producing bacteria from offshore oil and gas platforms in north atlantic canada. *Environmental Monitoring and Assessment, 187*(5), 284.

Camacho, M., Boada, L. D., Orós, J., Calabuig, P., Zumbado, M., & Luzardo, O. P. (2012). Comparative study of polycyclic aromatic hydrocarbons (PAHs) in plasma of eastern atlantic juvenile and adult nesting loggerhead sea turtles (caretta caretta). *Marine Pollution Bulletin, 64*(9), 1974-1980.

Camus, L., Brooks, S., Geraudie, P., Hjorth, M., Nahrgang, J., Olsen, G., & Smit, M. (2015). Comparison of produced water toxicity to arctic and temperate species. *Ecotoxicology and Environmental Safety, 113*, 248-258.

Carp, O., Huisman, C. L., & Reller, A. (2004). Photoinduced reactivity of titanium dioxide. *Progress in Solid State Chemistry, 32*(1-2), 33-177.

Cazoir, D., Fine, L., Ferronato, C., & Chovelon, J. -. (2012). Hydrocarbon removal from bilgewater by a combination of air-stripping and photocatalysis. *Journal of Hazardous Materials, 235-236*, 159-168.

Chen, Z., Zhao, L., & Lee, K. (2010). Environmental risk assessment of offshore produced water discharges using a hybrid fuzzy-stochastic modeling approach. *Environmental Modelling and Software, 25*(6), 782-792.

Cheng, M., Zeng, G., Huang, D., Lai, C., Xu, P., Zhang, C., & Liu, Y. (2016). Hydroxyl radicals based advanced oxidation processes (AOPs) for remediation of soils contaminated with organic compounds: A review. *Chemical Engineering Journal, 284*, 582-598.

Cho, I. H., Kim, Y. G., Yang, J. K., Lee, N. H., & Lee, S. M. (2006). Solar-chemical treatment of groundwater contaminated with petroleum at gas station sites: Ex situ remediation using solar/TiO_2 photocatalysis and solar photo-fenton. *Journal of Environmental Science and Health - Part A Toxic/Hazardous Substances and Environmental Engineering, 41*(3), 457-473.

Cho, I., Kim, L., Zoh, K., Park, J., & Kim, H. (2006). Solar photocatalytic degradation of groundwater contaminated with petroleum hydrocarbons. *Environmental Progress, 25*(2), 99-109.

Chong, M. N., Jin, B., Chow, C. W. K., & Saint, C. (2010). Recent developments in photocatalytic water treatment technology: A review. *Water Research, 44*(10), 2997-3027.

Cochran, R. E., Jeong, H., Haddadi, S., Fisseha Derseh, R., Gowan, A., Beránek, J., & Kubátová, A. (2016). Identification of products formed during the heterogeneous nitration and ozonation of polycyclic aromatic hydrocarbons. *Atmospheric Environment, 128*, 92-103.

Coelho, A., Castro, A. V., Dezotti, M., & Sant'Anna Jr., G. L. (2006). Treatment of petroleum refinery sourwater by advanced oxidation processes. *Journal of Hazardous Materials, 137*(1), 178-184.

Corrêa, A. X., Tiepo, E. N., Somensi, C. A., Sperb, R. M., & Radetski, C. M. (2009). Use of ozone-photocatalytic oxidation (O_3/UV/TiO_2) and biological remediation for

treatment of produced water from petroleum refineries. *Journal of Environmental Engineering, 136*(1), 40-45.

da Rocha, O. R. S., Dantas, R. F., Duarte, M. M. M. B., Duarte, M. M. L., & da Silva, V. L. (2010). Oil sludge treatment by photocatalysis applying black and white light. *Chemical Engineering Journal, 157*(1), 80-85.

D'Auria, M., Emanuele, L., Racioppi, R., & Velluzzi, V. (2009). Photochemical degradation of crude oil: Comparison between direct irradiation, photocatalysis, and photocatalysis on zeolite. *Journal of Hazardous Materials, 164*(1), 32-38.

De Torres-Socías, E., Fernández-Calderero, I., Oller, I., Trinidad-Lozano, M. J., Yuste, F. J., & Malato, S. (2013). Cork boiling wastewater treatment at pilot plant scale: Comparison of solar photo-fenton and ozone (O_3, O_3/H_2O_2). toxicity and biodegradability assessment. *Chemical Engineering Journal, 234*, 232-239.

De, A. K., Chaudhuri, B., Bhattacharjee, S., & Dutta, B. K. (1999). Estimation of ·OH radical reaction rate constants for phenol and chlorinated phenols using UV/H2O2 photo-oxidation. *Journal of Hazardous Materials, 64*(1), 91-104.

Dionysiou, D. D., Puma, G. L., Ye, J., Schneider, J., & Bahnemann, D. (2016). *Photocatalysis: Applications* Royal Society of Chemistry.

Dolinová, J., Ružička, R., Kurková, R., Klánová, J., & Klán, P. (2006). Oxidation of aromatic and aliphatic hydrocarbons by OH radicals photochemically generated from H2O2 in ice. *Environmental Science & Technology, 40*(24), 7668-7674.

Dórea, H. S., Bispo, J. R., Aragão, K. A., Cunha, B. B., Navickiene, S., Alves, J. P., . . . Garcia, C. A. (2007). Analysis of BTEX, PAHs and metals in the oilfield produced water in the state of sergipe, brazil. *Microchemical Journal, 85*(2), 234-238.

Ekins, P., Vanner, R., & Firebrace, J. (2005). Management of produced water on offshore oil installations: A comparative assessment using flow analysis.

Elias-Samlalsingh, N., & Agard, J. B. (2004). Application of toxicity identification evaluation procedures for characterizing produced water using the tropical mysid, metamysidopsis insularis. *Environmental Toxicology and Chemistry, 23*(5), 1194-1203.

Enguita, F. J., & Leitao, A. L. (2013). Hydroquinone: Environmental pollution, toxicity, and microbial answers. *BioMed Research International, 2013*, 542168.

Erjavec, B., Hudoklin, P., Perc, K., Tišler, T., Dolenc, M. S., & Pintar, A. (2016). Glass fiber-supported TiO_2 photocatalyst: Efficient mineralization and removal of toxicity/estrogenicity of bisphenol A and its analogs. *Applied Catalysis B: Environmental, 183*, 149-158.

Fakhru'l-Razi, A., Pendashteh, A., Abdullah, L. C., Biak, D. R. A., Madaeni, S. S., & Abidin, Z. Z. (2009). Review of technologies for oil and gas produced water treatment. *Journal of Hazardous Materials, 170*(2-3), 530-551.

Flynn, S. A., Butler, E. J., & Vance, I. (1996). Produced water composition, toxicity, and fate. *Produced water 2* (pp. 69-80) Springer.

Gao, Y. H., Chen, Y., Wang, Z. X., & Wang, X. L. (2013). Treatment of oily wastewater by photocatalytic degradation using nano Fe-TiO_2. *Advanced Materials Research, 781-784*, 2241-2244.

Ghaly, M. Y., Jamil, T. S., El-Seesy, I. E., Souaya, E. R., & Nasr, R. A. (2011). Treatment of highly polluted paper mill wastewater by solar photocatalytic oxidation with synthesized nano TiO_2. *Chemical Engineering Journal, 168*(1), 446-454.

Ghasemi, Z., Younesi, H., & Zinatizadeh, A. A. (2016). Preparation, characterization and photocatalytic application of TiO_2/Fe-ZSM-5 nanocomposite for the treatment of petroleum refinery wastewater: Optimization of process parameters by response surface methodology. *Chemosphere, 159*, 552-564.

Ghosh, J. P., Achari, G., & Langford, C. H. (2016). Design and evaluation of a UV LED photocatalytic reactor using anodized TiO_2 nanotubes. *Water Environment Research, 88*(8), 785-791.

Gimeno, O., Rivas, F., Beltrán, F., & Carbajo, M. (2007). Photocatalysis of fluorene adsorbed onto TiO_2. *Chemosphere, 69*(4), 595-604.

Grzechulska, J., Hamerski, M., & Morawski, A. W. (2000). Photocatalytic decomposition of oil in water. *Water Research, 34*(5), 1638-1644.

Gulyas, H., Jain, H. B., Susanto, A. L., Malekpur, M., Harasiuk, K., Krawczyk, I., . . . Furmanska, M. (2005). Solar photocatalytic oxidation of pretreated wastewaters: Laboratory scale generation of design data for technical-scale double-skin sheet reactors. *Environmental Technology, 26*(5), 501-514.

Gupta, K. K., Jassal, M., & Agrawal, A. K. (2008). Sol-gel derived titanium dioxide finishing of cotton fabric for self cleaning. *Csir,* , 443-450.

Gupta, S., Pathak, B., & Fulekar, M. (2015). Molecular approaches for biodegradation of polycyclic aromatic hydrocarbon compounds: A review. *Reviews in Environmental Science and Bio/Technology, 14*(2), 241-269.

Gupta, S. M., & Tripathi, M. (2011). A review of TiO_2 nanoparticles. *Chinese Science Bulletin, 56*(16), 1639.

Haag, W. R., & Hoigne, J. (1983). Ozonation of bromide-containing waters: Kinetics of formation of hypobromous acid and bromate. *Environmental Science & Technology, 17*(5), 261-267.

Han, W., Zhang, P., Zhu, W., Yin, J., & Li, L. (2004). Photocatalysis of p-chlorobenzoic acid in aqueous solution under irradiation of 254 nm and 185 nm UV light. *Water Research, 38*(19), 4197-4203.

Hashimoto, K., Kawai, T., & Sakata, T. (1984). Photocatalytic reactions of hydrocarbons and fossil fuels with water. hydrogen production and oxidation. *Journal of Physical Chemistry, 88*(18), 4083-4088.

Hasselberg, L., Meier, S., & Svardal, A. (2004). Effects of alkylphenols on redox status in first spawning atlantic cod (gadus morhua). *Aquatic Toxicology, 69*(1), 95-105.

Heller, A., Nair, M., Davidson, L., Schwitzgebel, J., Luo, Z., Norrell, J. L., . . . Ekerdt, J. G. (1993). Application of photocatalytic hollow glass microbeads in the cleanup of oil spills. Paper presented at the *International Oil Spill Conference, , 1993*(1) 623-627.

Hempoonsert, J., Tansel, B., & Laha, S. (2010). Effect of temperature and pH on droplet aggregation and phase separation characteristics of flocs formed in oil-water emulsions after coagulation. *Colloids and Surfaces A: Physicochemical and Engineering Aspects, 353*(1), 37-42.

Henderson, S., Grigson, S., Johnson, P., & Roddie, B. (1999). Potential impact of production chemicals on the toxicity of produced water discharges from north sea oil platforms. *Marine Pollution Bulletin, 38*(12), 1141-1151.

Hidaka, H., Honjo, H., Horikoshi, S., & Serpone, N. (2003). Photocatalyzed degradations on a TiO_2-coated quartz crystal microbalance. I. adsorption/desorption processes in the degradation of phenol and catechol. *New Journal of Chemistry, 27*(9), 1371-1376.

Hoffmann, M. R., Martin, S. T., Choi, W., & Bahnemann, D. W. (1995). Environmental applications of semiconductor photocatalysis. *Chemical Reviews, 95*(1), 69-96.

Hoigne, J., & Bader, H. (1976). The role of hydroxyl radical reactions in ozonation processes in aqueous solutions. *Water Research, 10*(5), 377-386.

Holth, T. F., Beylich, B. A., Skarphédinsdóttir, H., Liewenborg, B., Grung, M., & Hylland, K. (2009). Genotoxicity of environmentally relevant concentrations of water-soluble oil components in cod (gadus morhua). *Environmental Science & Technology, 43*(9), 3329-3334.

Hsu, Y. Y., Hsiung, T. L., Wang, H. P., Fukushima, Y., Wei, Y. L., & Chang, J. E. (2008). Photocatalytic degradation of spill oils on TiO_2 nanotube thin films. *Marine Pollution Bulletin, 57*(6-12), 873-876.

Hu, D., Yu, X., Zhang, M., Guo, J., & Zheng, X. (2012). Study on the photocatalytic degradation of diesel pollutants in seawater by a sonochemically prepared nano zinc oxide. *Advanced Materials Research, 476-478*, 1939-1942.

Huang, C., & Shu, H. (1995). The reaction kinetics, decomposition pathways and intermediate formations of phenol in ozonation, UV O_3 and UV H_2O_2 processes. *Journal of Hazardous Materials, 41*(1), 47-64.

Huang, W., Chang, C., & Shih, F. (2009). Disinfection by-product formation and mutagenic assay caused by preozonation of groundwater containing bromide. *Environmental Monitoring and Assessment, 158*(1), 181-196.

Ibhadon, A. O., & Fitzpatrick, P. (2013). Heterogeneous photocatalysis: Recent advances and applications. *Catalysts, 3*(1), 189-218.

Igunnu, E. T., & Chen, G. Z. (2012). Produced water treatment technologies. *International Journal of Low-Carbon Technologies, 9*(3), 157-177.

Jaji, K. T. (2012). *Treatment of oilfield produced water with dissolved air flotation*

Jamaly, S., Giwa, A., & Hasan, S. W. (2015). Recent improvements in oily wastewater treatment: Progress, challenges, and future opportunities. *Journal of Environmental Sciences (China), 37*, 15-30.

Janknecht, P., Lopes, A. D., & Mendes, A. M. (2004). Removal of industrial cutting oil from oil emulsions by polymeric ultra-and microfiltration membranes. Environmental science & technology, 38(18), 4878-4883.

Jing, L., Chen, B., & Zhang, B. (2014a). Modeling of UV-induced photodegradation of naphthalene in marine oily wastewater by artificial neural networks. *Water, Air, & Soil Pollution, 225*(4), 1906.

Jing, L., Chen, B., Zhang, B., & Li, P. (2015). Process simulation and dynamic control for marine oily wastewater treatment using UV irradiation. *Water Research, 81*, 101-112.

Jing, L., Chen, B., Zhang, B., & Peng, H. (2012). A review of ballast water management practices and challenges in harsh and arctic environments. *Environmental Reviews, 20*(2), 83-108.

Jing, L., Chen, B., Zhang, B., Zheng, J., & Liu, B. (2014b). Naphthalene degradation in seawater by UV irradiation: The effects of fluence rate, salinity, temperature and initial concentration. *Marine Pollution Bulletin, 81*(1), 149-156.

Johnsen, S., Smith, A. T., & Brendehaug, J. (1994). Identification of acute toxicity sources in produced water. Paper presented at the *SPE Health, Safety and Environment in Oil and Gas Exploration and Production Conference,*

Karakulski, K., Morawski, W. A., & Grzechulska, J. (1998). Purification of bilge water by hybrid ultrafiltration and photocatalytic processes. *Separation and Purification Technology, 14*(1-3), 163-173.

Katz, A., McDonagh, A., Tijing, L., & Shon, H. K. (2015). Fouling and inactivation of titanium dioxide-based photocatalytic systems. *Critical Reviews in Environmental Science and Technology, 45*(17), 1880-1915.

King, S. M., Leaf, P. A., Olson, A. C., Ray, P. Z., & Tarr, M. A. (2014). Photolytic and photocatalytic degradation of surface oil from the deepwater horizon spill. *Chemosphere, 95*, 415-422.

Kuhn, H., Braslavsky, S., & Schmidt, R. (2004). Chemical actinometry. *Pure and Applied Chemistry, 76*(12), 2105-2146.

Lair, A., Ferronato, C., Chovelon, J., & Herrmann, J. (2008). Naphthalene degradation in water by heterogeneous photocatalysis: An investigation of the influence of inorganic anions. *Journal of Photochemistry and Photobiology A: Chemistry, 193*(2–3), 193-203.

Laoufi, N., Tassalit, D., & Bentahar, F. (2008). The degradation of phenol in water solution by TiO_2 photocatalysis in a helical reactor. *Global NEST Journal, 10*(3), 404-418.

Lazar, M. A., Varghese, S., & Nair, S. S. (2012). Photocatalytic water treatment by titanium dioxide: Recent updates. *Catalysts, 2*(4), 572-601.

Leshuk, T., Wong, T., Linley, S., Peru, K. M., Headley, J. V., & Gu, F. (2016a). Solar photocatalytic degradation of naphthenic acids in oil sands process-affected water. *Chemosphere, 144*, 1854-1861.

Leshuk, T., de Oliveira Livera, D., Peru, K. M., Headley, J. V., Vijayaraghavan, S., Wong, T., & Gu, F. (2016b). Photocatalytic degradation kinetics of naphthenic acids in oil sands process-affected water: Multifactorial determination of significant factors. *Chemosphere, 165*, 10-17.

Levchuk, I., Rueda-Márquez, J., Suihkonen, S., Manzano, M., & Sillanpää, M. (2015). Application of UVA-LED based photocatalysis for plywood mill wastewater treatment. *Separation and Purification Technology, 143*, 1-5.

Li, G., An, T., Chen, J., Sheng, G., Fu, J., Chen, F., . . . Zhao, H. (2006). Photoelectrocatalytic decontamination of oilfield produced wastewater containing refractory organic pollutants in the presence of high concentration of chloride ions. *Journal of Hazardous Materials, 138*(2), 392-400.

Li, W., Ni, C., Lin, H., Huang, C., & Shah, S. I. (2004). Size dependence of thermal stability of ti O 2 nanoparticles. *Journal of Applied Physics, 96*(11), 6663-6668.

Li, Z., Gao, B., Chen, G. Z., Mokaya, R., Sotiropoulos, S., & Puma, G. L. (2011). Carbon nanotube/titanium dioxide (CNT/TiO_2) core–shell nanocomposites with tailored shell thickness, CNT content and photocatalytic/photoelectrocatalytic properties. *Applied Catalysis B: Environmental, 110*, 50-57.

Li, C., Wang, D., Xu, X., & Wang, Z. (2017). Formation of known and unknown disinfection by-products from natural organic matter fractions during chlorination, chloramination, and ozonation. *Science of the Total Environment, 587,* 177-184

Li, S., Wang, L., & Li, L. (2005). Degradation of oily wastewater in refinery with photocalysis technology. *Petroleum Refinery Engineering, 35*(12), 48-50.

Lin, H. F., & Valsaraj, K. T. (2003). A titania thin film annular photocatalytic reactor for the degradation of polycyclic aromatic hydrocarbons in dilute water streams. *Journal of Hazardous Materials, 99*(2), 203-219.

Ling, C. M., Mohamed, A. R., & Bhatia, S. (2004). Performance of photocatalytic reactors using immobilized TiO_2 film for the degradation of phenol and methylene blue dye present in water stream. *Chemosphere, 57*(7), 547-554.

Liu, B., Chen, B., Lee, K., Zhang, B., Ma, Y., & Jing, L. (2016a). Removal of naphthalene from offshore produced water through immobilized nano-TiO_2 aided photo-oxidation. *Water Quality Research Journal of Canada, 51*(3), 246-255.

Liu, B., Chen, B., Zhang, B., Zheng, J., & Jing, L. (2017). Toxicity and biodegradability study on enhanced photocatalytic oxidation of polycyclic aromatic hydrocarbons in offshore produced water. *2017 CSCE Annual General Conference,* Vancouver, Canada.

Liu, B., Chen, B., Zhang, B. Y., Jing, L., Zhang, H., & Lee, K. (2016b). Photocatalytic degradation of polycyclic aromatic hydrocarbons in offshore produced water: Effects of water matrix. *Journal of Environmental Engineering (United States), 142*(11)

Liu, B., Zheng, J., Chen, B., & Zhang, B. (2013). A preliminary study on nano-catalyst enhanced heterogeneous photodegradation of polycyclic aromatic hydrocarbons (PAHs) in produced water. Paper presented at the *The 36th AMOP Technical Seminar on Environmental Contamination and Response,* Halifax, Canada. 618-628.

Lundstedt, S., White, P. A., Lemieux, C. L., Lynes, K. D., Lambert, I. B., Öberg, L., . . . Tysklind, M. (2007). Sources, fate, and toxic hazards of oxygenated polycyclic aromatic hydrocarbons (PAHs) at PAH-contaminated sites. *AMBIO: A Journal of the Human Environment, 36*(6), 475-485.

Luo, J., Ma, M., Liu, C., Zha, J., & Wang, Z. (2009). Impacts of particulate organic carbon and dissolved organic carbon on removal of polycyclic aromatic hydrocarbons, organochlorine pesticides, and nonylphenols in a wetland. *Journal of Soils and Sediments, 9*(3), 180-187.

Marci, G., Sclafani, A., Augugliaro, V., Palmisano, L., & Schiavello, M. (1995). Influence of some aromatic and aliphatic compounds on the rate of photodegradation of phenol in aqueous suspensions of TiO_2. *Journal of Photochemistry and Photobiology A: Chemistry, 89*(1), 69-74.

Mascolo, G., Comparelli, R., Curri, M., Lovecchio, G., Lopez, A., & Agostiano, A. (2007). Photocatalytic degradation of methyl red by TiO_2: Comparison of the efficiency of immobilized nanoparticles versus conventional suspended catalyst. *Journal of Hazardous Materials, 142*(1), 130-137.

Matthews, R. W. (1987). Photooxidation of organic impurities in water using thin films of titanium dioxide. *Journal of Physical Chemistry, 91*(12), 3328-3333.

McCullagh, C., Skillen, N., Adams, M., & Robertson, P. K. (2011). Photocatalytic reactors for environmental remediation: A review. *Journal of Chemical Technology and Biotechnology, 86*(8), 1002-1017.

McLaughlin, C., Falatko, D., Danesi, R., & Albert, R. (2014). Characterizing shipboard bilgewater effluent before and after treatment. *Environmental Science and Pollution Research, 21*(8), 5637-5652.

McQueen, A. D., Kinley, C. M., Kiekhaefer, R. L., Calomeni, A. J., Rodgers Jr, J. H., & Castle, J. W. (2016). Photocatalysis of a commercial naphthenic acid in water using fixed-film TiO_2. *Water, Air, and Soil Pollution, 227*(5), 132.

Mehrjouei, M., Müller, S., & Möller, D. (2015). A review on photocatalytic ozonation used for the treatment of water and wastewater. *Chemical Engineering Journal, 263*, 209-219.

Meier, S., Andersen, T. E., Norberg, B., Thorsen, A., Taranger, G. L., Kjesbu, O. S., . . . Svardal, A. (2007). Effects of alkylphenols on the reproductive system of atlantic cod (gadus morhua). *Aquatic Toxicology, 81*(2), 207-218.

Minero, C., Maurino, V., & Pelizzetti, E. (1997). Photocatalytic transformations of hydrocarbons at the sea water / air interface under solar radiation. *Marine Chemistry, 58*(3-4), 361-372.

Momeni, M. M., & Hosseini, M. G. (2014). Different TiO_2 nanotubes for back illuminated dye sensitized solar cell: Fabrication, characterization and electrochemical impedance properties of DSSCs. *Journal of Materials Science-Materials in Electronics, 25*(11), 5027-5034.

Nakata, H., Sakai, Y., Miyawaki, T., & Takemura, A. (2003). Bioaccumulation and toxic potencies of polychlorinated biphenyls and polycyclic aromatic hydrocarbons in tidal flat and coastal ecosystems of the ariake sea, japan. *Environmental Science & Technology, 37*(16), 3513-3521.

NEB, CNLOPB & CNSOPB. (2010). Offshore waste treatment guideline. Retrieved Apr. 15, 2017, from http://www.cnlopb.ca/legislation/guidelines.php

Neff, J. M. (2002). *Bioaccumulation in marine organisms: Effect of contaminants from oil well produced water.* Elsevier.

Neff, J. (1985). Polycyclic aromatic hydrocarbons. In G. M. Rand, Petrocelli & S.R. (Eds.), ***Fundamentals of aquatic toxicology**: **methods and applications*** (). New York, NY: Hemisphere Publishing.

Neff, J., Lee, K., & DeBlois, E. M. (2011). Produced water: Overview of composition, fates, and effects. In K. Lee, & J. Neff (Eds.), *Produced water: Environmental risks and advances in mitigation technologies* (pp. 3-54). New York, NY: Springer New York.

Ni, L., Li, Y., Zhang, C., Li, L., Zhang, W., & Wang, D. (2016). Novel floating photocatalysts based on polyurethane composite foams modified with silver/titanium dioxide/graphene ternary nanoparticles for the visible-light-mediated remediation of diesel-polluted surface water. *Journal of Applied Polymer Science, 133*(19)

Ni, M., Leung, M. K., Leung, D. Y., & Sumathy, K. (2007). A review and recent developments in photocatalytic water-splitting using TiO_2 for hydrogen production. *Renewable and Sustainable Energy Reviews, 11*(3), 401-425.

NLOPB. (2017). Resource management statistics. Retrieved Oct. 20, 2017, from http://www.cnlopb.ca/information/statistics.php

Nweke, C., & Okpokwasili, G. (2010). Influence of exposure time on phenol toxicity to refinery wastewater bacteria. *Journal of Environmental Chemistry and Ecotoxicology, 2*(2), 020-027.

OECD. (1992). Test no. 306: Biodegradability in seawater. *OECD guidelines for the testing of chemicals, section 3 Environmental fate and behaviour* ()

OGP. (2002). *Aromatics in produced water: Occurrence, fate & effects and treatment.* (No. Report OGP No. 1.20/324). London, United Kingdom: International Association of Oil and Gas Producers.

Oil & Gas UK. (2017). *Environment report 2016*. Oil & Gas UK, London.

Orem, W., Tatu, C., Varonka, M., Lerch, H., Bates, A., Engle, M., . . . McIntosh, J. (2014). Organic substances in produced and formation water from unconventional natural gas extraction in coal and shale. *International Journal of Coal Geology, 126*, 20-31.

OSPAR Commission. (2012). Discharges, spills and emissions from offshore oil and gas installations in 2010. *OSPAR Commission, Paris,*

Pablos, C., Van Grieken, R., Marugan, J., & Muñoz, A. (2012). Simultaneous photocatalytic oxidation of pharmaceuticals and inactivation of escherichia coli in wastewater treatment plant effluents with suspended and immobilised TiO_2. *Water Science and Technology, 65*(11), 2016-2023.

Pavelescu, G., Uyguner-Demirel, C., Bekbolet, M., Ghervase, L., & Ioja, C. (2014). Comparison of photocatalytic treatment effectiveness on sewage and industrial

wastewaters. *Environmental Engineering and Management Journal, 13*(8), 2015-2021.

Pearlman, R. S., Yalkowsky, S. H., & Banerjee, S. (1984). Water solubilities of polynuclear aromatic and heteroaromatic compounds. *Journal of Physical and Chemical Reference Data, 13*(2), 555-562.

Pekakis, P. A., Xekoukoulotakis, N. P., & Mantzavinos, D. (2006). Treatment of textile dyehouse wastewater by TiO_2 photocatalysis. *Water Research, 40*(6), 1276-1286.

Zhang, P.Y., Liang, F.Y., Gang, Y., Chen, Q., & Zhu, W.P. (2003). A comparative study on decomposition of gaseous toluene by O_3/UV, TiO_2/UV and O_3/TiO_2/UV. *Journal of Photochemistry and photobiology A: Chemistry, 156*(1), 189-194.

Peres, J. C. G., Silvio, U. d., Teixeira, A. C. S., & Guardani, R. (2015). Study of an annular photoreactor with tangential inlet and outlet: I. fluid dynamics. *Chemical Engineering & Technology, 38*(2), 311-318.

Pérez-Casanova, J. C., Hamoutene, D., Hobbs, K., & Lee, K. (2012). Effects of chronic exposure to the aqueous fraction of produced water on growth, detoxification and immune factors of atlantic cod. *Ecotoxicology and Environmental Safety, 86*, 239-249.

Pernyeszi, T., & Dékány, I. (2003). Photocatalytic degradation of hydrocarbons by bentonite and TiO_2 in aqueous suspensions containing surfactants. *Colloids and Surfaces A: Physicochemical and Engineering Aspects, 230*(1-3), 191-199.

Pozzo, R. L., Baltanas, M. A., & Cassano, A. E. (1997). Supported titanium oxide as photocatalyst in water decontamination: State of the art. *Catalysis Today, 39*(3), 219-231.

Radwan, E. K., Yu, L., Achari, G., & Langford, C. H. (2016). Photocatalytic ozonation of pesticides in a fixed bed flow through UVA-LED photoreactor. *Environmental Science and Pollution Research, 23*(21), 21313-21318.

Rubio-Clemente, A., Torres-Palma, R. A., & Peñuela, G. A. (2014). Removal of polycyclic aromatic hydrocarbons in aqueous environment by chemical treatments: A review. *Science of the Total Environment, 478*, 201-225.

Saien, J., & Nejati, H. (2007). Enhanced photocatalytic degradation of pollutants in petroleum refinery wastewater under mild conditions. *Journal of Hazardous Materials, 148*(1-2), 491-495.

Saien, J., Delavari, H., & Solymani, A. (2010). Sono-assisted photocatalytic degradation of styrene-acrylic acid copolymer in aqueous media with nano titania particles and kinetic studies. *Journal of Hazardous Materials, 177*(1), 1031-1038.

Saien, J., & Shahrezaei, F. (2012). Organic pollutants removal from petroleum refinery wastewater with nanotitania photocatalyst and UV light emission. *International Journal of Photoenergy, 2012*

Santos, F. V., Azevedo, E. B., Sant'Anna Jr., G. L., & Dezotti, M. (2006). Photocatalysis as a tertiary treatment for petroleum refinery wastewaters. *Brazilian Journal of Chemical Engineering, 23*(4), 451-460.

Shahrezaei, F., Mansouri, Y., Zinatizadeh, A. A. L., & Akhbari, A. (2012). Process modeling and kinetic evaluation of petroleum refinery wastewater treatment in a photocatalytic reactor using TiO_2 nanoparticles. *Powder Technology, 221*, 203-212.

Shon, H., Vigneswaran, S., Ngo, H., Kim, J., & Kandasamy, J. (2007). Effect of flocculation as a pretreatment to photocatalysis in the removal of organic matter from wastewater. *Separation and Purification Technology, 56*(3), 388-391.

Srinivasan, A., & Viraraghavan, T. (2010). Oil removal from water using biomaterials. *Bioresource Technology, 101*(17), 6594-6600.

Thomas, K. V., Balaam, J., Hurst, M. R., & Thain, J. E. (2004). Identification of in vitro estrogen and androgen receptor agonists in north sea offshore produced water discharges. *Environmental Toxicology and Chemistry, 23*(5), 1156-1163.

Torimoto, T., Ito, S., Kuwabata, S., & Yoneyama, H. (1996). Effects of adsorbents used as supports for titanium dioxide loading on photocatalytic degradation of propyzamide. *Environmental Science & Technology, 30*(4), 1275-1281.

U.S. EPA. (1999). Surface vessel bilgewater/oil water separator: Nature of discharge.

Ukiwe, L. N., Egereonu, U. U., Njoku, P. C., Nwoko, C. I., & Allinor, J. I. (2013). Polycyclic aromatic hydrocarbons degradation techniques: A review. *International Journal of Chemistry, 5*(4), 43.

Uyguner-Demirel, C. S., Birben, N. C., & Bekbolet, M. (2017). Elucidation of background organic matter matrix effect on photocatalytic treatment of contaminants using TiO_2: A review. *Catalysis Today, 284*, 202-214.

Vargas, R., & Núñez, O. (2010). Photocatalytic degradation of oil industry hydrocarbons models at laboratory and at pilot-plant scale. *Solar Energy, 84*(2), 345-351.

Veil, J., & Clark, C. (2011). Produced water volume estimates and management practices. *SPE Production & Operations, 26*(03), 234-239.

Venkataramani, S., Davitt, K. M., Xu, H., Zhang, J., Song, Y., Connors, B. W., & Nurmikko, A. V. (2007). Semiconductor ultra-violet light-emitting diodes for flash photolysis. *Journal of Neuroscience Methods, 160*(1), 5-9.

Von Gunten, U. (2003). Ozonation of drinking water: Part II. disinfection and by-product formation in presence of bromide, iodide or chlorine. *Water Research, 37*(7), 1469-1487.

Wan, L., & Xu, Y. (2013). Iodine-sensitized oxidation of ferrous ions under UV and visible light: The influencing factors and reaction mechanism. *Photochemical & Photobiological Sciences, 12*(12), 2084-2088.

Wang, B., Chen, Y., Liu, S., Wu, H., & Song, H. (2006). Photocatalytical visbreaking of wastewater produced from polymer flooding in oilfields. *Colloids and Surfaces A: Physicochemical and Engineering Aspects, 287*(1-3), 170-174.

Wang, L., Kong, D., Ji, Y., Lu, J., Yin, X., & Zhou, Q. (2017). *Transformation of iodide and formation of iodinated by-products in heat activated persulfate oxidation process*

Wells, P. G., Lee, K., & Blaise, C. (1997). *Microscale testing in aquatic toxicology: Advances, techniques, and practice* CRC Press.

WHO. (2017). Trihalomethanes in drinking water. Retrieved Dec. 12, 2017, from http://www.who.int/water_sanitation_health/dwq/chemicals/THM200605.pdf

Wiszniowski, J., Robert, D., Surmacz-Gorska, J., Miksch, K., & Weber, J. (2003). Photocatalytic mineralization of humic acids with TiO_2: Effect of pH, sulfate and chloride anions. *International Journal of Photoenergy, 5*(2), 69-74.

Wu, L., Li, X., Yuan, Z., & Chen, Y. (2009). The fabrication of TiO_2-supported zeolite with core/shell heterostructure for ethanol dehydration to ethylene. *Catalysis Communications, 11*(1), 67-70.

Wunderlich, W., Oekermann, T., Miao, L., Hue, N. T., Tanemura, S., & Tanemura, M. (2004). Electronic properties of nano-porous TiO_2- and ZnO thin films- comparison of simulations and experiments. *Journal of Ceramic Processing & Research, 5*(4), 343-354.

Xu, J., Xiao, X., Stepanov, A. L., Ren, F., Wu, W., Cai, G., . . . Jiang, C. (2013). Efficiency enhancements in ag nanoparticles-SiO_2-TiO_2 sandwiched structure via plasmonic effect-enhanced light capturing. *Nanoscale Research Letters, 8*(1), 73.

Xue, G., Liu, H., Chen, Q., Hills, C., Tyrer, M., & Innocent, F. (2011). Synergy between surface adsorption and photocatalysis during degradation of humic acid on TiO_2/activated carbon composites. *Journal of Hazardous Materials, 186*(1), 765-772.

Yahia Cherif, L., Yahiaoui, I., Aissani-Benissad, F., Madi, K., Benmehdi, N., Fourcade, F., & Amrane, A. (2014). Heat attachment method for the immobilization of TiO_2 on glass plates: Application to photodegradation of basic yellow dye and optimization of operating parameters, using response surface methodology. *Industrial & Engineering Chemistry Research, 53*(10), 3813-3819.

Yakimov, M. M., Timmis, K. N., & Golyshin, P. N. (2007). Obligate oil-degrading marine bacteria. *Current Opinion in Biotechnology, 18*(3), 257-266.

Yao, J., Huang, Z., & Masten, S. J. (1998). The ozonation of pyrene: Pathway and product identification. *Water Research, 32*(10), 3001-3012.

Yeber, M., Paul, E., & Soto, C. (2012). Chemical and biological treatments to clean oily wastewater: Optimization of the photocatalytic process using experimental design. *Desalination and Water Treatment, 47*(1-3), 295-299.

Yıldırım, A. Ö, Gül, Ş, Eren, O., & Kuşvuran, E. (2011). A comparative study of ozonation, homogeneous catalytic ozonation, and photocatalytic ozonation for CI reactive red 194 azo dye degradation. *CLEAN–Soil, Air, Water, 39*(8), 795-805.

Yu, H., Song, L., Hao, Y., Lu, N., Quan, X., Chen, S., . . . Feng, Y. (2016). Fabrication of pilot-scale photocatalytic disinfection device by installing TiO_2 coated helical support into UV annular reactor for strengthening sterilization. *Chemical Engineering Journal, 283*, 1506-1513.

Yue, X., Zhang, R., Wang, H., & Zhang, F. (2009). Sorption and decomposition of crude oil using exfoliated graphite/ZnO composites. *Journal of Physics and Chemistry of Solids, 70*(11), 1391-1394.

Zaleska, A. (2008). Doped-TiO_2: A review. *Recent Patents on Engineering, 2*(3), 157-164.

Zhang, H., Xing, Z., Zhang, Y., Li, Z., Wu, X., Liu, C., . . . Zhou, W. (2015). Ni 2 and ti 3 co-doped porous black anatase TiO_2 with unprecedented-high visible-light-driven photocatalytic degradation performance. *RSC Advances, 5*(129), 107150-107157.

Zhang, J., Wang, X., Wang, X., Song, J., Huang, J., Louangsouphom, B., & Zhao, J. (2015). Floating photocatalysts based on loading Bi/N-doped TiO_2 on expanded graphite C/C (EGC) composites for the visible light degradation of diesel. *RSC Advances, 5*(88), 71922-71931.

Zhang, T., Wang, X., & Zhang, X. (2014). Recent progress in TiO_2-mediated solar photocatalysis for industrial wastewater treatment. *International Journal of Photoenergy, 2014*

Zhang, Z., Hossain, M. F., & Takahashi, T. (2010). Photoelectrochemical water splitting on highly smooth and ordered TiO_2 nanotube arrays for hydrogen generation. *International Journal of Hydrogen Energy, 35*(16), 8528-8535.

Zhao, Y., Hoivik, N., & Wang, K. (2016). Recent advance on engineering titanium dioxide nanotubes for photochemical and photoelectrochemical water splitting. *Nano Energy, 30*, 728-744.

Zheng, J., Liu, B., Ping, J., Chen, B., Wu, H., & Zhang, B. (2015). Vortex-and shaker-assisted liquid–liquid microextraction (VSA-LLME) coupled with gas chromatography and mass spectrometry (GC-MS) for analysis of 16 polycyclic

aromatic hydrocarbons (PAHs) in offshore produced water. *Water, Air, & Soil Pollution, 226*(9), 318.

Zheng, J., Chen, B., Thanyamanta, W., Hawboldt, K., Zhang, B., & Liu, B. (2016). Offshore produced water management: A review of current practice and challenges in harsh/arctic environments. *Marine Pollution Bulletin, 104*(1–2), 7-19.

Zhu, B., & Zou, L. (2009). Trapping and decomposing of color compounds from recycled water by TiO_2 coated activated carbon. *Journal of Environmental Management, 90*(11), 3217-3225.

Ziolli, R. L., & Jardim, W. F. (2002). Photocatalytic decomposition of seawater-soluble crude-oil fractions using high surface area colloid nanoparticles of TiO_2. *Journal of Photochemistry and Photobiology A: Chemistry, 147*(3), 205-212.

Ziolli, R. L., & Jardim, W. F. (2003). Photochemical transformations of water-soluble fraction (WSF) of crude oil in marine waters. A comparison between photolysis and accelerated degradation with TiO_2 using GC-MS and UVF. *Journal of Photochemistry and Photobiology A: Chemistry, 155*(1-3), 243-252.

Zulfakar, M., Hairul, N. A. H., Akmal, H. M. R., & Rahman, M. A. (2011). Photocatalytic degradation of phenol in a fluidized bed reactor utilizing immobilized TiO_2 photocatalyst: Characterization and process studies. *Journal of Applied Sciences, 11*(13), 2320-2326.